INFORMATION TO USERS

This manuscript has been reproduced from the microfilm master. UMI films the text directly from the original or copy submitted. Thus, some thesis and dissertation copies are in typewriter face, while others may be from any type of computer printer.

The quality of this reproduction is dependent upon the quality of the copy submitted. Broken or indistinct print, colored or poor quality illustrations and photographs, print bleedthrough, substandard margins, and improper alignment can adversely affect reproduction.

In the unlikely event that the author did not send UMI a complete manuscript and there are missing pages, these will be noted. Also, if unauthorized copyright material had to be removed, a note will indicate the deletion.

Oversize materials (e.g., maps, drawings, charts) are reproduced by sectioning the original, beginning at the upper left-hand corner and continuing from left to right in equal sections with small overlaps. Each original is also photographed in one exposure and is included in reduced form at the back of the book.

Photographs included in the original manuscript have been reproduced xerographically in this copy. Higher quality 6" x 9" black and white photographic prints are available for any photographs or illustrations appearing in this copy for an additional charge. Contact UMI directly to order.

UMI®

Bell & Howell Information and Learning
300 North Zeeb Road, Ann Arbor, MI 48106-1346 USA
800-521-0600

PHASE SEPARATION OF SOLVENT MIXTURES WITH A CRITICAL POINT OF MISCIBILITY

by

RAJAN GUPTA

A dissertation submitted to the Graduate Faculty in Engineering in partial fulfillment of the requirements for the degree of Doctor of Philosophy, The City University of New York

1999

This manuscript has been read and accepted for the Graduate Faculty in Engineering in satisfaction of the dissertation requirement for the degree of Doctor of Philosophy.

Date — Professor Reuel Shinnar, Chair of Examining Committee

Date — Professor Roberto Mauri, Co-Mentor

Date — Professor Mumtaz K. Kassir, Acting Executive Officer

Professor Charles Maldarelli

Professor Alexander Couzis

Dr. Michael Midler

Supervisory committee
The City University of New York

ABSTRACT

PHASE SEPARATION OF SOLVENT MIXTURES WITH A CRITICAL POINT OF MISCIBILITY

by

Rajan Gupta

Advisors: Professors Reuel Shinnar and Roberto Mauri

In this work, the dynamics of phase separation in liquid mixtures, phase separation in the presence of surfactants, and a novel separation process of liquid-liquid extraction have been studied.

In the first part of this work, we study the phase segregation of a partially miscible liquid mixture when it is quenched to a temperature T deeply below its critical point of miscibility T_c, with $|T-T_c| / T_c \sim 0.1$. In the case of initially homogeneous mixture, we observe the formation of single phase microdomains, which grow linearly in time in the range of 10-400 μm, indicating that phase segregation is driven by convection, and not by diffusion. While these domains are interconnected dendritic structures when the mixture had critical composition, they appear to be spherical drops in the off-critical case. On the other hand, when the mixture is initially segregated everywhere, with the exception of a millimeter-thick region, a sharp interface appears a few seconds after the quench, with no visible drops forming. Using a dimensional analysis of the governing equations based on the model H, we show that phase separation is governed by the convection induced by capillary forces, and not by diffusion. In addition, we determine an expression estimating

the growth rate of single-phase domains, which is in very good agreement with our experimental results.

In the second part of this work, we show that the presence of surface-active compounds does not influence the settling time of a partially miscible liquid mixture as it phase separates. On the other hand, when the same mixture, in its two-phase state, is agitated isothermally, its settling time greatly increases if surfactants are added. This phenomenon is monitored microscopically, and is explained theoretically applying the model *H*, showing that during phase transition the capillary forces induce a net attraction between droplets which greatly dominates the repulsive forces due to the presence of surfactants.

Finally, we describe a new liquid-liquid extraction process, which capitalizes on the properties of partially miscible solvents. It consists in first mixing the system to be extracted with a primary solvent, which is soluble with the native solvent, and subsequently adding a modifier, which is insoluble with either the native or the primary solvent. This process has the advantage that the resulting separation of the solvents is very rapid, even in the presence of emulsion-forming impurities. In addition, the extraction efficiency of the new process may be ten times higher than that of the traditional liquid-liquid extraction. The new process is thought of having significant advantages in the extraction of products from fermentation broths, plants and other natural sources.

Acknowledgements

I wish to express my profound appreciation and gratitude to Professors Reuel Shinnar and Roberto Mauri for their guidance, inspiration and contribution at all times during the course of this work.

I am also indebted to Professors Charles Maldarelli and Alexander Couzis for their valuable suggestions and encouragement. Sincere thanks are due to Mr. Andrew Eng and Mr. Zhen Rong Xu for their help in my experimental work.

Financial assistance was made available by the Research Foundation of The City University of New York, which came from NSF. This aid is gratefully acknowledged.

Table of Contents

List of Figures

List of Tables

Table

Chapter 1

Introduction

Despite the extensive application of liquid extraction over the past fifty years, and the extensive amount of research that has been done, liquid extraction is nevertheless a relatively immature unit operation. The large number of variables, which apparently influence the rate of mass transfer, makes it necessary to have a special treatment for each different case. One common case in most of the liquid-liquid extraction processes is the formation of emulsions and slow coalescence due to impurities. In many cases, to break these emulsions, centrifuges are used. However, this requires intense agitation, which may be detrimental for the product. To ameliorate this problem, a novel separation technique, the Phase Transition Extraction (PTE) process, was proposed (Ullmann *et al.*, 1997, 1995; Ullmann, 1993; Ludmer *et al.* 1990). The process consists of two steps: (a) extraction is performed in the homogeneous region by heating two partially miscible solvents above their critical temperature, and thus eliminating the need for intense agitation, and (b) separation is performed by rapidly cooling at a temperature below the

coexistence curve. In Ullmann *et al.* (1995), the new process was applied to extract an antibiotic, i.e. ephretomycin, from a fermentation broth containing fractured cells, obtaining the two startling and unexpected following results:

- Phase separation was very fast (it was completed within few minutes), whereas conventional extraction produced a stable emulsion that required a centrifuge to separate.
- The extraction yield was very high, and could not be duplicated even when conventional extraction in multiple stages was performed. This was surprising, as the partition coefficient for the conventional solvent was higher.

More recently, Eliyahu and Ludmer (1995) have confirmed these results using different systems, and in particular they achieved very high yields when extracting compounds from microbial cells that had not been fractured. These results are potentially of great relevance, especially in the extraction of biological compounds from fermentation broths, mammalian cells and plants.

In the present work we explain these unexpected results, and present a scientific basis for the absence of emulsion formation and the higher yields in the PTE process. We investigate the process microscopically, and provide a firm understanding of the different features and phenomena involved during the phase separation. During the course of this work, we also study another process, the Composition-Induced Phase Separation (CIPS) process, in which the phase transition of partially miscible mixtures is achieved by adding a modifier, i.e. changing the mixture composition instead of its temperature.

Essential content of the work

In section 2.1 we summarize the basic principles of the liquid-liquid extraction (LLE) process, discussing the extraction operation, properties of dispersions, and the stability of the emulsions. Some common problems with the LLE process are also identified, and the prevailing methods to handle them are discussed. Since our whole work is related to partially miscible solvents, in Section 2.2, we explain their miscibility behavior and the phase-equilibria thermodynamics. Then, after explaining the characteristics of the two modes of phase separation, nucleation and spinodal decomposition, we discuss the earlier work done on the dynamics of phase separation.

In Chapter 3 we explain the Phase Transition Extraction (PTE) process, in which the phase transition of partially miscible mixtures is induced by changing either the composition or the temperature of the mixture. Here, we investigate this process macroscopically, and analyze the difference between the PTE phase separation process and the usual LLE process.

Chapter 4 is devoted to the microscopic visualization of the liquid mixtures morphology during the phase separation. Here, we study the phase separation of both critical and off-critical fluid mixtures, following a deep temperature quench into the unstable region of mutual miscibility, by direct visual observations. We also present a dimensional analysis, and try to explain theoretically how the system behavior, like the growth rate of single-phase microdomains, depends on its fluidity and initial conditions.

Chapter 5 demonstrates that the PTE process is a useful tool for dealing with difficult separation processes. In section 5.1, we discuss the extraction of solutes from the

porous media, showing that the new process can be used in the extraction of products from fermentation broths, plants and other natural sources. In Section 5.2, we study the phase separation process in the presence of surfactants, and explain why the separation process in liquid mixtures is independent of the presence of emulsifying compounds. The applications of these results can be found in any liquid-liquid operation involving phase separation, both when emulsions are the final product of the process, and when they are detrimental to it. In section 5.3, an application of the extraction process on a more intricate problem is presented. Here, we propose a method for *in situ* remediation of contaminated soil from heavy or radioactive metal.

Finally, in the last Chapter 6 we summarize our work and suggest some advantages of the new extraction process.

Chapter 2

Background

2.1 Liquid-Liquid Extraction

Liquid-liquid extraction, or solvent extraction, was carried out as early as Roman times when silver and gold were extracted from molten copper using lead as a solvent. The first significant industrial application of solvent extraction was in the petrochemical industry. This was followed by its application in recovery of vegetable oil, purification of penicillin, refining of radioisotopes and nonferrous metals, and, more recently, in biotechnology.

The liquid-liquid extraction operation consists of the following steps: (a) intimate contacting of the solvent with the solution containing the component to be extracted (extractant or solute), so that the solute will be transferred from the solution to the solvent and (b) separation of the two immiscible phases. The solvent must, to a certain extent, be

immiscible with the original mixture and must be capable of preferentially dissolving the component to be extracted.

When separation by distillation is ineffective or very difficult, liquid extraction is one of the main alternatives to consider. Close-boiling mixtures or substances that cannot withstand the temperature of distillation, even under a vacuum, may often be separated from impurities by extraction, by exploiting their chemical differences instead of vapor-pressure differences. For example, penicillin is recovered from fermentation broths by solvent extraction, using a solvent such as butyl acetate, after lowering the pH to get a favorable partition coefficient. The solvent is then treated with a buffered phosphate solution to extract the penicillin from the solvent and give a purified aqueous solution, from which penicillin is eventually produced by drying. Solvent extraction is also used to recover acetic acid from dilute aqueous solutions; distillation would be possible in this case, but the extraction step considerably reduces the amount of water to be distilled.

One of the major uses of solvent extraction is to separate petroleum products that have different chemical structures but the same boiling range. Lube oil fractions (bp > 300°C) are treated with low-boiling polar solvents such as phenol, furfural, or methyl pyrrolidone to extract the aromatics and leave an oil that contains paraffins and napththenes. The aromatics have poor viscosity-temperature characteristics, but they cannot be removed by distillation because of the overlapping boiling-point range.

2.1.1 Extraction equipment

Extraction equipment may be operated batchwise or continuously. A quantity of feed liquid may be mixed with a quantity of solvent in an agitated vessel, after which the

layers are settled and separated. The extract is the layer of solvent plus extracted solute, and the raffinate is the layer from which solute has been removed. The extract may be lighter or heavier than the raffinate, and so the extract may be shown coming from the top of the equipment in some cases and from the bottom in others. The operation may of course be repeated if more than one contact is required, but when the quantities are large and several contacts are needed, continuous flow becomes economical. Most extraction equipment are continuous with either successive stage contacts or differential contacts. Representative types are mixed-settlers, vertical towers of various kinds which operate by gravity flow, agitated tower extractors, and centrifugal extractors, and are discussed in detail in most of the Separation Processes texts.

2.1.2 Emulsions and Dispersions

The mixture of immiscible liquids resulting from agitation or mixing is an emulsion or dispersion of one liquid in a continuum of the other (Figure 2.1). Dispersions are generally considered to be unstable or temporary emulsions, the dispersed-phase droplets of which are coarse. It is customary to speak of these as "water-in-oil" or "oil-in-water" emulsions, referring to whether water or oil, respectively, forms the dispersed phase. Though it was long considered that emulsions cannot exist that contain more than 74% by volume of the dispersed phase, emulsions containing much more than 74% dispersed phase have been made. The dispersed droplets are ordinarily not of uniform size. High viscosity of one of the liquid favors its forming the continuum phase. The presence of an emulsifying substance, or surface-active agent, is of great influence, and it is generally recognized that the liquid in which the emulsifying reagent is soluble has the

greater tendency to form the continuous phase (Adamson, 1967). If solids are present that are preferentially wet by one of the liquids, that liquid will likely become continuous. Unstable dispersions can be stabilized by controlled agitation in a stirred vessel (Church and Shinnar, 1961).

Inversion is the change from one phase dispersed to the other, and presumably it occurs when the existing form of the emulsion is the less stable under the prevailing conditions. Inversions may be caused by dilution of the emulsion with the dispersed phase, by increasing the agitator speed in stirred vessel, or by using appropriate solids or surface-active agents. Occasionally dual emulsions, where the continuous phase is also present as very droplets inside larger drops of the other phase, are formed. Dilution of this emulsion may indicate to which type it belongs.

2.1.2.1 Stability of emulsions

From the liquid extraction point of view, the stability of an emulsion is its most important property, since it is necessary to separate the phases at each extraction stage. Stability represents the resistance offered by the dispersion to ultimate coalescence of the dispersed phase droplets. In order for a dispersion to "break" or separate into its bulk, the droplets must experience the following sequence of events: (a) collision, (b) flocculation or agglomeration, and (c) coalescence.

Collision. In the case of dispersions of very fine droplets, the rate of collision is given by their Brownian movement. However, in the dispersions with drop diameter 100 μm or more, rapid settling or sedimentation occurs, thus bringing droplets into contact with each other fairly rapidly. In this research work, drop size ranges from 1 μm to 1000

μm, and thus both Brownian motion and sedimentation will be responsible for drop collision, depending on the size considered. The settling is more rapid when the continuous liquid is less viscous and the density difference of two phases is large.

Flocculation. Not every collision of droplets is effective in bringing about an ultimate "break" of the dispersion, and if the collisions are completely ineffective, the emulsion is said to be stable. Stable emulsions are usually characterized by small droplet size, of the order of 1 to 1.5 *μm* in diameter and less. Two pure liquids rarely form stable emulsions, and a third substance nearly always must be present. This is always the case in extraction processes. Such an additional substance will ordinarily lower the interfacial tension. Surface-active agents, which are adsorbed at the liquid-liquid interface, are particularly effective in lowering the tension and increasing the stability. If the contact angle between the solids and the two liquids is finite, then the solids accumulate at the interface, with the majority of the volume of each particle lying in the continuous phase. These can prevent flocculation.

Coalescence. This refers to the merging of two or more drops with each other, requiring a puncturing of the film surrounding the drops. Interfacial tension is the driving force, and for liquids in equilibrium the higher the tension, the more rapid is the coalescence rate. If the continuous phase is very viscous, the longer time required for drainage and thinning of the film between the droplets slows down the overall process, and changes of temperature, which affect both viscosity and interfacial tension, have a strong influence.

2.1.3 Common problems encountered with LLE

Traditional liquid-liquid extraction (LLE) is simple in concept and usually requires the contacting of a feed containing the solute to be extracted with a solvent. This solvent/feed mixture is usually immiscible, but may be partially miscible (Treybal, 1963). The extraction and the stripping involve liquid-liquid contacting in which the droplets of one phase are initially dispersed in a second phase to facilitate mass transfer across the liquid-liquid boundary. Now, to form small drops and ensure good contact between the phases in slow mass-transfer systems, high intensity mixing is required. However, the shear stress induced by such a mixing can, in many cases, either damage high molecular weight solute molecules or form fine dispersions which reduce the coalescence rate. In the presence of surface-active impurities, this intense mixing may even cause emulsion formation, which is a common problem in the pharmaceutical industry, where the desired products are frequently extracted from fermentation broths containing surface-active impurities. In addition, the active compounds to be extracted from the fermentation broths are often "imprisoned" within cell debris, which makes the penetration of the solvents even more difficult to achieve. Similarly, in the extraction of products from natural plants and animal sources, it is important that the solvent can penetrate the solids to be extracted.

Therefore the efficiency of an LLE process is directly related to the wettability of the particles on which the solute molecules are adsorbed, while the workable throughput depends on the coalescence rates of the liquid drops that form during the mixing. It is clear, therefore, that systems with wettability problems or emulsification tendencies

cannot be operated by conventional extractors. Commonly such systems are handled using centrifugal extractors or, in some cases, adding compounds that break the emulsion.

Rapid extraction with very low hold-up of liquid per stage in an extractor is required for many products, such as antibiotics. For example, Penicillin, a most common antibiotic, has a very short half-life at low pH, which makes the extraction from an acidified solution the most critical stage. Thus a fast extraction, with minimal emulsion formation, is desired in this case. The current practice to perform rapid extraction is to add a precise quantity of deemulsifying agent to the aqueous stream just prior to the extraction. An example for such a treatment is given by Stround and Ransley (1956).

Another application of solvent extraction is in the extraction of hazardous waste from contaminated soil. Examples of contaminants are nuclear waste products, heavy metals, PCB, chlorinated solvents, polynuclear aromatics and similar organic compounds. In the case of soil contaminated with organic compounds, excavation and incineration under controlled conditions is a technical option. In some other cases, biological methods can be used for *in situ* removal of pollutants. On the other hand, for nuclear waste there is no cost-efficient *in situ* method, and even the removal of metal ions after excavation is difficult. The main difficulty in using conventional solvent extraction to remediate contaminated soils is in the insufficient contacting between soil and solvents, due to the preferential absorption of water on the soil and the fact that the solvents usually used are water insoluble.

2.2 Properties of Solvent Systems with a Critical Point of Miscibility

As our whole work deals with the use of partially miscible solvents, in this section we discuss briefly their properties.

2.2.1 Introduction to partially miscible solvents systems

When two liquids, *A* and *B*, combined in any ratio form only one phase, they are called completely (or homogeneously) miscible. However, if *A* and *B* are not miscible in all ratios, then they are called partially miscible.

In the case of partially miscible solvents, in a given range of ratios of *A* and *B*, mixture will form two liquid phases that are not miscible. Each phase will then consist of a saturated solution of one component in another. This solubility of one liquid in another is a function of temperature, and in general, the concentration of a liquid in another increases as the temperature is increased (assuming that pressure remains constant during heating).

Let us first understand the miscibility behavior at isothermal conditions for partially miscible solvents. While complete miscibility is obtained whenever a small amount of *A* is added to *B* or vice versa, as more *A* is added to the solution, eventually the limit of solubility of *A* in *B* at the current temperature is reached. Then, further addition of *A* will result in the appearance of two liquid phases that are saturated solutions of *A* in *B* and of *B* in *A*. Finally, sufficient addition of *A* will again bring the system to a condition of one liquid phase. Thus, for a substantial range of the system composition at a given

temperature, two liquid phases of constant composition, the saturated solutions, will coexist. The variation in the composition of these saturated solutions with temperature is conveniently shown graphically in the so-called miscibility curves (sometimes also called solubility or coexistence curves).

Figure 2.2 is a plot of the composition of the saturated liquid phases at equilibrium as a function of temperature. The area above the curve represents mixtures that form a single liquid phase, and that below the curve represents mixtures that form two mutually saturating liquid solutions. A mixture whose overall composition and temperature are given by point *F* will form saturated solutions of compositions *D* and *E*, and the horizontal line *DE* is named a tie line.

In the case described in Figure 2.2, as the temperature is increased, mutual solubilities of *A* in *B* increases, and points *D* and *E* move towards each other. Finally *D* and *E* coincide on further heating, which implies that there is then no longer a heterogeneous area in the binary system of liquids *A* and *B*, and a complete miscibility occurs. The minimum temperature at which this happens, point *C* in Figure 2.2, is termed the critical solution temperature (CST), or consulate temperature, T_C, and in the case described in Figure 2.2, point *C* is in fact an upper critical solution temperature (UCST).

There are other systems whose mutual solubility increases with decreasing temperature, as exemplified by the system triethylamine-water, and described in Figure 2.3a. In this case the point, at which the compositions of the two phases approach each other, is a lower critical solution temperature (LCST). In our further discussion on phase

equilibria thermodynamics and dynamics of phase separation, we will consider only the case of UCST systems.

Figures 2.3b and 2.3c describe two-component systems with both UCST and LCST. Some systems do show a tendency to form a closed two-phase region if a wide enough temperature range is explored (Walas, 1985). The temperature difference between the LCST and the UCST is at least 80°C (Ullman, 1993).

A large number of liquid pairs form systems without upper or lower critical points. In these cases vaporization may occur before an UCST or freezing before a LCST can be obtained (Treybal, 1963). However the most unusual behavior is that of sulfur-benzene system, Figure 2.3c, which has an UCST that is lower than a LCST.

Several comprehensive collections of liquid-liquid equilibrium data are available, such as Stephen, Stephen, and Silcock (1979) in seven volumes, and Landolt-Bornstein (1964), where more than 2,000 binary systems are represented graphically in without any correlation or predictive theory. The most comprehensive collection of liquid-liquid equilibria in graphical as well as tabular form is that of Sorensen and Arlt (DECHEMA Chem. Data Series V/1,2,3, 1979-80). Also, more than 6,000 critical solution temperature observations are listed by Francis (1961, 1963), with more than 300 involving water as one of the solvents.

The physical explanation of the critical miscibility phenomena is based upon the interplay of molecular forces (Rowlinson, 1969; Domb and Green, 1972).

For example, the existence of UCST can be explained assuming that the A $-B$ molecular bond is weaker than the individual interaction A- A and B $-$ B, then at high

temperatures (above UCST) the entropy effects are favored, and complete miscibility results. At low temperatures the free energy of interactions is favored and phase separation occurs.

Explanations of the LCST (Domb and Green, 1972) revolve around the highly directional short-range interaction of the entities *A* and *B* as in the hydrogen bonding case. At low temperatures the decrease in free energy of solution due to specific interaction of *A* with *B* gives rise to miscibility. However, as temperature rises above the LCST the entropy effects take over favoring a more random orientation of the entities. This then destroys the directional bonds resulting in unfavorable free energy of solution and thus phase separation.

The temperature-composition diagrams discussed above were considered to be obtained at the equilibrium vapor pressure of the system, which varies both with temperature and in the one liquid phase region with composition. However, the change in externally applied pressure is very small and may be neglected in most situations (Treybal, 1963). The nature of the effect may be predicted be Le-Chatilier's principle, i.e., if the solution of the two components is accompanied by an increase in volume, it follows that an increased pressure will favor a decreased solubility (UCST will be raised, and LCST will be lowered), and vice versa.

The addition of even small amount of a third component to a two-component liquid may alter the CST considerably. Typically, when the third component is much more soluble in one of the binary mixture components, its addition raises the UCST (Hales et al., 1966). When the third component distributes in roughly equal proportions

between the two components, its addition tends to lower the UCST (Snydey and Eckert, 1973). Therefore, toluene for example, raises the UCST of water/acetonitrile mixture (Ullman, 1993), whereas acetone, as third component, lowers the UCST of methanol/cyclohexane by 3.5°C per percent of acetone dissolved (Cohn and Jacobs, 1984). In similar way, the addition of a third component that is soluble in both liquids raises the LCST, and addition of a third component that is mainly soluble in one of the binary solution mixture lowers the LCST.

Due to the addition of a third component to a two-liquid system and its distribution between the equilibrium phases, the critical composition will be altered as well. However, for a small amount of third component, the solvent mixture can be regarded as a pseudo two-component system, and the changes in the critical temperature and critical composition can be considered linear (Tveekrem and Jacobs, 1983; Cohn and Jacobs, 1984).

2.2.2 Phase-Equilibria Thermodynamics

The mutual solubility of solvents and the critical solution temperature phenomena can be examined by using the classical phase-equilibria thermodynamics and performing thermodynamic stability analysis.

Let us consider the homogeneous mixture of two species A and B, as discussed earlier, with molar fractions x_A and x_B, respectively. At constant temperature T and pressure P, the equilibrium state of this system is such that it minimizes the Gibbs energy of mixing, Δg^{eq},

$$\Delta g^{eq} = g^{eq} - (g_A x_A + g_B x_B), \tag{2.1}$$

where g^{eq} is the energy of the mixture at equilibrium, while g_A and g_B are the molar free energy of the pure species A and B, respectively at temperature T and pressure P. Δg^{eq} is the sum of an ideal part Δg^{id} and a so-called excess part of Δg^{ex}, with

$$\Delta g^{id} = RT[x_A \log x_A + x_B \log x_B], \tag{2.2}$$

where R is the gas constant, while the excess molar free energy can be expressed as,

$$\Delta g^{ex} = RT\Psi x_A x_B, \tag{2.3}$$

where Ψ is a function of T and P. Eq. (2.3), known as one-parameter Margules correlation, assumes that $A - A$ and the $B - B$ intermolecular forces are equal to each other, so that g - x_A phase diagram is symmetric. Here, Δg^{id} and Δg^{ex} are the entropic and enthalpic counterpart of the Δg^{eq}, respectively.

Using the above quasi-chemical treatment, an approximate calculation of the position of miscibility gap for simple and regular system can be made. From Eqs. (2.2) and (2.3)

$$\Delta g^{eq} = RT[x_A \log x_A + x_B \log x_B + \Psi x_A x_B] \tag{2.4}$$

Plots of eq. (2.4) at different temperature are illustrated in Figure 2.4. At temperature $T_1 > T_C$, the minima of Δg^{eq} is the lowest-free-energy-condition, and corresponds to single solution at all compositions. However, there is a tendency of the system for ordering at lower temperatures. At low temperatures, the maximum positive magnitude of the entropy term relative to the magnitude of the enthalpy term is such that the $\Delta g^{id} - x$ curve inflects in the central composition range (T_3 and T_4, Figure 2.4). As the temperature is raised and the entropy term becomes important the inflection in the free-

energy curve disappears; the temperature at which this just takes place (T_2 in Figure 2.4) is the *critical temperature* T_C.

2.2.3 Spinodal and Coexistence Curves

A mixture of solvents will split to separated phases whenever the total Gibbs energy of the heterogeneous solution is less than that of the homogeneous solution. In Figure 2.5 the Gibbs energy Δg^{eq} (or G) of binary mixture is plotted as function of the composition x at temperature $T < T_C$. The convex portion a-d-h of the curve represents an unstable region of which the stable Gibbs energy is along the straight-line *a-f-h*. For any overall mixture composition between "*a*" and "*h*" the mixture will split into two coexisting phases with equilibrium compositions of points a and h, and with an equal chemical potential (or partial molal Gibbs energy). Such a curve always has at least one local maxima and two or more minima, and is described as having convex portions. The mathematical condition for convexity and therefore the mixture instability is that

$$\frac{\partial^2 G}{\partial x^2} < 0 \qquad (2.5)$$

The inflection points at which $\partial G^2/\partial x^2 = 0$ separate the regions of instability and stability (with respect to small concentration fluctuations), and is called "spinodal" point (see Figure 2.5).

If the range of immiscibility decreases gradually, by reason of temperature change or other factors, eventually it degenerates to a point. This point of incipient immiscibility, or critical solution, is mathematically characterized as having

$$\frac{\partial^2 G}{\partial x^2} = \frac{\partial^3 G}{\partial x^3} = 0 \qquad (2.6)$$

This behavior of binary mixtures, as well as the generalization to multi-component mixtures, was described by Lupis (1983).

When the relations between, composition, temperature, and the Gibbs free energy of the mixture are known, the above considerations and be used to evaluate the CST and the equilibrium compositions of the coexisting phases. The former can be determined by using the condition of eq. (2.6) (or their equivalents for multi-component systems), whereas the equilibrium composition can conveniently be evaluated by applying the principle of equality of chemical potentials. Various types of activity coefficient correlations, such as the Van-larr, NRTL, UNIQUAC, etc. are known in the literature and can be used for this purpose.

According to classical theory, the metastable and the unstable regions are sharply separated by spinodal curve for which $\partial G^2/\partial x^2 = 0$. However, recent research suggests that there is in fact no sharp distinction between such states (Gunton et al., 1983). A smooth transition zone between the two states (a spinodal nucleation zone) has been suggested by Binder (1984) and supported by the experimental findings of Jayalakshmi et al. (1992).

The above thermodynamic analysis can serve as an analytical tool to evaluate the behavior of solvent mixtures, namely to predict the existence of a critical point, and to estimate the composition of the coexisting liquid phases. It is particularly important for preliminary screening of solvents, and when feasibility study of a new extraction process.

2.2.4 Nucleation vs. Spinodal Decomposition

Consider the liquid mixture of liquids *A* and *B* cooled off-critically from an initial composition X_1 to some temperature T_1 (Figure 2.6). In order for a nucleus of ultimate composition X_2 to form, a small group of atoms, an embryo, must acquire a higher *B* content than the surroundings, and an interface must appear. It can be shown that when such a group of atoms is both small, and has not yet raised its *B* content very much above the average, the presence of interface and the composition change are accompanied by an increase in overall free energy rather than by the decrease associated with the final formation of a large particle of composition X_2. *Only* when this embryo has grown a certain *critical size* and *critical composition* is its further growth associated with a decrease in free energy. Thus this embryonic nucleus must overcome both a *size barrier* and a *compositional barrier* before it can grow stably. This growth behavior in metastable region is known as nucleation-and-growth.

At temperature *below* the spinodal, such as T_2 in Figure 2.6, the bulk-free-energy change on forming an embryo-plus-halo region is negative for even the smallest possible difference in composition between the embryo and parent solution. Thus, below the spinodal the compositional barrier disappears, and only the size barrier restrains phase separation. As a result, transformation in solutions quenched to temperatures somewhat below the spinodal is considerably less sluggish than in those quenched to temperatures somewhat above the spinodal. The type of transformation below the spinodal curve are termed as spinodal decomposition, a particular case of first-order phase transitions.

The morphology of the transformation product changes also in the spinodal region. Above the spinodal, the large compositional difference necessary for stable growth of the new phase ensures that there will be a discrete boundary between the phases, i.e., discrete nuclei will form, even in the early stages of decomposition. This is illustrated schematically in the composition plot of Figure 2.7. Below the spinodal, on the other hand, even regions of very small compositional difference from the matrix can grow stably provided there are large enough in extent; thus, in the early decompositional stages, the boundary regions between the phases will no longer be sharp: there will simply be a gradual and periodic compositional variation throughout the parent solution with quite *diffuse boundaries* between the high and low composition regions (Figure 2.7). In the later stages of the transformation, the appearance of the spinodal decomposition will approach nucleation and growth, and the two modes will then not be readily distinguishable.

2.3 Dynamics of Phase Separation

The phase separation in solids or fluids can occur either by nucleation (both heterogeneous and homogeneous) or by spinodal decomposition (Debenedetti, 1996). The former process describes the relaxation to equilibrium of a metastable system, while the second one is typical of unstable systems. Many theories have been developed to describe the kinetics and dynamics of phase separation. Studies have been carried out on various systems, including alloys (Hono and Hirano, 1987; Hashimoto *et al.*, 1978; Hennion *et al.*, 1982), polymers (Cumming *et al.*, 1992; de Gennes, 1980; Hashimoto, 1988; Bates and Wiltzius, 1989), and fluid systems (Chou and Goldburg, 1979, 1981; Wong and

Knobler, 1978, 1981, 1981; Siggia, 1979; Mauri, Shinnar and Triantafyllou, 1996). Most of the efforts have gone into describing the growth of domain size l, after the system is brought into two-phase region, by the power-law dependence in time, $l(t) \sim t^n$.

As described in section 2.2.4, nucleation is an activated process, where a free energy barrier has to be overcome in order to form embryos of a critical size, beyond which the new phase grows spontaneously; in most practical cases, suspended impurities or imperfectly wetted surfaces provide the interface on which the growth of the new phase is initiated. Based on this physical picture, a so-called classical theory of nucleation has been developed and can be found in the literature (Zettlemoyer, 1969). More recently, kinetic theories of nucleation proposed by Katz, Ruckenstein and their coworkers (Katz and Wiederisch, 1977; Nowakowski and Ruckenstein, 1991) provide an important step for future non-equilibrium treatments.

Contrary to nucleation, spinodal decomposition occurs spontaneously, without any energy barrier to be overcome, and involves the growth of fluctuations of any amplitude that exceed a critical wavelength. The theoretical basis of this process is the Cahn-Hilliard theory (Cahn and Hilliard 1958, 1959), later extended by other authors (Langer, 1980; Gunton, Miguel and Sahni, 1983; Domb and Lebowitz, 1983), that generalizes the previous approach by Van der Waals, 1984. In principle, nucleation and spinodal decomposition are fundamentally different from each other, as metastable systems relax via the activated growth of localized fluctuations of large amplitude, whereas unstable systems do so via spontaneous growth of long-wavelength fluctuations of any amplitude. However, for deeply quenched systems, the distinction between the two regimes becomes

murky, as both the critical nucleus size and the critical fluctuation wavelength decrease. In fact, a rigorous treatment of the transition between these two basic mechanisms of phase transition does not exist, and neither of the classical theories of nucleation and spinodal decomposition seems to be able to describe the behavior of a deeply quenched system. Progress towards this goal has been made, mainly by Binder, Klein and their coworkers (Binder, 1984), but, quoting Debenedetti (Debenedetti, 1996), "the formulation of a rigorous theory ... for deeply quenched systems remains a major challenge".

Following the temperature quench *into the unstable region* the system first quickly attains the state given by spinodal curve, and then subsequently reaches to the equilibrium state on the coexistence curve. Therefore, the process of phase transition is usually divided into two time regimes: the early spinodal decomposition stage, consisting of exponential growth of long wavelength (delocalized) concentration fluctuations, and a late stage given by nucleation and growth of localized microdomains. However, understanding the spinodal decomposition phenomenon has always been a complex problem.

The basis of most of the theoretical work on spinodal decomposition is the linear Cahn-Hilliard theory (Cahn and Hilliard 1958, 1959). Following a linearization of the generalized diffusion equation, and using the Landau-Ginsburg form for the free energy Cahn-Hilliard model, leads to the prediction of an exponential growth of the microdomains during the initial stages of the spinodal decomposition. The validity of Cahn-Hilliard theory is limited for very short times following the quench (Gunton *et al.*,

1983), and for later times non-linear terms neglected in their work become important. Recently, it was shown in 1D (Mauri *et al.*, 1996) that the non-linear terms saturate the exponential growth predicted by the linear theory, so that the concentration distribution tends to a steady-state, periodic profile.

The experimental study of spinodal decomposition in fluids is also a challenging task. The interdiffusion constant D in fluids is normally several orders of magnitude larger than alloys and polymers, and so the time scale for the spinodal decomposition in fluids is very small. However, near the critical point the diffusion rate is very low and the spinodal decomposition occurs on an experimentally observable time scale. Therefore, most of the experimental studies on liquid binary mixture (Chou and Goldburg, 1979, 1981; Wong and Knobler, 1978, 1981, 1981) were done by staying close to the critical temperature ($\varepsilon = |T - T_c|/T_c < 10^{-5}$). It was shown that while the initial stage of the phase separation is still too rapid to be observed, during the nucleation process the domain growth exponent $n \approx 0.3 - 0.4$ in the early diffusive stage, and $n \approx 1$ in the late stages. Guenoum *et al.* (1987) also studied the effect of gravity in the late stages of separation experimentally, and found that gravity effect was negligible during the whole separation process.

Most of the previous studies on the phase separation of liquid mixtures have used light scattering techniques. In the classic experiments by Goldburg and coworkers (Chou and Goldburg (1979,1981) and Knobler and coworkers (Wong and Knobler 1978), the phase separation process was critically retarded by quenching the system to a temperature T only by few millikelvin below the critical value T_c, i.e. with reduced temperature $\varepsilon = |T$

- $T_c|/T_c \times 10^{-5}$. Similar slowing can be achieved by studying polymer blends (Cumming et al., 1992) with viscosities hundreds of times larger than water's and reduced temperature $\varepsilon = 10^{-2}$. The dynamics of the phase separation process has been observed directly as well with, again, either very small quenches (Beysens *et al.,* 1994), or using high viscosity systems (White and Wiltzius, 1995). Most of these experimental studies observed that, right after the temperature of the system has crossed that of the miscibility curve, the solution starts to separate by diffusion only, leading to the formation of well-defined patches, whose average concentration is near its equilibrium value (Chou and Goldburg, 1979,1981; Wong and Knobler, 1978; Guenoun *et al.*, 1990). The shape of these patches appear to depend strongly on the composition of the system: for critical mixtures, they are dendritic, interconnected domains, while for off-critical systems they appear to be spherical drops. Then, in the so called, "late" stage of coarsening, these patches grow by diffusion and coalescence, until they become large enough that buoyancy dominates surface tension effects, and the mixture separates by gravity. This occurs when the size of the domains is $l_{max} = O(\sigma/g\Delta\rho)$, where σ is the surface tension, g the gravity field, and $\Delta\rho$ the density difference between the two separating phases (Siggia, 1979). In the case of a liquid mixture, that would correspond to is $l_{max} = O(1$ mm). Now, if diffusion were the only driving force, it is well known, both experimentally (Chou and Goldburg, 1979, 1981) and theoretically (Lifshitz and Slyozov, 1961) that the typical size of a phase separating domain grows with time as $l(t) = t^{1/3}$, and therefore it would take a time of $O(1$ hr) to form such millimeter-size drops. Obviously, while similar times are needed to phase segregate polymer melts and alloys, liquid mixtures separate within seconds of the

temperature quench, and therefore diffusion and buoyancy alone cannot explain the segregation process.

The other mechanism of growth is convection-driven coalescence, which implies that drops move against each other under the influence of an attractive force. Like all convective mechanisms, this coalescence predicts a linear growth law, $l(t) = t$, which agrees with most of the experimental measurements (Chou and Goldburg, 1979,1981; Wong and Knobler, 1978; Guenoun *et al.*, 1990). However, the exact nature of the convective driving force is not well known, although it has been conjectured that it must be due to a surface tension driven bulk flow (Siggia, 1979; Huse, 1986). More recently, Tanaka and coworkers (Tanaka and Araki, 1998) showed by numerical simulation that spinodal decomposition of fluid mixtures is strongly dependent on their "fluidity", which characterizes the relative importance of convection and diffusion. In fact, for fluid mixtures, the strong coupling between concentration and velocity fields is responsible for the enhanced coarsening rate of droplets in a phase-separating system.

It is to be noted here that most of the earlier experimental work was done near the critical point, while in our work we are interested in understanding phase separation phenomenon for large temperature quenches in the unstable region.

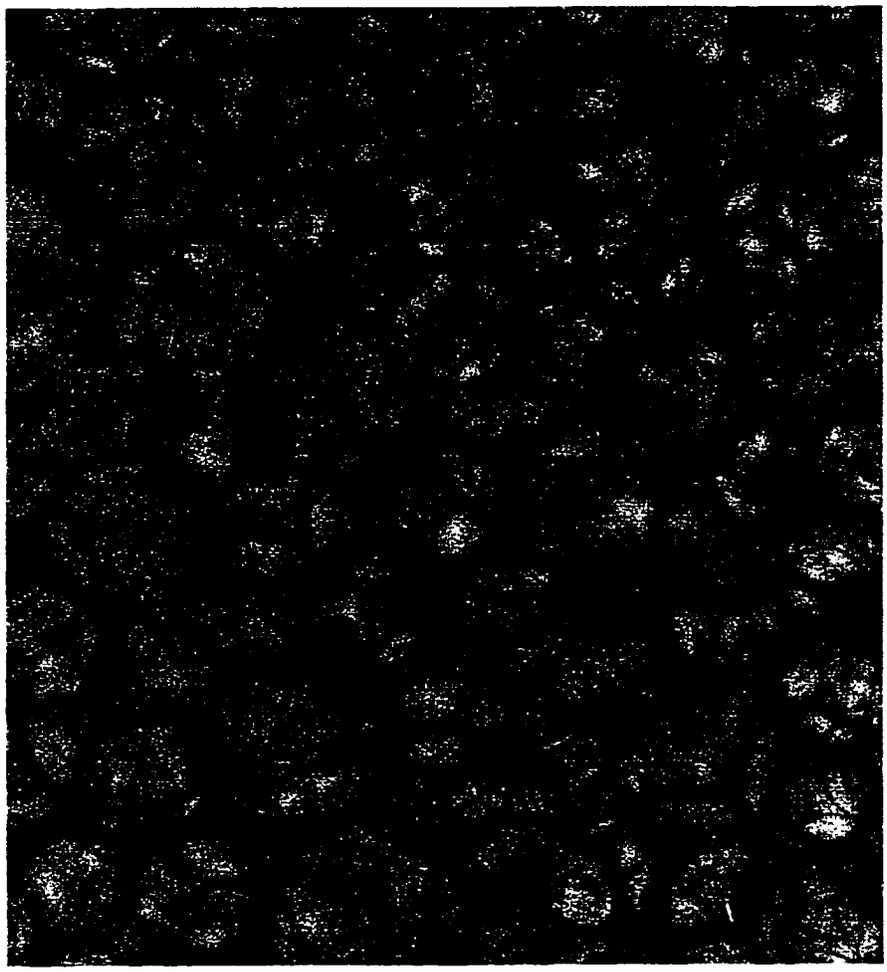

Figure 2.1: Morphology of a typical emulsion.

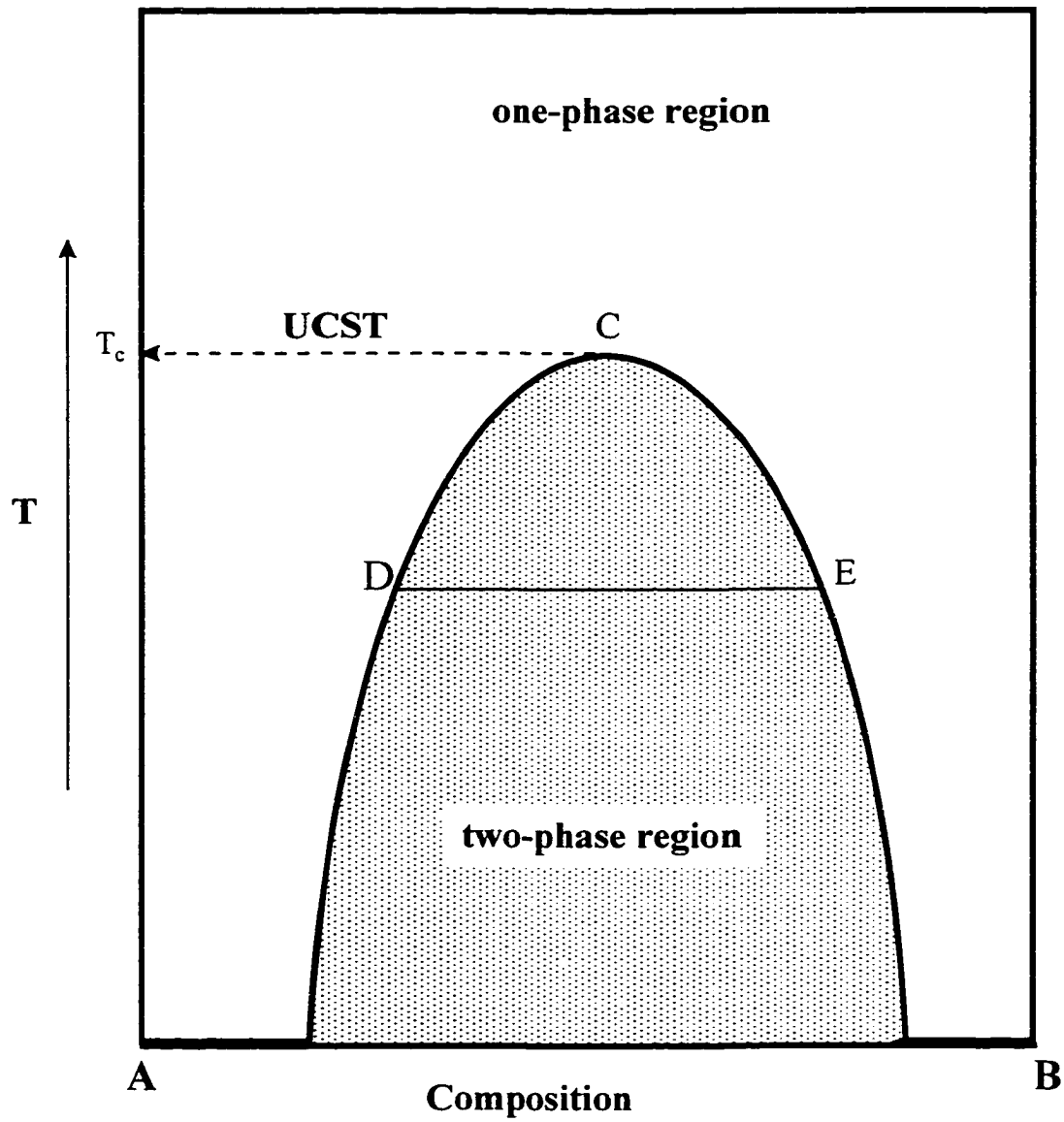

Figure 2.2: T-*x* diagram of a binary system with an upper critical solution temperature (UCST).

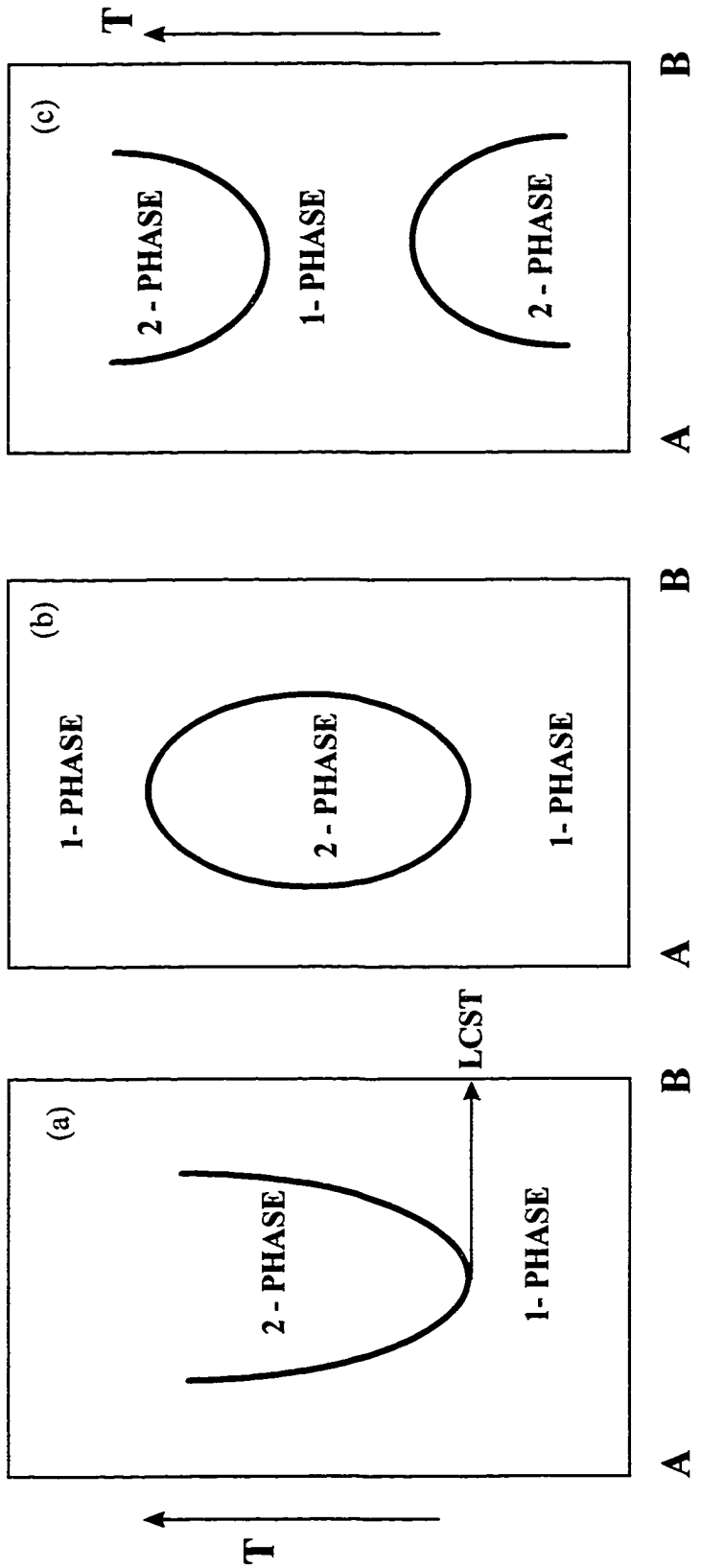

Figure 2.3: T-*x* diagram of a binary system with (a) LCST, (b) and (c) both upper and lower critical solution temperature.

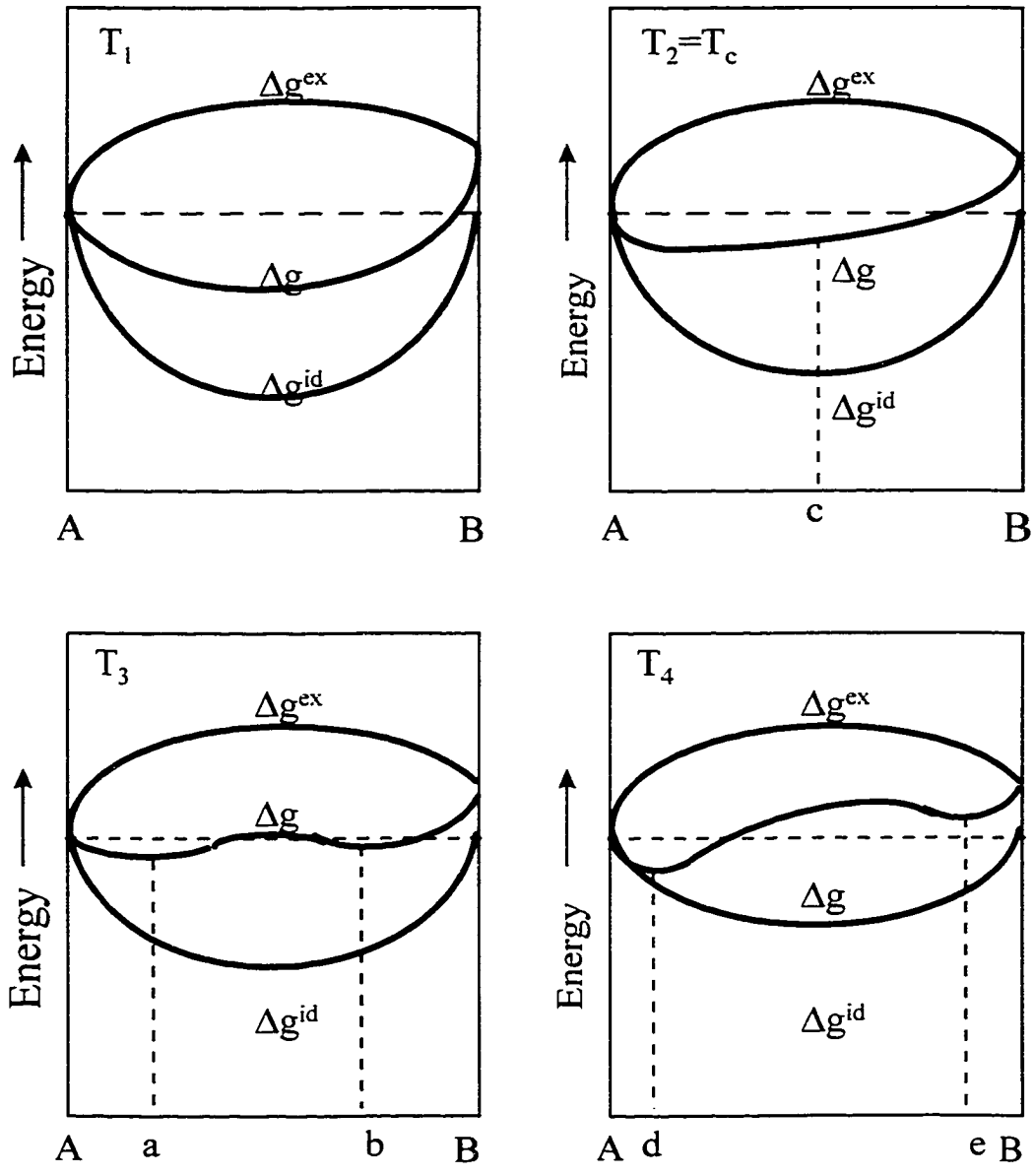

Figure 2.4: Energy-composition curves at several temperatures, $T_1 > T_2 > T_3 > T_4$.

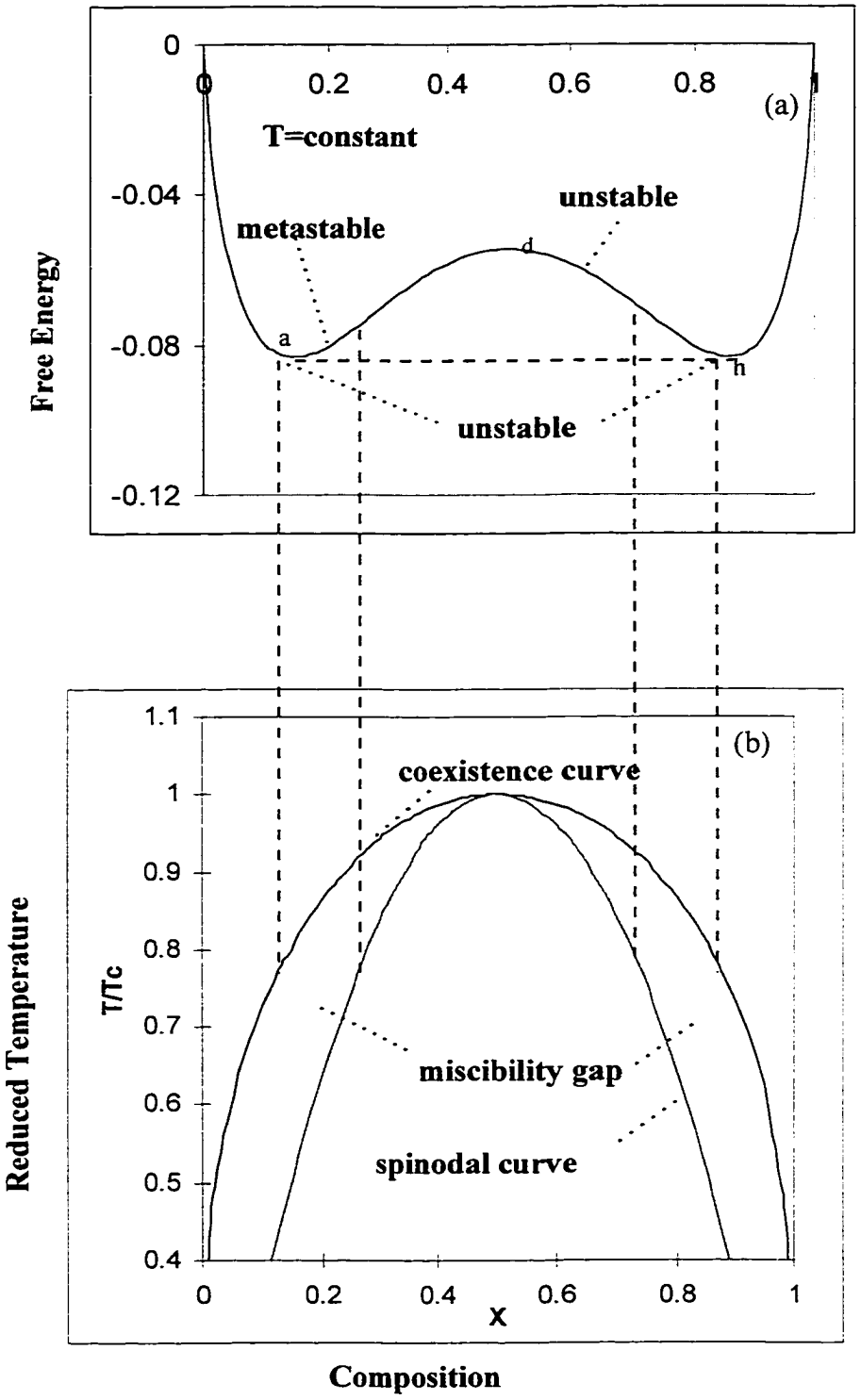

Figure 2.5: Gibbs energy of binary mixtures, (a) as a function of composition, and (b) coexistence curve and spinodal curve of binary mixture.

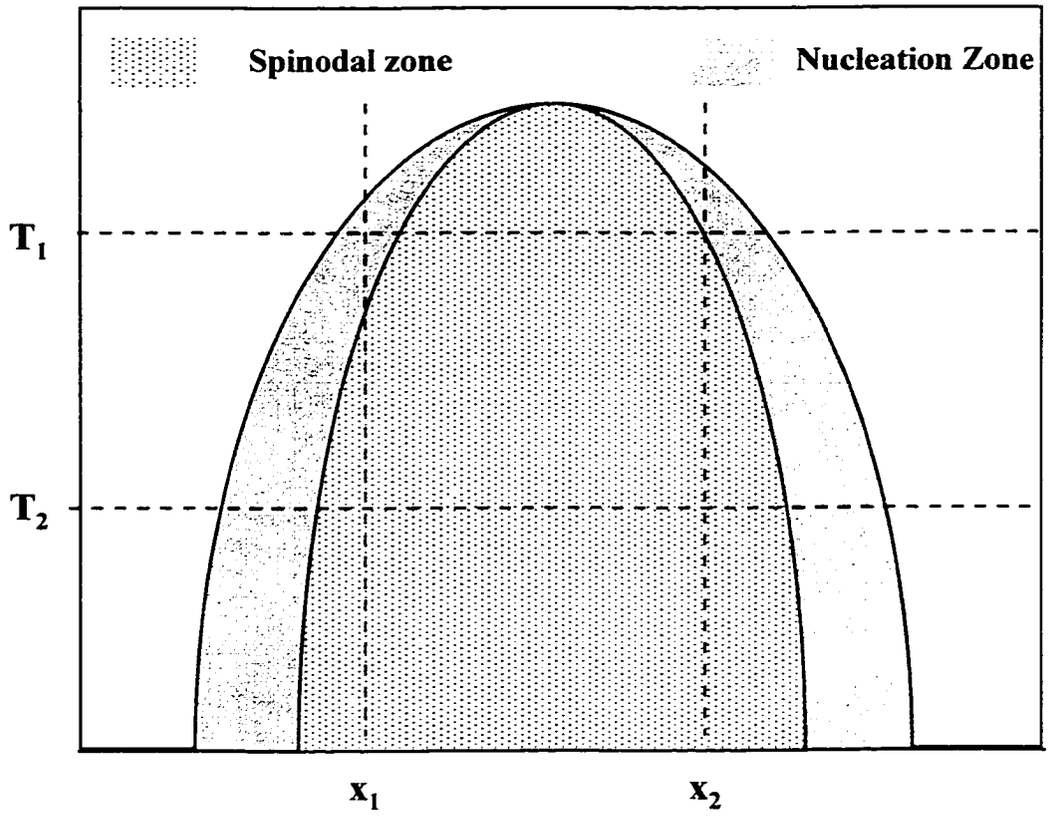

Figure 2.6: Nucleation and spinodal regions.

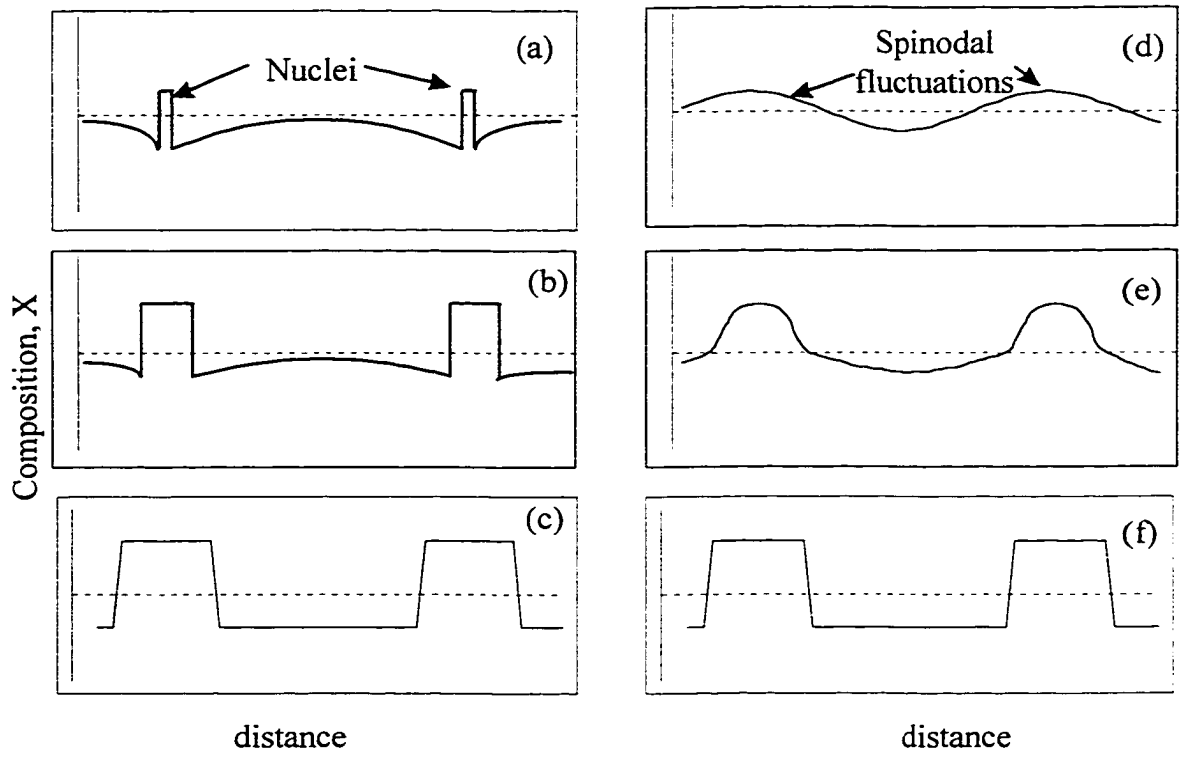

Figure 2.7: Schematic composition profiles during successive stages of phase separation by (a to c) nucleation and growth and by (d to f) spinodal decomposition.

Chapter 3

Phase Transition Extraction (PTE)

In this section we study the new separation process discovered over the past few years by our research group. In this process, named PTE (Phase Transition Extraction), the system is brought to its thermodynamically unstable region below the miscibility curve, either by crossing the miscibility curve through a temperature quench, or by changing the system composition. Two versions of this process were developed. In the first, so-called, TIPS (Temperature-Induced Phase Separation) process (Ullmann *et al.*, 1997, 1995; Ullmann, 1993), the liquid mixture, together with the solute to be separated, is first heated above its critical temperature, where it forms a uniform solution, and then cooled to the thermodynamically unstable region below the miscibility curve, where the solvents separate into two coexisting phases. In the second, so-called CIPS (Composition-Induced Phase Separation) process (Gupta, Mauri and Shinnar, 1996), we first mix the system to be extracted with a primary solvent, which is soluble with the native solvent,

and subsequently add a modifier, which is insoluble with either the native or the primary solvent. In both cases, either by cooling the system or by adding a modifier, the system undergoes a phase transition that we suppose is a spinodal decomposition. The important feature of this process is that the resulting separation of the solvents into two coexisting phases is very rapid, even in the presence of emulsion-forming impurities.

3.1 The PTE Process Using the Temperature-Induced Phase Separation (TIPS)

As mentioned above, TIPS, like all phase transition extraction (PTE) processes, capitalizes on the properties of partially miscible solvents with a critical point of solubility. In this process the liquid mixture, together with the solute to be separated, is first heated above the critical temperature, where it forms a uniform solution, and then cooled to the thermodynamically unstable region below the miscibility curve (see Figure 3.1). Ullmann *et al.* (1995) described an important application of this process to extract an antibiotic from a fermentation broth, finding, surprisingly, that the new process had higher yields than its conventional counterpart. In addition, coalescence was very rapid and phase separation was completed within few minutes, despite the fact that the broth was not filtered and that the suspended cells normally form a stable emulsion that need a centrifuge to separate. Eliyahu and Ludmer (1995) have confirmed these results using different systems, and in particular they achieved very high yields when extracting compounds from microbial cells that have not been fractured. These results are potentially of great relevance, especially in the extraction of biological compounds from

fermentation broths, mammalian cells and plants. More recently, Ullmann *et al.* (1997) described how this process can be used to design and operate a multistage countercurrent extraction column composed of successive heating and cooling units (Figure 3.2). In this new column, the process was modified by equipping each mixing section with a heater and each settling section with a cooler. In the hot (mixing) section, the temperature is kept higher than the critical temperature, so that the mixture forms an homogeneous phase. Therefore, a perfect mixing is achieved since the solute molecules can be thought of being in contact with both solvents. Now, in the cold (settling) section the mixture is cooled below the coexistence curve, leading to coalescence and phase separation.

The rapid coalescence of critical mixtures was studied in detail by Ullmann *et al.* (1995) using as model system a dye (i.e. crystal violet) dissolved in water. The dye allowed an easy visual observation of the coalescence process; in addition, since the dye acted as an emulsion stabilizer, the timescale of the hindered coalescence during conventional liquid-liquid extraction (LLE) could be varied from minutes to hours at will, by simply increasing the dye concentration from 2 to 50 *ppm*. As main solvent, Ullmann *et al.* used acetonitrile, to which they added 4% (molar) of a modifier, i.e. toluene, to raise the critical temperature of the solution from about 0°C to 40°C. The water-acetonitrile-toluene solution was put in a vial, heated to 50°C, where it became homogeneous, and then cooled back to ambient temperature, at which point the system phase-separated very quickly. On the other hand, when the system was agitated isothermally, separation occurred very slowly (up to several hours), as crystal violet had caused the formation of a

stable emulsion. Very similar results were obtained for the fermentation broth, where MIBK, instead of toluene, was used as a modifier.

Ullmann *et al.*'s results, although sufficient to clearly show the rapid coalescence phenomenon, had one limitation, namely the cooling was too slow (about one minute) to allow observations at short timescales. This is important because, when we perform TIPS, one minute after cooling the main phase separation has already been completed, and the small changes that are observed at later times are due to secondary nucleation. Therefore, we repeated Ullmann *et al.*'s separation experiments using a much thinner (i.e. 1.2 mm thick) glass cell, where cooling could be completed within two seconds. A mixture of 52 *cc* acetonitrile, 38 *cc* water and 10 *cc* MIBK was used, with a small quantity, 2 *ppm*, of crystal violet dye to facilitate visualization and retard coalescence. Finally, the phase separation resulting after isothermally shaking the system (i.e. performing LLE) was compared with that after heating and cooling (i.e. performing TIPS). As one can see from Figure 3.3, there is an inherent difference between the two processes. In LLE we see two, more or less defined, interfaces, which move towards the center of the cell until they merge. This behavior was observed also when the composition of the system was varied, and the time required to complete the process increased from 5 - 10 seconds, in the absence of dye, to two hours, with 20 *ppm* dye. On the other hand, during TIPS the interface appears almost immediately at its final position, and the solution clears up rapidly, with no emulsion formation, even in the presence of larger quantities of dye. This fast phase separation in the presence of emulsion-forming compounds is a special property of PTE.

These observations are clearly at odds with the explanation of the phenomenon that was put forward by Ullmann *et al.* (1995), who assumed (as most people do) that at the beginning of the process very small nuclei are formed, which subsequently grow by both diffusion and coalescence. The fact that coalescence is evidently not slowed down by the presence of emulsion-forming compounds was explained by the conjecture that there are no stable interfaces to which such compounds can adhere. However, as it was discussed in Section 2.4 that, following a temperature quenching, a process, generally referred to as spinodal decomposition, takes place which can lead to phase separation without nucleation. In fact, the process begins with the appearance of a uniformly dispersed phase that subsequently develops into distinct regions of coexisting equilibrium phases. To further investigate the initial stage of phase separation, the quenching experiment described above was repeated in a 40 inch long cylindrical tube, with a 4 *mm* inner diameter. After few seconds, large, centimeter-size drops were formed, as shown in Figure 3.4, indicating that during spinodal decomposition large drops can form very rapidly, without nucleation. This is the reason why separation during the PTE process is so fast, irrespective of the presence of emulsion-forming compounds.

3.2 The PTE Process using the Composition-Induced Phase Separation (CIPS)

CIPS was discovered as the natural extension of the Phase Transition Extraction (PTE) process. It takes place in a single vessel, and is divided into two stages. In the first, the system to be extracted is mixed isothermally with a primary solvent, which is soluble

with the native solvent. In the second stage, a modifier is added, which causes phase separation by reducing the solubility of the primary with the native solvent (Figure 3.5). When using the TIPS process, it was realized that very few solvents, when mixed with the native solvent, form a solvent mixture with a critical temperature that is suitable for simple laboratory experiments. This problem is even more acute when TIPS is used for extraction of biological compounds, as in these cases strong constraints about the temperature range apply. In Ullmann *et al.* (1995) this problem was overcome by using solvent mixtures with a low critical temperature, and then adding a modifier to change the miscibility curve. It was shown that the critical temperature of the water-acetonitrile mixture can be raised from 0°C to 120°C by adding 5% (molar) of toluene. In the same way, the critical temperature of any solvent mixture can be changed almost at will (obviously within the limitations of the boiling and freezing points) by adding a suitable modifier (Figure 3.6).

This simple observation suggested us a new way to perform spinodal decomposition. Let us suppose, for example, that our system has a 1.3% molar concentration of toluene, and is quenched from an initial 50°C temperature, where it forms a single phase, to 25°C, where it separates (as in Figure 3.6). Now, the same separation can be achieved isothermally, at 25°C, by raising the toluene molar concentration from 0%, where the system forms a single phase, to 1.3%, where it separates. In other words, the key of success of the PTE process is to bring the system to a point of thermodynamic instability under the miscibility curve. As shown in Figure 3.5, this can be achieved by changing its composition, as in the new process that we propose

here. In this, so-called CIPS (Composition-Induced Phase Separation) process (Shinnar and Mauri (1995)), the system to be extracted is first mixed with a primary solvent, which is soluble with the native solvent, and subsequently a modifier is added, which is insoluble with either the native or the primary solvent.

The "equivalence" between TIPS and CIPS is substantiated in the series of pictures of Figure 3.7, where we used the same water-acetonitrile-MIBK mixture as in Figure 3.3, only in the presence of a larger amount, 20 *ppm*, of the crystal violet dye. We see that, while after isothermal mixing a stable emulsion was obtained, with small, approximately 10 μm drops that remained suspended for about 2 hours, and when we used CIPS, within 30 seconds the mixture had completely separated. As in the case of temperature-induced phase separation, during CIPS we do not observe any moving interfaces, but instead a very fast phase separation takes place, which is almost unaffected by the presence of emulsion-forming compounds, with subsequent cleaning of the cloudy regions around the interface.

To have a completely satisfactory theory that can generalize our results to all cases is out of the scope of this study. So, we do not claim that adding any modifier to an otherwise single-phase binary mixture will always result in spinodal decomposition and fast coalescence, just as we cannot claim that cooling a mixture below its miscibility curve will always result in fast phase separation, independent of the rate of cooling and of the composition of the mixture. However, we have considered a significant number of cases, using different solvents and modifiers, under conditions in which isothermal intense mixing would form stable emulsions, and in all these cases our composition

induced phase separation process worked. In fact, separation was fast even when inorganic salts, instead of liquid solvents, were used as modifiers, and results identical to those of Figure 3.7 were obtained adding to a 50 *cc* water - 50 *cc* acetonitrile mixture, 5 *g* of sodium chloride. Clearly, this is not surprising, as salts too modify the critical temperature of liquid mixtures.

It is important to note that the addition of the modifier must result in a mixture composition, which is in the unstable, not the metastable, region below the miscibility curve. However, knowing exactly the miscibility curve is not essential to perform the CIPS process, while it is so for TIPS. For example, if we add 9% molar toluene to a water-acetonitrile mixture, the critical temperature would raise to 160°C (see Figure 3.6), so that TIPS could be performed only by pressurizing the system. On the other hand, CIPS could be performed easily, even without knowing how high the critical temperature is.

One difference between CIPS and TIPS is that TIPS can be performed, at least in principle, by heating and cooling the binary mixture composed of the native and primary solvents alone, i.e. without modifiers, provided that the critical temperature of the system is acceptable. A modifier is used in TIPS only to bring the critical temperature up or down to a convenient value, and is not essential to the process, while, on the other hand, adding a modifier is essential to CIPS. However, in practice it is very unlikely that one could find a primary solvent that, together with the native solvents, forms a mixture with the right critical temperature; in fact, modifiers were used in most of the experiments performed by Ullmann (1993) and Ullmann *et al.* (1995). On the other hand, adding a

modifier as in CIPS leaves us free to choose the operating temperature according to the process needs (such as low temperatures for sensitive materials). More importantly, in CIPS we are free to add the amount of modifier that is necessary to maximize the extraction efficiency of the process. In fact, increasing the relative amount of modifier generally means improving the separation between the two phases and therefore it increases the partition coefficient of the solute between the two phases. Instead, in TIPS the amount of modifier is limited by the fact that the critical temperature of the mixture increases as more modifier is added. Therefore, the partition coefficient here can be improved only at the cost of increasing the temperature excursion of the heating/cooling process, which is not only expensive (as in some cases pressurization would be required), but often it is not even feasible. For example, in most biological extractions the samples cannot be heated above 60°C. So, in conclusion, CIPS is equivalent to a TIPS process with a large temperature differential and rapid cooling. Its advantage is that it achieves the same results (i.e. high yield and no emulsion formation) and yet it is performed isothermally.

Finally, it should be stressed that for modifiers which are themselves good solvents, the operating conditions can be predicted using the large amount of available data. For example, one can use the triangular diagrams given in Sorensen and Arlt (1980), or generate them using thermodynamic data to predict the compositions of the phases after separation, and also check whether the operating point is in the unstable region, therefore insuring that the separation process is a spinodal decomposition.

3.3 PTE vs. Emulsification

In the previous two Sections we saw that the phase separation of a liquid binary mixture can take place with two very different modalities, according to whether the system is mixed isothermally, or it is heated and then rapidly cooled. In the first case, phase separation involves the formation of an emulsion, that is a suspension of closely packed, micron-size drops, while in the second case a single interface (or a collection of large drops) appears, well before the formation of small drops. At this point, we investigated whether the fast temperature-induced phase separation is a process that is experienced 'in the real world', or it is a special prerogative of a restricted number of processes and solvent systems. To do that, first we considered many solvent systems, composed of two partially miscible solvents plus, when needed, a modifier (which is soluble with one solvent and insoluble with the other), and saw that their behavior was virtually identical to that of our original water-acetonitrile-toluene system. Examples of such systems are water-acetone-MIBK, hexane-methanol and water-ethanol-ethyl acetate. We even studied the system composed of 34% water, 33% acetonitrile, 33% triethylamine in volume concentration, characterized by a lower, 22°C critical temperature, and saw that after heating the system rapidly from 18°C to 30°C, phase separation was, again, rapid and emulsion-free. The only case where temperature-induced phase separation was slow and involved the formation of stable emulsions was when the liquid solvents were very viscous.

In conclusion, emulsification of liquid mixtures in the presence of emulsifiers is clearly very important when the system is mixed isothermally, while it is marginal during PTE process. In the first case, we observed that drops were closely packed in the

emulsion region, and would not move, if not for the coalescence occurring at the interface. Therefore, since hardly any coalescence took place within the emulsion region, it took a long time for the emulsion to settle. On the other hand, during the phase separation induced by rapid quenching or composition change, although in some cases we did observe the formation of a so-called secondary emulsion, that happened only after most of the separation had been completed. In addition, as the drops in the secondary emulsion amounted to only few percents in volume, they were free to move, so that the emulsion could rapidly settle.

In the next section, we further investigate the PTE process. We study the process experimentally by directly observing the phase transition process. Since we believe that both TIPS and CIPS undergo through the same separation mechanism, we study only the TIPS process in detail. The choice to study TIPS over CIPS was based on: (a) more controlled experiments are possible in case of the TIPS, and (b) most of the literature is based on the temperature quench rather than on the composition change.

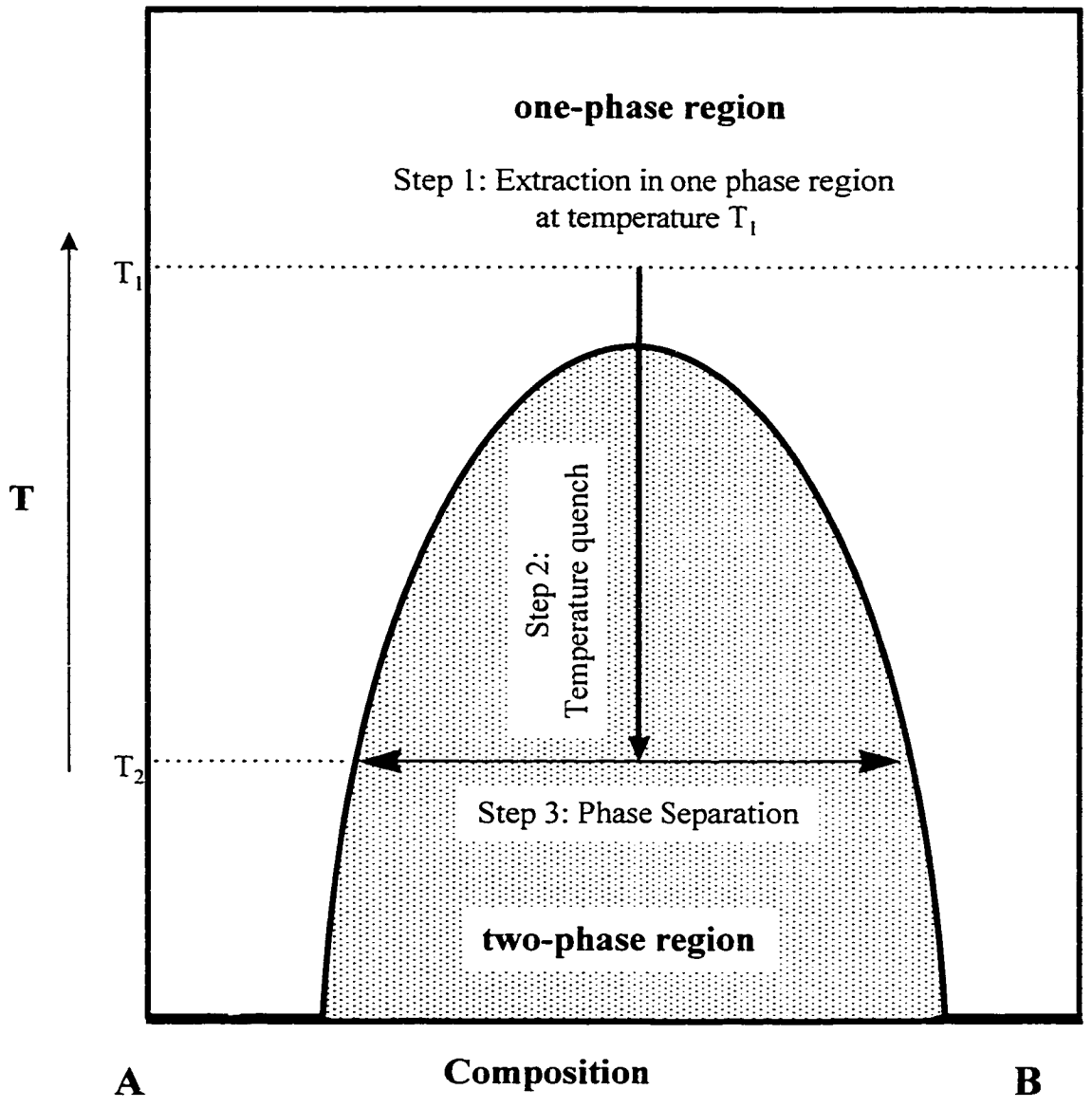

Figure 3.1: PTE process using Temperature-Induced Phase Separation.

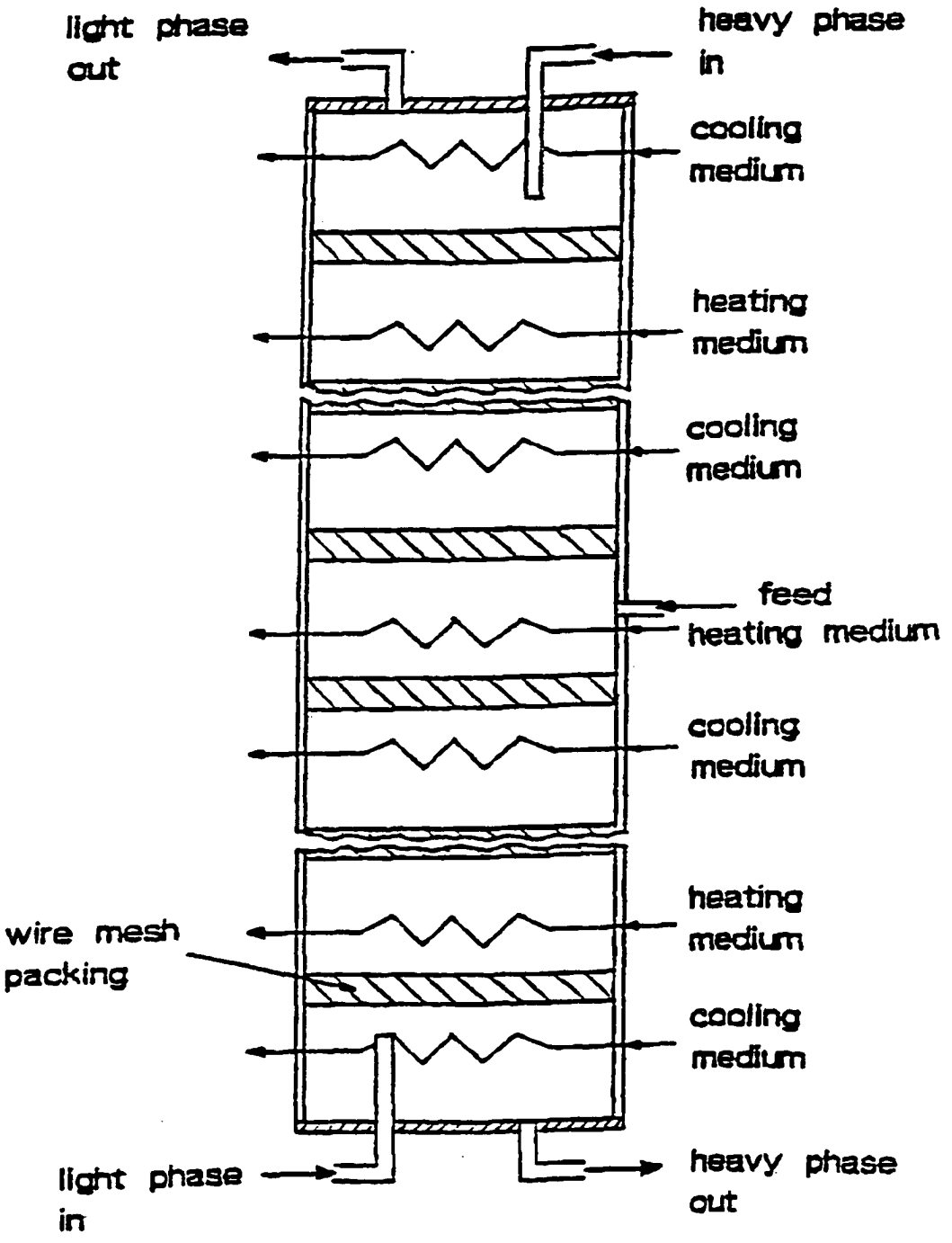

Figure 3.2: Schematic of the PTE Column (Ullman, Ludmer and Shinnar, 1997).

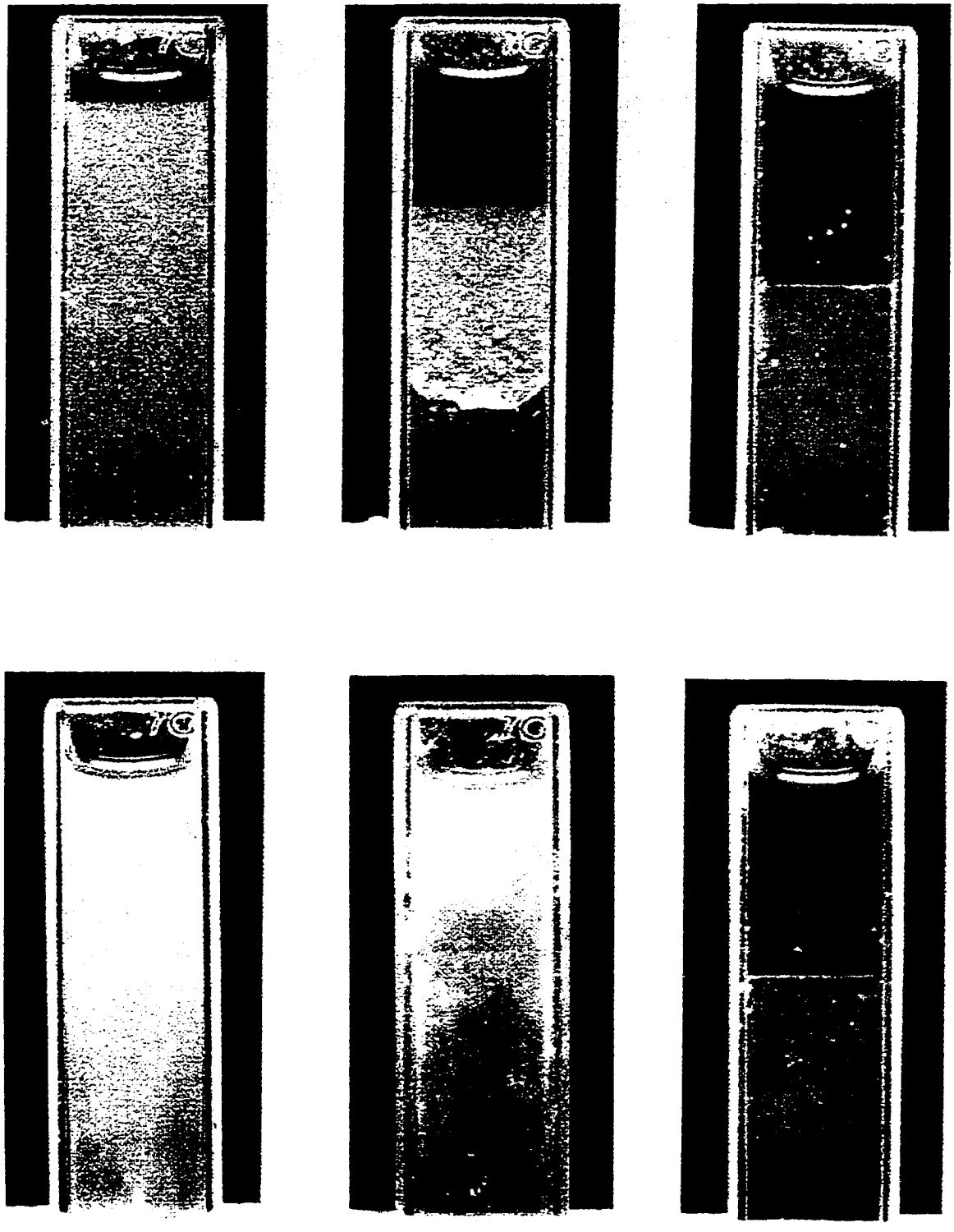

Figure 3.3: Phase separation of a water-ACN-MIBK mixture using LLE (top) and TIPS (bottom) in the presence of 2 *ppm* of crystal violet dye.

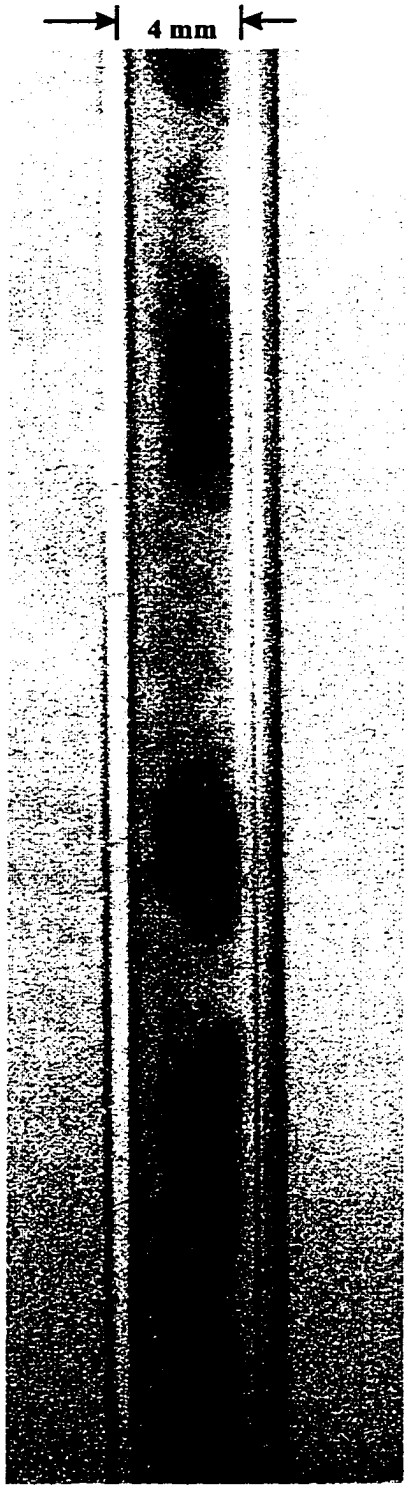

Figure 3.4: Phase separation of a water-ACN-MIBK mixture in a long tube.

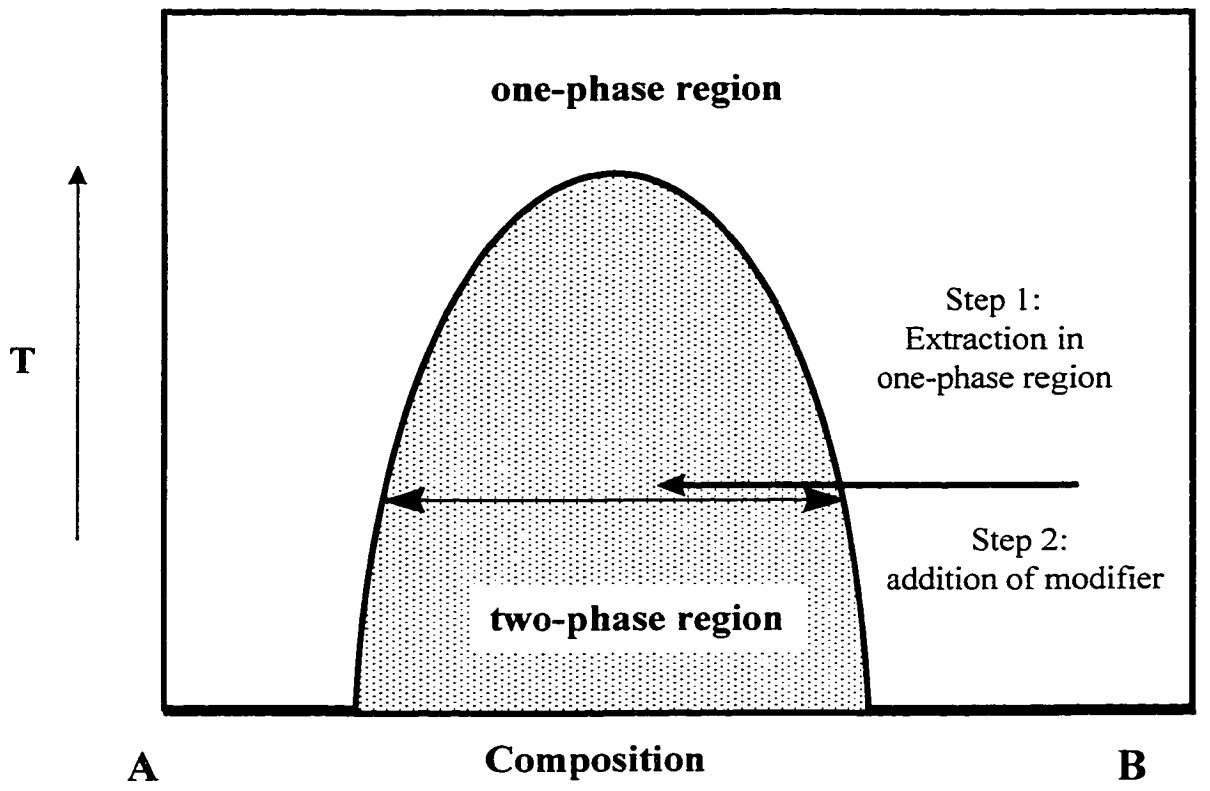

Figure 3.5: PTE process using Composition-Induced Phase Separation.

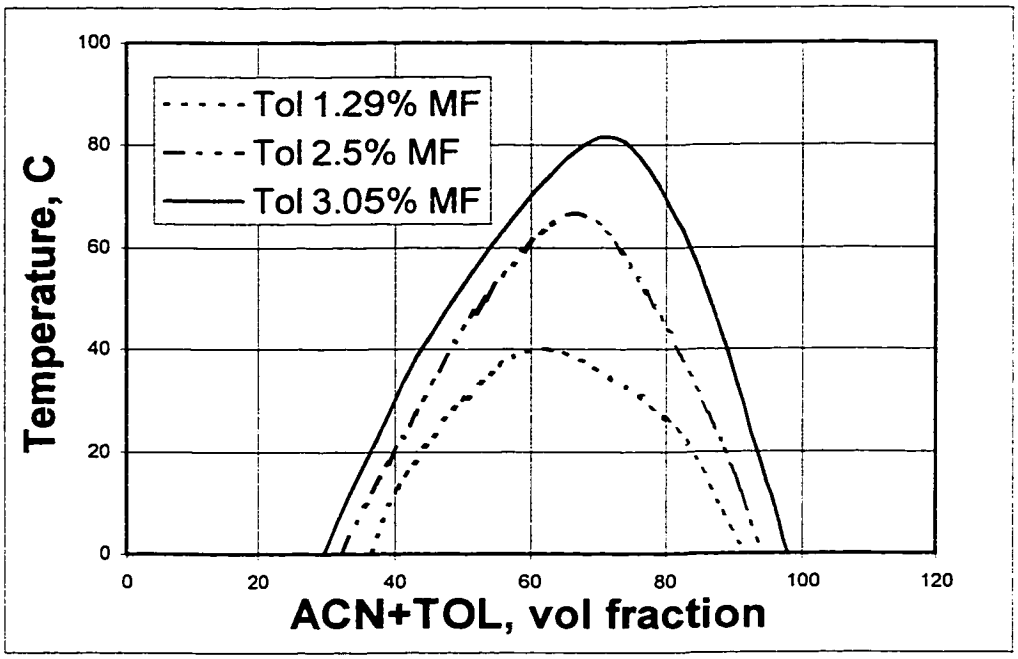

Figure 3.6: Phase diagram of the water-ACN-toluene system with three different toluene concentrations.

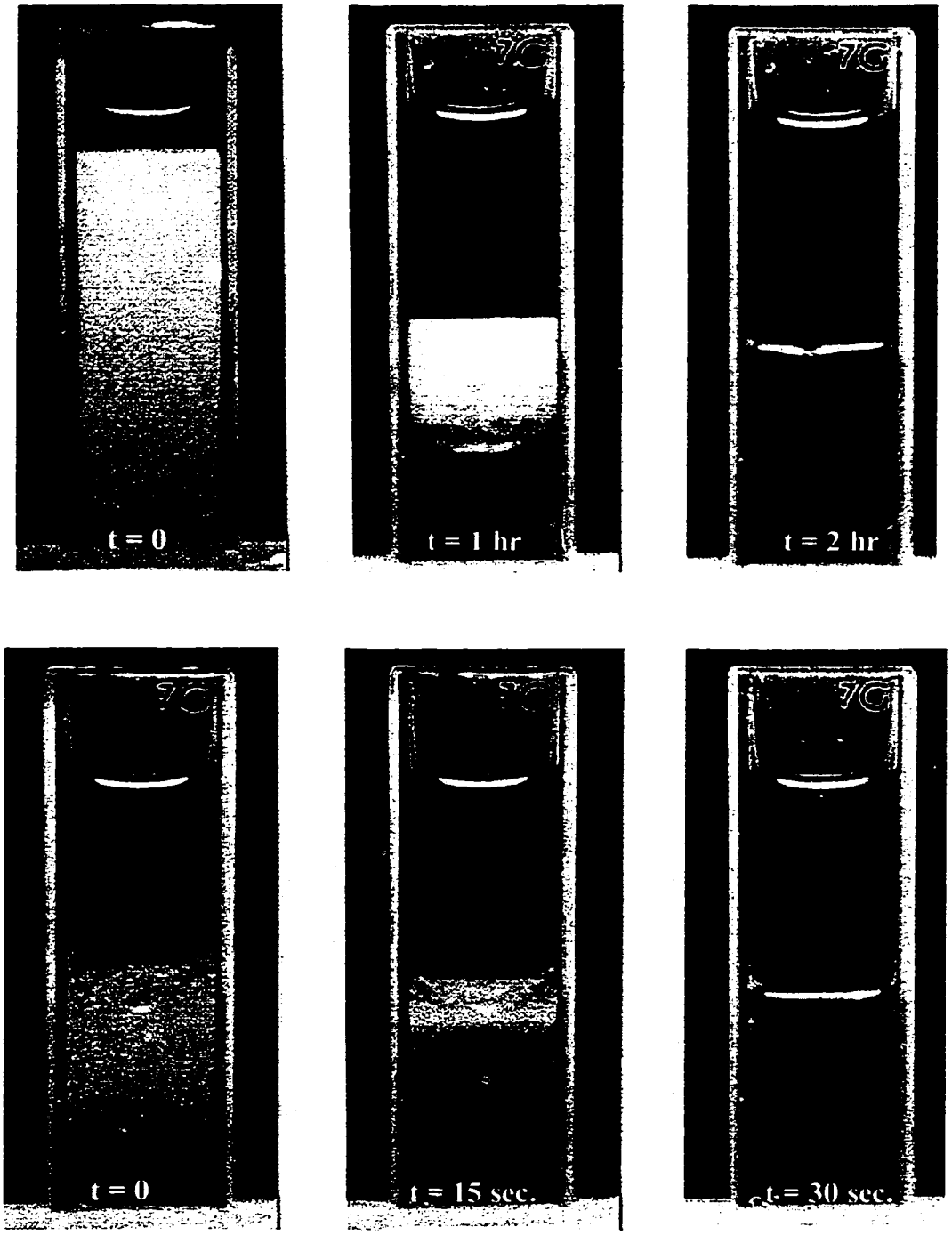

Figure 3.7: Phase separation of a water-ACN-MIBK mixture using LLE and CIPS in the presence of 20 *ppm* of crystal violet dye.

Chapter 4

Phase Separation of Deeply Quenched Liquid Mixtures

In this section, we present a visualization of the morphology of liquid mixtures during phase separation, following a deep temperature quench into the unstable region of mutual miscibility. Here, we intend to study the phase separation of both critical and off-critical fluid mixtures by direct visual observations. Unlike previous studies, we will consider deep quenches, with $\varepsilon = |T - T_c|/T_c \sim 0.1$. In addition, we want to determine the behavior of- initially demixed systems, whose initial (i.e. before the temperature quench) composition is non-uniform. Finally, we will present a dimensional analysis based on the "model *H*" (Hohenberg and Halperin), and try to explain theoretically how the system

behavior, like the growth rate of single-phase microdomains, depends on its fluidity and initial conditions.

4.1 The experimental setup

An experimental setup (Figure 4.1) was designed and built to allow the observation of the phase separation process in the size range of 10 *μm* to 7 *mm*. It consisted of a temperature-regulated, 1 *mm*-thick, 40 *mm*-high sample cell, an optical microscope (Nikon Optiphot-2), and a video camera (Sony XC-711) or still camera (Nikon F-5 with Data Back MF-28) mounted on the microscope. Alternately, instead of the microscope, we used bellows to get a field of view of 2.5 *mm* to 4 *cm*. The Nikon F-5 camera was chosen for its high-speed film advance (up to 8 frames per second). The temperature was regulated by placing the sample cell into an 8 *mm*-thick water jacket, into which temperature-controlled water was circulated. Initially the solution, having an upper critical temperature (UCT), was kept at a temperature above the critical point of miscibility, where at equilibrium the system is one-phase and homogeneous. Then, the solution was quenched below the critical point of miscibility by quickly changing the temperature of the water circulating within the jacket.

This experimental setup allowed us to obtain an initial quenching rate of ~ 3°C/*s*. Temperatures were measured by inserting 350 *μm* thermocouples, with 0.04 *s* response time, at various locations inside the cell, and connecting them with a data acquisition system. All the pictures, obtained both through the microscope and the bellows, were taken with a fast shutter speed of 1/100 *s* or more, and professional Kodak Gold 100 film

was chosen for all the exposures. A video camera was used to capture up to 20 frames per second, using a Matrox Meteor frame grabber. Matrox Inspector software was used to grab images, make movie files, enhance the image quality, and for image analysis.

In our experiments we used a liquid mixture composed of water, acetonitrile and toluene, whose thermodynamic properties were determined in previous works (Ullmann *et al.*, 1995; Gupta *et al.*, 1996). Two types of solutions were considered, with molar compositions of toluene equal to 1.25% and 2.5%, and critical temperatures of 35°C and 67°C, respectively (see their phase diagrams in Figure 4.2). The first mixture has a critical volumetric composition of 38% water, 58% acetonitrile, 4% toluene, and it undergoes phase transition at 35°C, while the second solution is off-critical, with volumetric composition of 54% water, 41% acetonitrile, 5% toluene, undergoing phase transition at the same, 35°C temperature as the critical mixture. In addition, up to 150 *ppm* of Oil Red O dye was added to the system to enhance the visualization of the process. This non-surface-active dye dissolves preferentially in the upper, solvent-rich phase, with a partition coefficient of about 20, and does not change the characteristics of the phase separation process. All the solvents were HPLC grade, while the water was double distilled. The analysis of the phase composition was conducted using an HP 5890 Gas Chromatograph.

In all our experiments, we started with the mixture in its phase-separated state at a constant temperature of 15°C (see Figure 4.2). Then, two experimental procedures were considered. In the first (to be referred to as the homogeneous case), the solution was first heated from 15°C to 38°C, then mixed thoroughly, and finally it was quenched back to 15

°C. In the second case (to be referred to as the gradient case) after being heated, the solution was kept at 38°C for two hours without mixing, and only then it was quenched. In both cases, the quench rate was about 3°C/*s* (see Figure 4.3). Mixing the solution before the quench is extremely important, because when an initially phase-segregated mixture is heated above its miscibility curve, the spontaneous mixing process is governed by diffusion alone, as the solution is gravity stabilized. In fact, in the gradient case we saw that, after we kept our system at 38°C for two hours, the mixture was still mostly demixed, with the exception of a thin, few millimeters thick layer around the phase interface, where a concentration gradient was present. The thickness of the mixing layer could be easily estimated observing that the color of the mixture in the interface region was gradually changing from the bright red of the upper, solvent-rich phase, to the plain white of the lower, water-rich phase. This thickness was in agreement with an estimate based on the value of the solvent diffusivities. These, in turn, were measured experimentally (please see Appendix I), using both GC techniques and laser absorption, obtaining a value of 3×10^{-5} cm^2/s, which was in good agreement with the theoretical prediction based on the Wilke-Chang equation.

4.2 The experimental results

4.2.1 Homogenous Case

The results of our visualization in the homogeneous case are shown in Figures 4.4, 4.5 and 4.7, with the time $t = 0$ corresponding to the moment when the temperature

of the mixture crosses the miscibility curve. All pictures were taken using either a digital camera or a 35-mm camera, as explained earlier.

In Figures 4.4 and 4.5 the phase separation of a critical liquid mixture is shown, using a field of view of 300 μm and 2.5 mm, respectively. We see at first the appearance of ~ 10 μm microdomains (smaller objects cannot be observed, due to limitations in the optical resolution of our apparatus), which subsequently grow into regions of interconnected domains. Clearly, after reaching millimeter size, domains start to experience gravitational effects and the system rapidly separates into two gravity-stabilized regions. Similar interconnected domains were also observed, among others, by Guenoum and coworkers (Guenoun *et al.*, 1987) and Cumming and coworkers (Cumming *et al.*, 1992), although only for very small temperature quenches and in the late stage of phase separation. The growth rate of these fast coarsening structures can be determined defining the equivalent radius of the domains as a function of time,

$$R(t) = \frac{\int \phi(k,t) d^3k / |k|}{\int \phi(k,t) d^3k}, \tag{4.1}$$

where $\phi(k,t)$ is the Fourier transform of the composition $\phi(x,t)$ of the mixture at location x and time t. Experimentally, we verified that in the range of concentrations considered in our experiments, the dye concentration was proportional to the solvent volume fraction, so that $\phi(x,t)$ is proportional to the degree of greyness of the pixel located at x, and $R(t)$ can be evaluated using Eq. (4.1). As we see in Figure 4.6, the drop size grew linearly throughout the phase separation process from 10 to 400 μm, indicating that phase segregation is governed by convective forces. The growth rate was 76 $\mu m/s$ as

long as the phase domains were separate from each other; as soon as they became interconnected, i.e. for times $t \geq 0.5$ *s*, the growth rate increased to 200 *μm/s*. Although it was well known experimentally (Chou and Goldburg, 1979,1981; Wong and Knobler, 1978; Guenoun *et al.*, 1990) that the size of the microdomains grows linearly in time, this is the first time that this linear growth is measured for large temperature quenches $\varepsilon \sim 0.1$, and, in fact, our measured growth rate is one or two order of magnitude larger that obtained with small temperature quenches. In addition, it is the first time that the change in the morphology of the system, from well-separated droplets to interconnected domains, is linked to an increase of the their growth rate (almost three-fold, in our case). This result clearly indicates that, as stated by Guenoum and coworkers (Beysens *et al.*, 1994), the mechanism of coalescence cannot be separated from the morphology of the drop pattern.

For off-critical mixtures, we basically obtained similar results as those for critical mixtures, as one can see from Figure 4.7. The basic difference is that, as one would expect, in this case we observed the formation of isolated drops of the minority phase (in our case, the solvent-rich phase), instead of the interconnected domains that were observed in the critical case. However, once formed, these drops grew linearly, as shown in Figure 4.8, with a growth rate of 68 *μm/s*, which is comparable with that of the critical case, before phase domains became interconnected. This result was somewhat unexpected, as during the temperature quench the mixture had to cross the metastable region of the phase diagram, where drops are expected to grow at a much slower pace.

Our measurements showed that within one second, phase domains of deeply quenched liquid mixtures (both critical and off-critical) reach 100 *μm* size. Now, after 1

second, the temperature of our system was about 32°C (see Figure 4.3), and it took another 6 seconds to reach the 15°C steady state temperature. However, during these last 6 seconds the morphology of the system did not change appreciably, indicating that most of the relaxation towards equilibrium occurs during the initial temperature quench, when the temperature of the system crosses the miscibility curve, as it was conjectured by Chou and Goldburg (Chou and Goldburg, 1981). In addition, since the equilibrium composition of the system kept changing as the temperature of the mixture decreased, phase separation continued to occur even within the domains which had already formed, although to a lesser extent because of the smaller quench depth and concentration gradients available. This is evident in the last two pictures of Figure 4.5, where we see small drops inside larger domains. A similar effect, called "double phase separation", was obtained by Tanaka (Tanaka, 1995), applying a slow quench (i.e. 3°C/*s*, like in our experiments) to a polymer solution.

Examining the pictures (and the computer movies that we grabbed) of the process of phase separation, we concluded that small, 10-100 μm drops move fast. In fact, in the typical case shown in Figure 4.9, monitoring the movement of single-phase domains we show that a 50 μm drop can move at a speed exceeding 100 $\mu m/s$, which is of the same magnitude as the growth rate of the microdomains. In addition, the motion of the single-phase domains appears to have random orientations and does not depend strongly on the drop dimensions. The source of this rapid movement cannot be gravity nor molecular diffusion, as these mechanisms would predict drop velocities a few orders of magnitude smaller than the those observed experimentally. The effect of gravity is further weakened

by the fact that when the temperature is near its critical value, the density difference between the two phases is very small. As we indicate in the next section, the driving force which is responsible for the rapid movement of the drops and, ultimately, for the rapid phase separation, is the concentration-gradient-induced body force predicted by the model *H* (Hohenberg and Halperin, 1977).

4.2.2 Gradient Case

Remarkable and unexpected results were obtained in the gradient case, where the liquid mixture was initially demixed, with the exception of a millimeter-thick region in which the composition varied gradually from that of the lower, water-rich phase to that of the upper, solvent-rich one. Focusing the experimental apparatus on that region, we saw that, after the quench, the system remained unchanged for about 3 seconds, until suddenly (see Figure 4.10), a sharp interface appeared. Only then, we saw drops appearing and moving towards the interface, where they coalesced. So, unlike what we observed in the homogeneous case, in the gradient case we did not see drops forming at an early stage and then growing by coalescence, although we cannot rule out the possibility that small drops do form, as our apparatus can only detect drops larger than 10 μm. A possible explanation of this experimental result is given in the next Section, but we can already state that this phenomenon is too rapid to be due to diffusion alone, and must instead be driven by convection.

Analyzing the regions above and below the interface (see Figure 4.11) a long time (20 seconds) after quenching, we observed that few scattered drops were suspended within the mixture, forming what in the engineering literature is called secondary

emulsion. As these drops were almost at equilibrium with the surrounding mixture, their motion towards the interface was gravity-driven, and therefore had a much longer timescale (i.e. minutes) than that of the interface formation (i.e. seconds). Following the motion of a large number of drops, we saw that, prior to them reaching the interface, they all moved with roughly the same speed, hardly ever coalescing, and only growing by diffusion. As shown in Figure 4.12, their mean radius R was found to grow in time as t_γ, where $\gamma = 0.30 \pm 0.04$, in agreement with the value $\gamma = 1/3$ predicted by Lifshitz and Slyozov (Lifshitz and Slyozov, 1961). As the LS theory neglects coalescence and hydrodynamic interactions between droplets, it is comforting that our experimental results agree with it, since those effects were negligible in our experiments.

4.3 Discussion

The motion of an incompressible binary fluid mixture composed of two species A and B is described through the so-called model H (Hohenberg and Halperin, 1977). Here, A and B are assumed to have equal viscosities, densities, and molecular weights, with the composition of the system uniquely determined through the molar fraction ϕ of, say, species A.

If the flow is assumed to be slow enough to neglect the dynamic terms in the Navier-Stokes

$$\frac{\partial \phi}{\partial t} + v.\nabla\phi = -\frac{1}{\rho}\nabla.J, \tag{4.2}$$

$$\eta\nabla^2 v - \nabla p = F_\phi, \tag{4.3}$$

$$\nabla . v = 0, \tag{4.4}$$

where $\boldsymbol{v}$ is the average local fluid velocity, $\boldsymbol{J}$ is the diffusion flux (Landau and Lifshitz, 1978) and F_ϕ is a body force. As shown in previous works (Mauri *et al.*, 1996), $\boldsymbol{J}$ is determined through the relation,

$$J = -\rho\phi(1-\phi)D\nabla\tilde{\mu}, \tag{4.5}$$

where ρ is the density of the system, D the molecular diffusivity, and $\tilde{\mu} = \mu_A - \mu_B$ (see appendix II) is the generalized chemical potential defined as (Landau and Lifshitz, 1978),

$$\tilde{\mu} = \frac{\delta(g/RT)}{\delta\phi}, \tag{4.6}$$

with g denoting the molar Gibbs free energy, defined as (Cahn and Hilliard, 1961),

$$\begin{aligned} g = {} & [g_A\phi + g_B(1-\phi)] + RT[\phi\log\phi + (1-\phi)\log(1-\phi)] \\ & + RT\psi\phi(1-\phi) - \frac{1}{2}RTa^2(\nabla\phi)^2, \end{aligned} \tag{4.7}$$

where g_A and g_B are the molar free energies of the pure species A and B, respectively, at temperature T and pressure P, R is the gas constant, ψ is the Flory parameter, and a is a characteristic microscopic length. As shown by Van der Waals (Van der Waals, 1894), a is proportional to the surface tension at equilibrium σ,

$$a \sim \frac{1}{\sqrt{\psi - 2}(\Delta\phi)_{eq}}\frac{\sigma M_W}{\rho RT}, \tag{4.8}$$

where $(\Delta\phi)_{eq}$ is the composition difference between the two phases at equilibrium, while M_W is the molecular weight of species A and B. This relation can be easily derived

considering that $\sigma \sim l(\Delta g)_{eq}$, where $l \sim a/\sqrt{\psi - 2}$ denotes a characteristic interface thickness (Mauri *et al.*, 1996), while $(\Delta g)_{eq}$ is the jump in free energy across an interface, which can be estimated from Eq. (4.7).

The body force $\mathbf{F}_\phi$ appearing in Eq. (4.3) equals the gradient of the free energy (Hohenberg and Halperin, 1977), and therefore it is driven by the concentration gradients within the mixture, Farrell and Valls, 1989; Jasnow and Vinals, 1996; Tanaka, 1997),

$$F_\phi = \frac{\rho}{M_W}\nabla g = \left(\frac{\rho RT}{M_W}\right)\tilde{\mu}\nabla\phi. \tag{4.9}$$

This force, being proportional to $\tilde{\mu} = \mu_A - \mu_B$, is driven by the surface energy, and therefore can be interpreted as a Marangoni force. Physically, it tends to minimize the energy stored at the interface, driving, say, A-rich drops towards A-rich regions, and therefore enhancing coalescence. The ratio between the convective and diffusive mass fluxes defines the Peclet number, $\alpha = Va/D$, where V is a characteristic velocity, which can be estimated through Eqs. (4.3 and 4.9) as $V \sim F_\phi\, a^2/\eta$, with $F_\phi \sim \rho RT/(aM_W)$, obtaining,

$$\alpha = \frac{a^2}{D}\frac{\rho}{\eta}\frac{RT}{M_W}. \tag{4.10}$$

This coefficient coincides with the "fluidity" parameter defined by Tanaka and Araki (1998). For systems with very large viscosity, α is small, so that the model describes the diffusion-driven separation process of polymer melts and alloys (Mauri *et al.*, 1996). For most liquids, however, α is very large. In our case, for example, with $a \sim 10^{-5}$ cm^2/s, [cf. Eq. (4.8), with $\sigma = 10$ *dyne/cm*] and $D \sim 10^{-5}$ cm^2/s, we find $\alpha \sim 10^5$.

Therefore, it appears that in our case diffusion is important only at the very beginning of the separation process, in that it creates a non-uniform concentration field. Then, the concentration gradients within the system will drive the subsequent convection, which, as it happens, becomes the dominant mechanism for mass transport. A simple mass balance indicates that the growth rate is $dR/dt = \rho^{-1}|J|$, where R is the drop radius and J the antidiffusive flux which, in turn, can be estimated using Eqs. (4.5 - 4.7) as $|J| \sim \rho(a/l)(D/a)(\Delta\phi)_{eq}[2\phi(1-\phi)\psi - 1]$, obtaining

$$\frac{dR}{dt} = (\psi - 2)^2\left(\frac{D}{a}\right), \tag{4.11}$$

where we have considered that $(\Delta\phi)_{eq} \sim \sqrt{\psi - 2}$. Therefore, since for our solvent mixture we have ψ = 2.15, we predict a growth rate $dR/dt \sim 10^{-2}$ *cm/s*, in excellent agreement with our experimental results.

The above dimensional analysis can be rewritten substituting Eqs. (4.8 and 4.10 into 4.11), obtaining,

$$\frac{dR}{dt} = k_b\frac{\sigma}{\eta}, \tag{4.12}$$

where,

$$k_b = \alpha^{-1}.$$

Equation (4.15) was obtained by Siggia (Siggia, 1979) and San Miguel and coworkers (San Miguel *et al.*, 1985) although their prediction $k_b \sim 10^{-2}$ far overestimates our growth rate results, where $k_b \sim 10^{-5}$. However, as the experimental findings (Chou and

Goldburg, 1979,1981; Wong and Knobler, 1978; Guenoun *et al.*, 1990) can all be fitted by the curve (Guenoun *et al.*, 1990; Furukawa, 1985),

$$\frac{dR^*}{dt^*} = B^*, \tag{4.13}$$

where $R^* = R/l$ and $t^* = tD/l^2$, while $B^* = 0.022$, it should be stressed that, remarkably, the curve (Eq. (4.13)) is in good agreement with our experimental results, too, despite the fact that, unlike those previous studies, we considered deep temperature quenches.

Let us consider now the gradient case, where the mixture is initially demixed everywhere, with the exception of a region where the composition varies gradually from one equilibrium value to the other. According to the theoretical model, the very early separation stage is the same as that for an initially homogeneous system, leading to the formation of small drops, which then grow by convection. Now, however, driven by the Marangoni force, these drops will start moving towards one or the other of the homogeneous regions, where they will be assimilated. Therefore, since in our visualization we could not see drops larger than 10 μm prior to the formation of the interface, we can conclude that such assimilation of the drops occurred very fast. Further studies are required to explain this phenomenon.

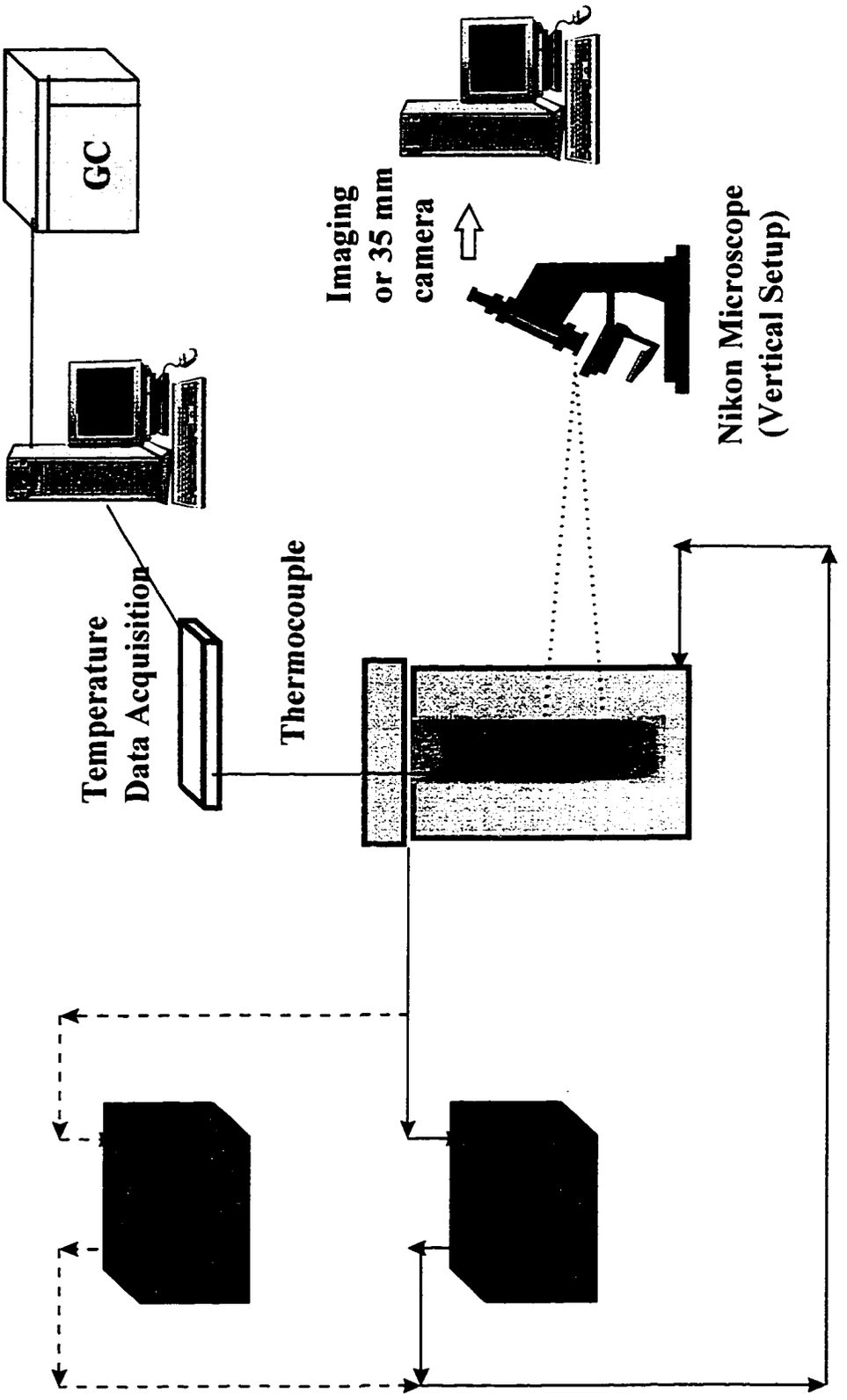

Figure 4.1: Schematic of the experimental setup.

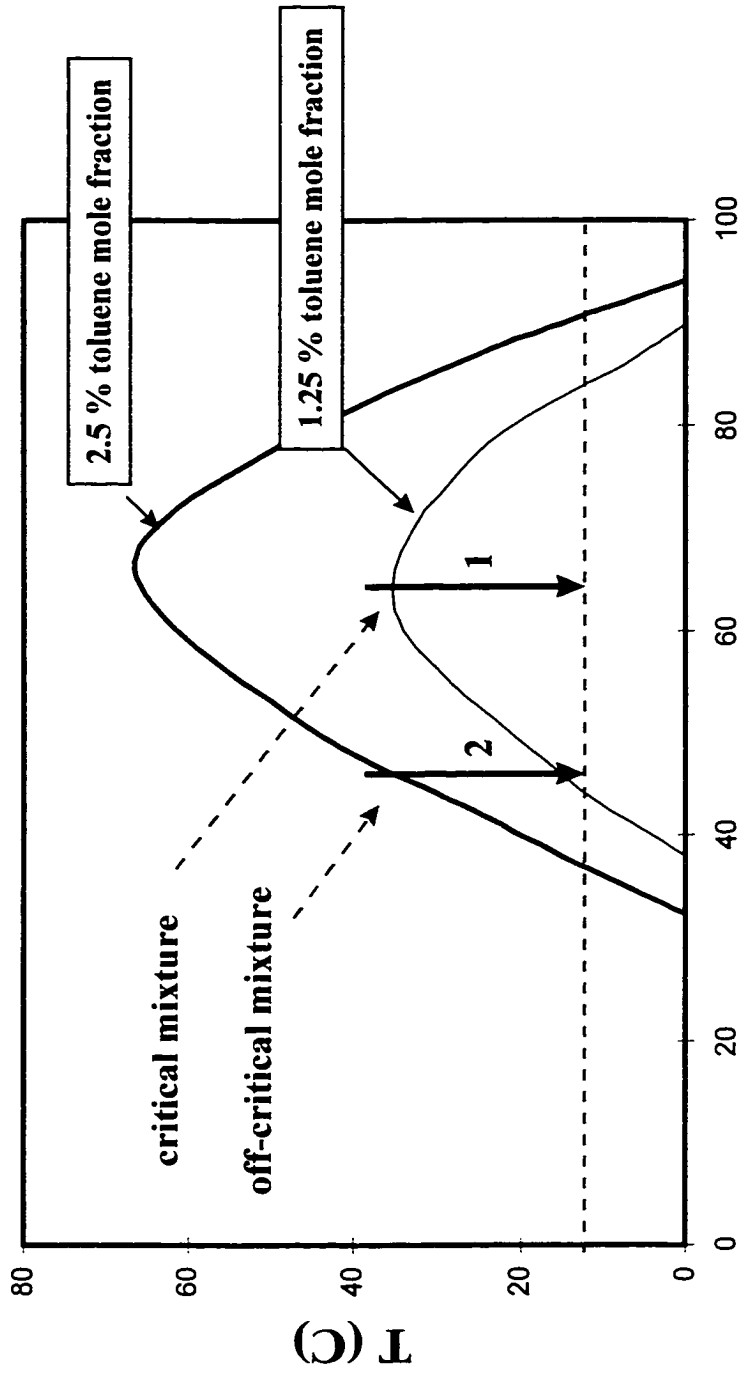

Figure 4.2: Phase separation in a water-ACN-toluene mixture.
Vertical arrows represent the critical (1) and the off-critical (2) temperature quench, both equal to 23 C .

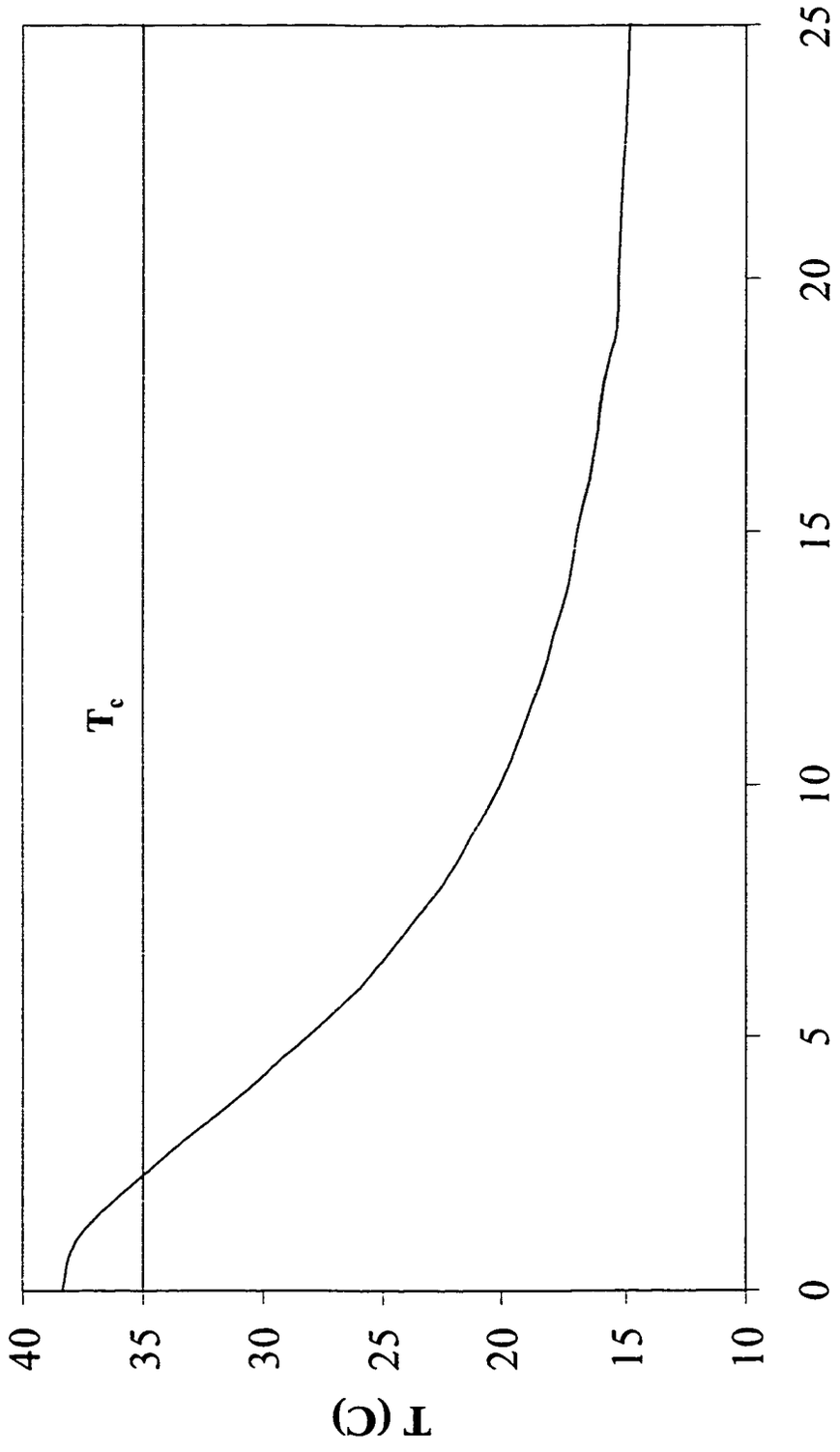

Figure 4.3: Temperature drop of the solvent mixture.

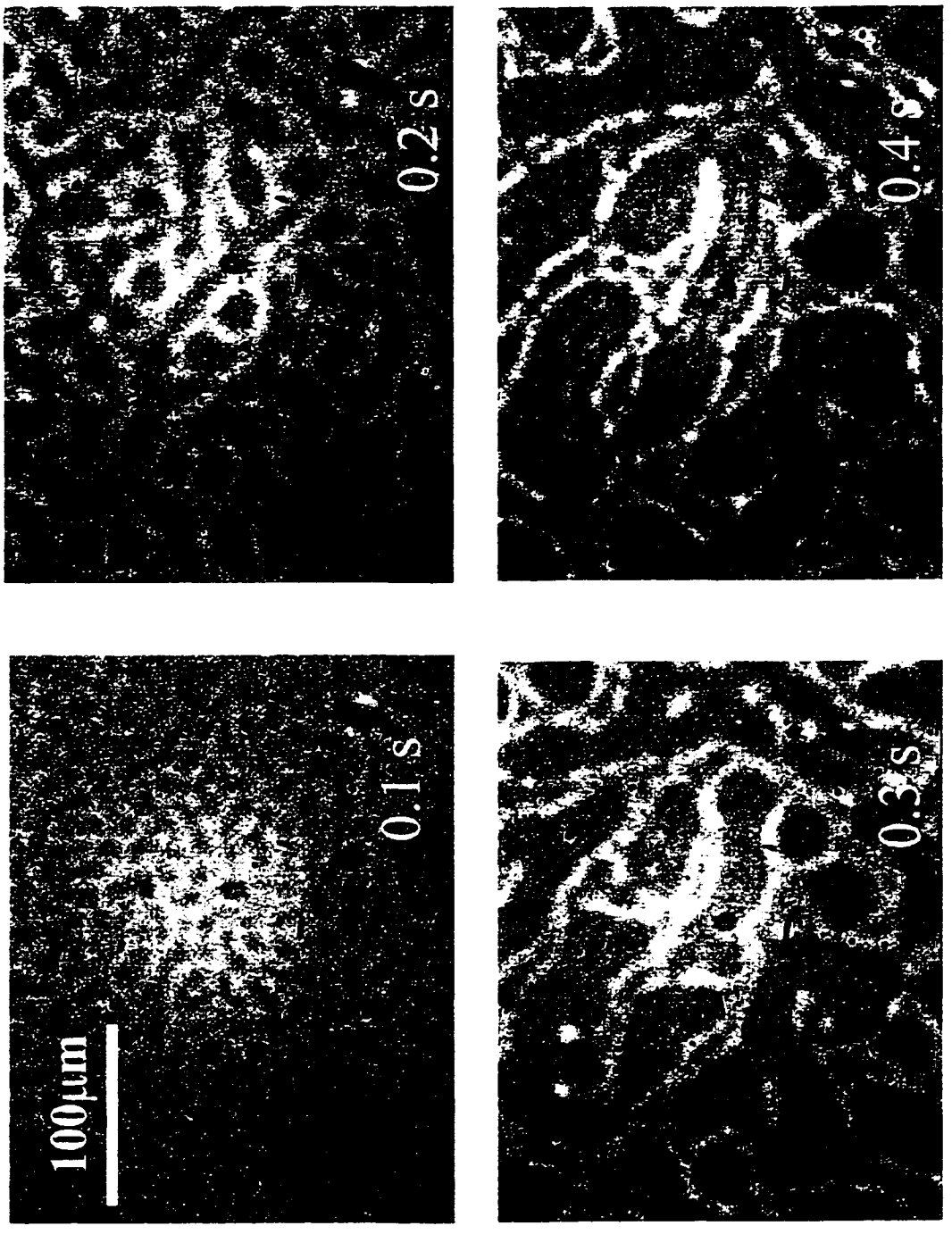

Figure 4.4: Phase separation in a critical liquid mixture with 300 μm field of view. Time is measured from the moment when $T = T_c$.

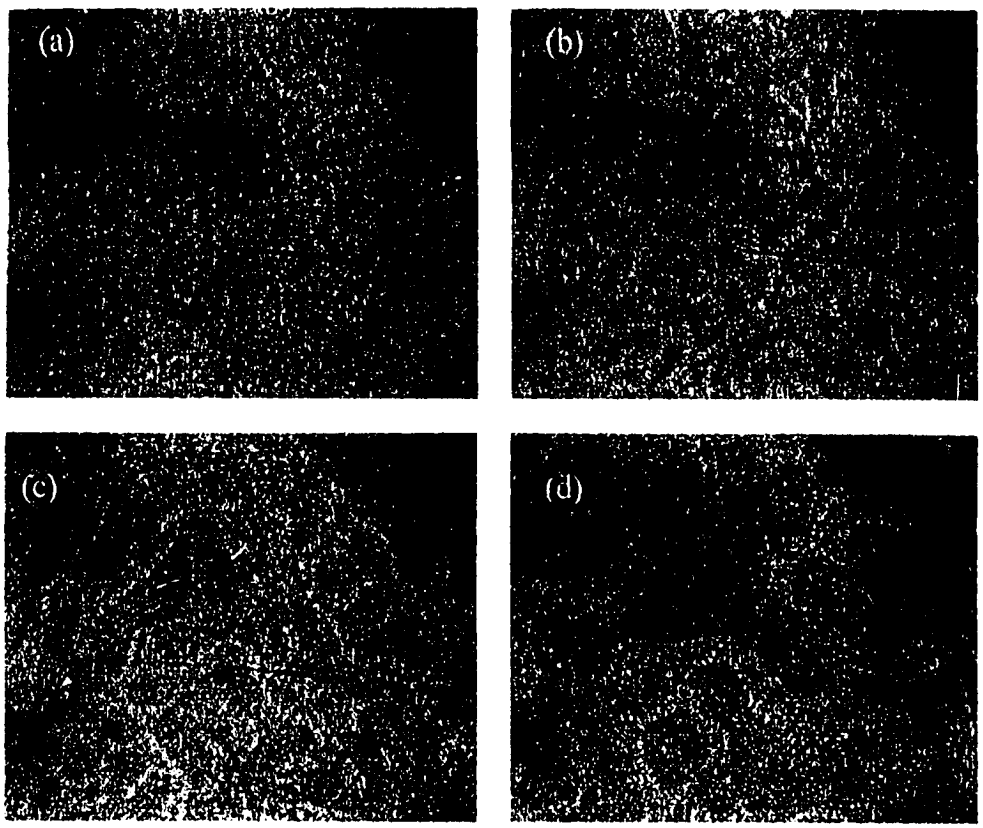

Figure 4.5: Phase separation in a critical liquid mixture with 2.25 *mm* field of view. Pictures were taken at times t = 0.6, 0.9, 1.2 and 1.5 *s*.

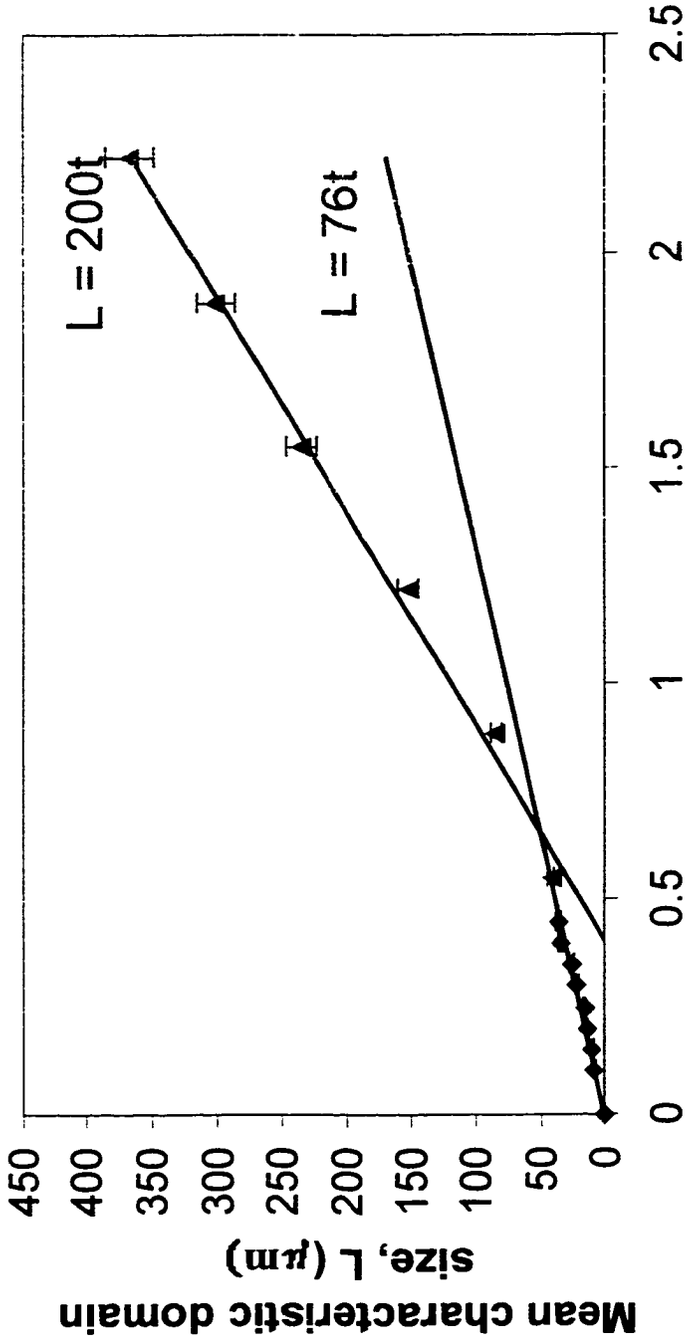

Figure 4.6: Domain growth during critical quench.

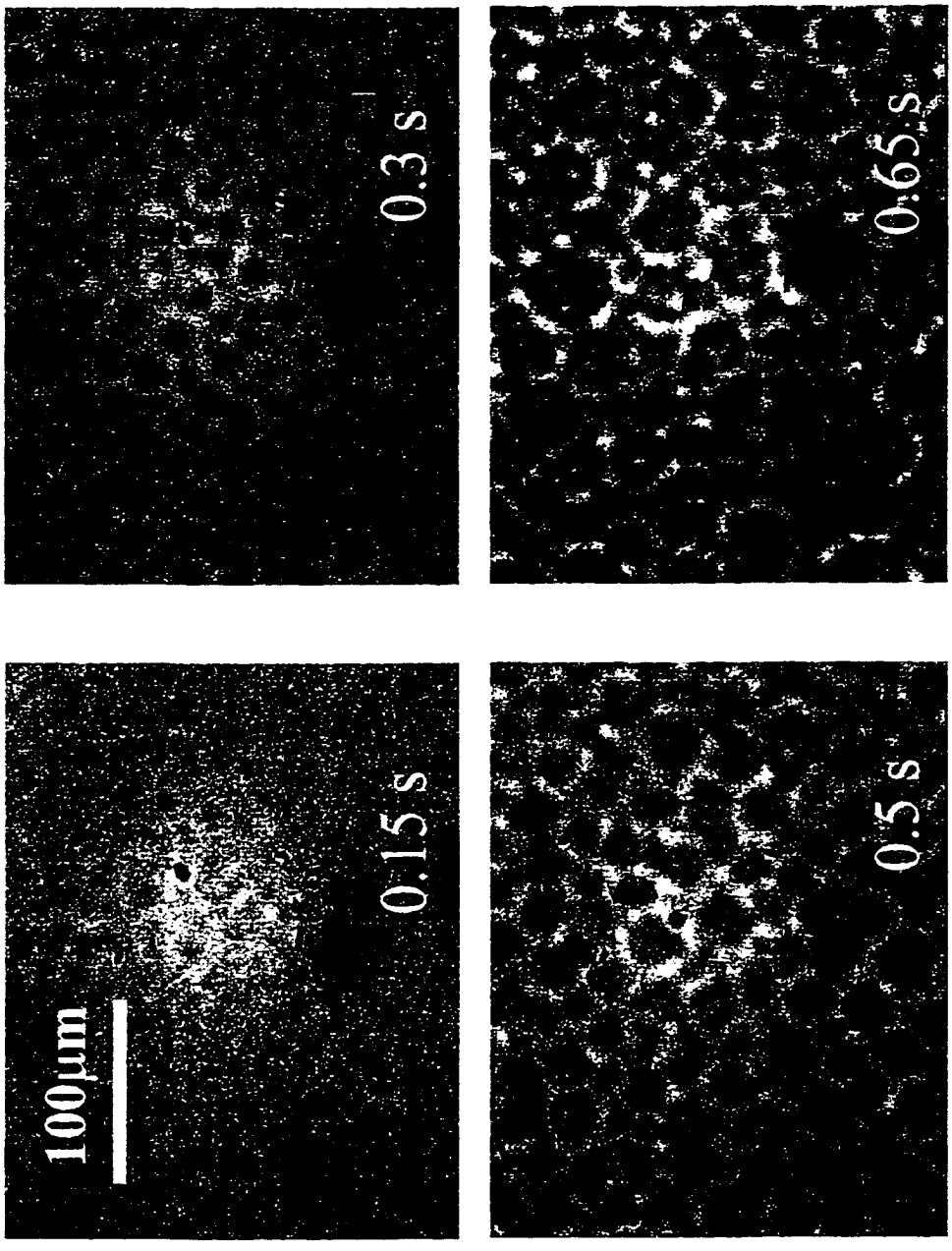

Figure 4.7: Phase separation in an off-critical liquid mixture. Time is measured from the moment when $T = T_c$.

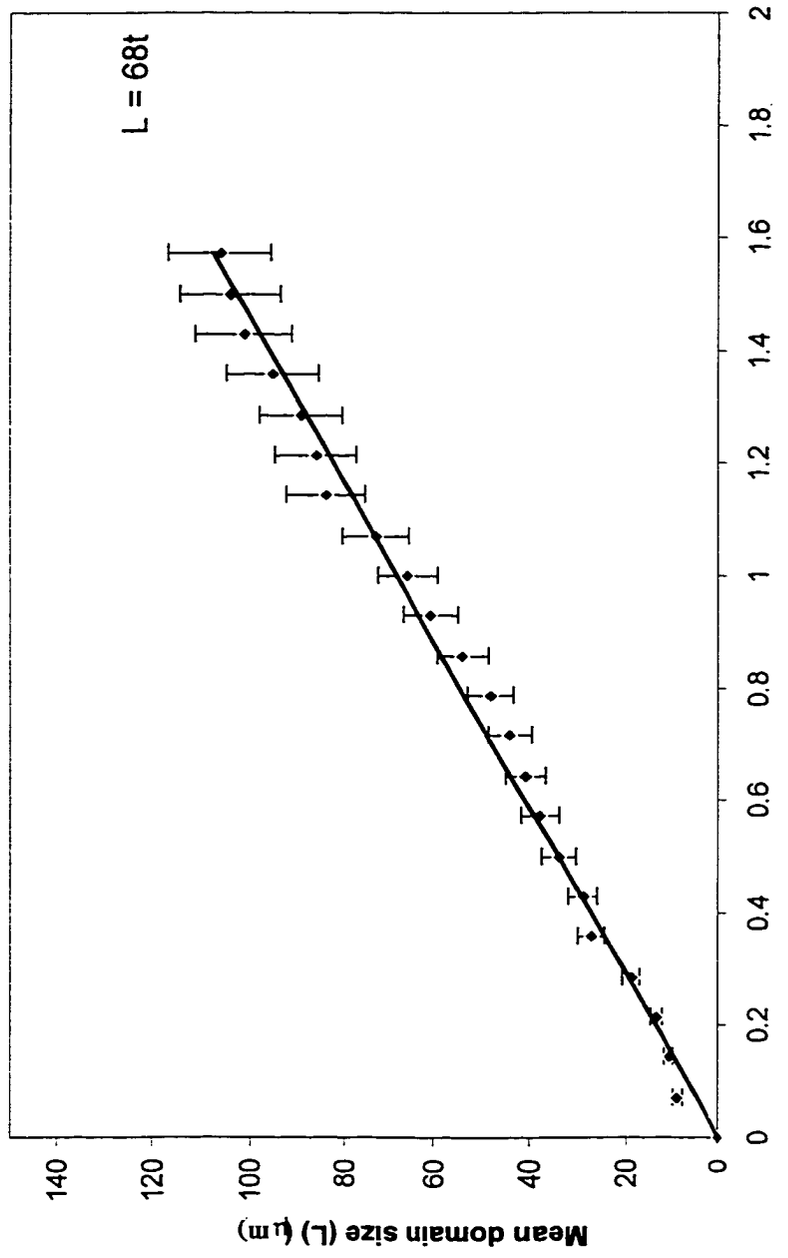

Figure 4.8: Domain growth during off-critical quench.

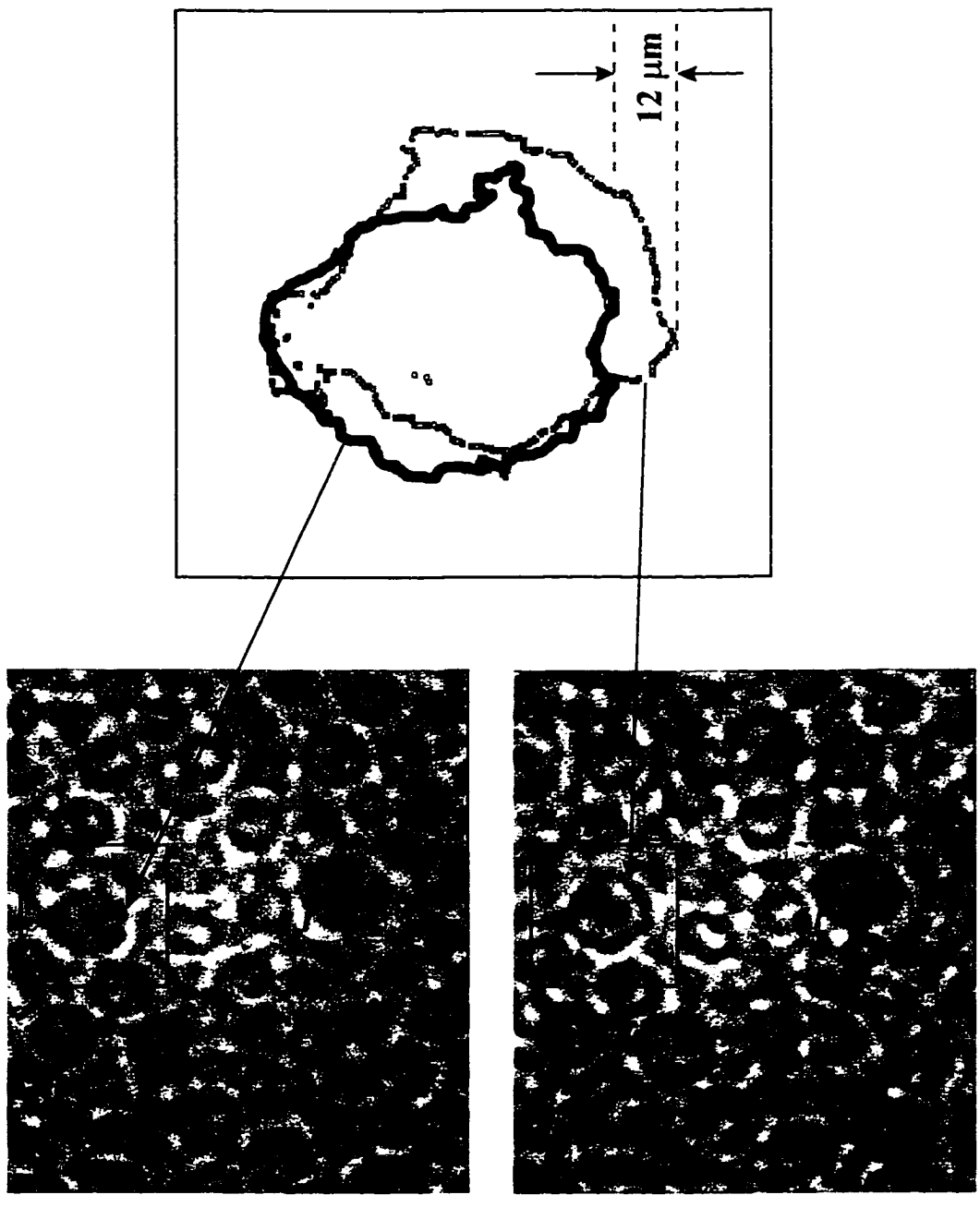

Figure 4.9: Movement of a single drop. The two pictures are 0.07 s apart.

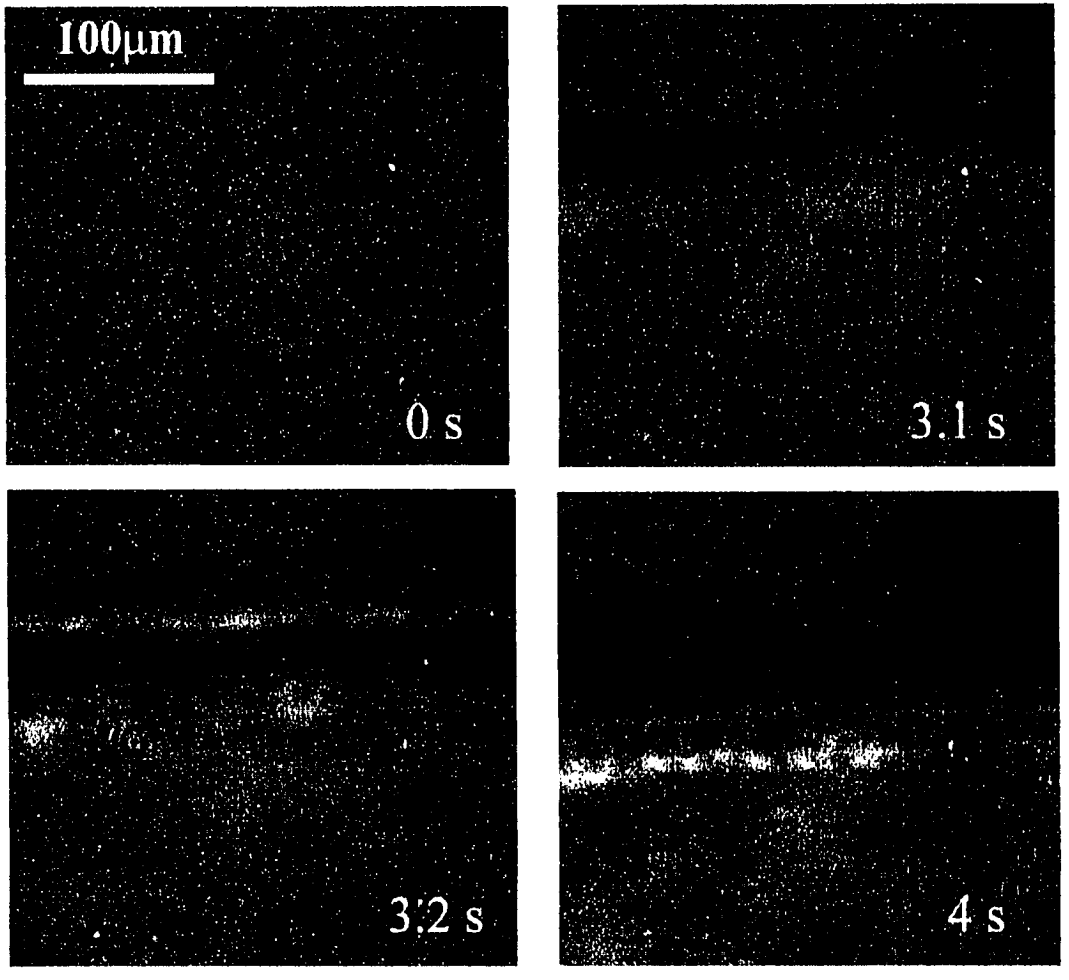

Figure 4.10: Phase separation in a critical liquid mixture with an initial concentration gradient. Time is measured from the moment when $T = T_c$.

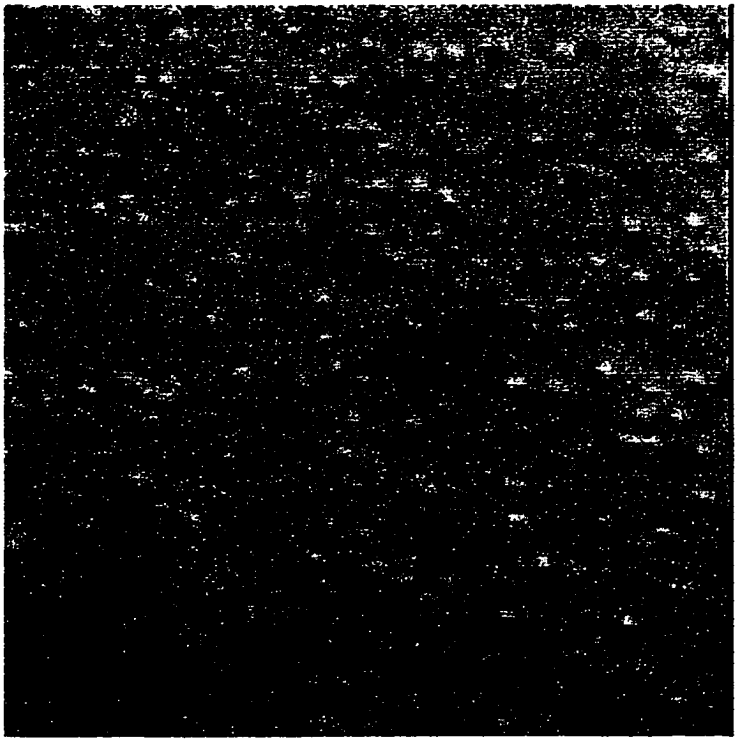

Figure 4.11: Region above the interface, about 20 s after the temperature quench.

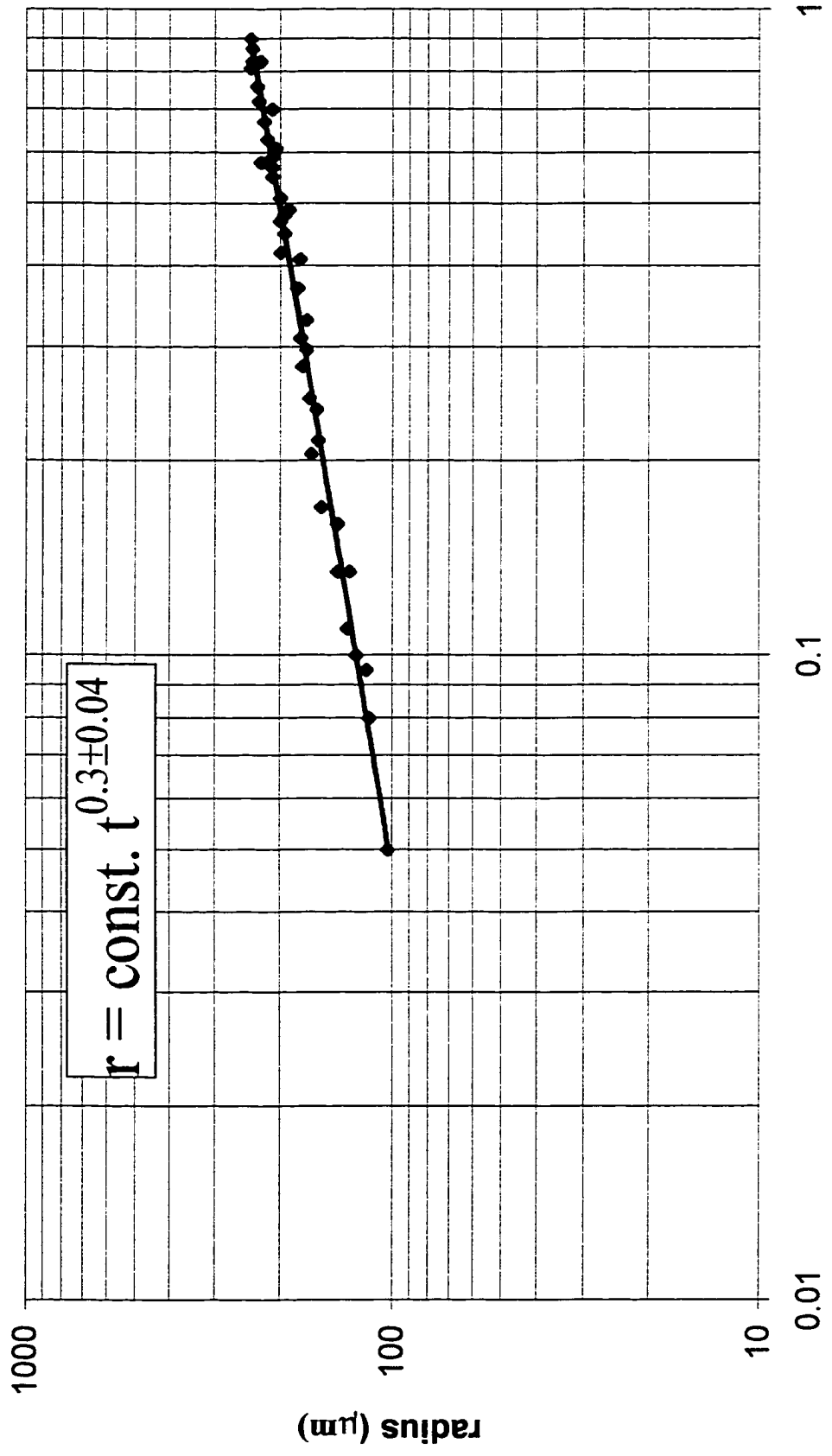

Figure 4.12: Drop size during the secondary nucleation. Time is measured starting 20 s after the temperature quench.

Chapter 5

Applications of the Phase Transition Extraction Process

The features of the novel PTE process, and the fact, which we established in the last section, that phase separation during the PTE process is governed by convection rather than diffusion, could open a new avenue of possibilities for difficult separations that have been either economically unfeasible or operationally limited. Such cases include: separations of systems that emulsify easily; difficult separations which require a large number of theoretical stages; separations of large molecules that can be damaged by high shear stress; separations of irradiated compounds where remote operation, low maintenance and heavy shielding are essential; extractions of radioactive materials from contaminated soils. In this section we apply the PTE process to some of these cases. In section 5.1, we discuss the extraction from porous media using the Composition-Induced Phase Separation. In Section 5.2, we study the

phase separation process in the presence of surfactants, and explain why the separation process in liquid mixtures is independent of the presence of emulsifying compounds. Finally, in section 5.3, an application of CIPS on a more intricate problem is discussed. It was explained in Section 2 that *in situ* remediation of contaminated soils from heavy or radioactive metals is a very serious problem. We propose a method here which can be useful for both *in situ* recovery as well as for treatment of excavated soils and sediments.

5.1 Extraction from Porous Solids

To better understand the physical reasons of the higher yields obtained using PTE, we developed a model system, consisting of solid particles whose size is similar to the cells of a typical fermentation broth, using a dye as our solute. This allowed us to perform a series of controlled and reproducible experiments, and to compare our results with the theoretical predictions. Our work on the model system provides a physical explanation of the experimental results obtained by Ullmann *et al.* (1995), and shows under which conditions PTE can lead to higher extraction yields. This is of special relevance in the extraction of large and sensitive molecules from broths, mammalian cells or plants, where the high shear required to break the cells could deteriorate the solute molecules.

The performances of the composition-induced phase separation process were compared in detail with those of both conventional liquid extraction and the temperature-induced phase separation process. From our results it appears that the new, CIPS process could lead to substantially higher yields and provides a useful tool

for dealing with difficult separation processes, which are hard to handle using currently-used methods.

In Chapter 3 we have seen how the PTE processes (both TIPS and CIPS) work, with rapid phase separation even in the presence of emulsion-forming compounds. However, the most important characteristic of the PTE processes is their ability to obtain higher yields when applied to the extraction of compounds from porous solid particles or membranes. This was first shown by Ullmann *et al.* (1995) for the extraction of efrotomycin from a fermentation broth containing fractured cells. However, quantitative scientific studies of the extraction of compounds from fermentation broths, plants and other systems containing a solid phase, have one difficulty, namely it is hard to get a completely reproducible system and, in addition, due to the complexity of the system, it is difficult to know how the extraction process takes place microscopically. Therefore, we decided to develop a well-defined system of solute and solvents, so that we could perform a series of controlled experiments.

5.1.1 The model system

This model system was intended to mimic a "real" fermentation broth, which typically consists of an aqueous solution of cell debris containing the solute to be extracted, such as the active compounds resulting from fermentation. Our model system consisted of water, a dye (2 *mg/lt* of crystal violet), playing the role of the solute, and 2% (dry weight) of silica gel particles, which are intended to model the cell debris. These particles are S-662 silica gel macroporous beads, with sizes ranging

from 70 to 250 μm, purchased from Fisher and commonly used in gas chromatography.

Using a dye as our solute had the advantage that its concentration could be readily measured with a spectrophotometer. In fact, using a Lambda 2 Perkin Elmer UV/Vis spectrophotometer one can see (Ullmann (1993)) that the absorption spectra of crystal violet show a maximum at a wavelength of 590 *nm*, and that this value is unchanged whether the dye is dissolved in water or in a solvent. Therefore a calibration line was determined, finding that the crystal violet concentration is linearly related to the absorbance of the sample at 590 *nm*, provided that the concentration is smaller than 12 *mg/lt* (Figure C1, Appendix C).

The most interesting aspect of our system (and the reason why it is a good model of fermentation broths) is that when the silica gel particles were added to the water/dye system, after 10 minutes stirring 97%, of the dye was adsorbed on the particles. In fact, the absorbance of the water/dye system decreased when the silica gel particles were added, until, after stirring for 2 and 10 minutes, it became 15% and 3% of its initial value (i.e. without particles), respectively. This value did not change when we stirred the system for longer times. Now, considering that the diffusion time of the dye in the particle pores is about 30 seconds (see Section 5.1.5), this measurements show that the adsorption/desorption time of the dye is no longer than few minutes.

In the following we will denote by "model system" the water/particles/dye suspension, with 97% of the dye adsorbed on the particles. This system is a good

model of a "real" fermentation broths, where the active compounds are often "imprisoned" within approximately 50 μm cell debris.

5.1.2 The solvents

Three solvents were used in our experiments, namely pure MIBK (Methyl Iso Butyl Ketone), and two mixtures of MIBK and ACN (Acetonitrile) in a 1:1 and 1:4 volumetric ratios, respectively. In all cases, the solvents were added to equal volumes of our model system, composed of 98% water and 2% dye-saturated particles. Now, MIBK is almost insoluble with water, and when 50 *cc* of MIBK were added to 50 *cc* of water containing 2 *ppm* of crystal violet, then, after agitation, the dye was found to distribute between the two phases, with a $p_{sw} = 5$ partition coefficient. Here and in the following the partition coefficient p_{sw} is defined as the ratio between the dye concentration in the upper, solvent-rich phase and that in the water-rich phase.

Studying the second solvent system, we must consider that the ACN/MIBK mixture is partially soluble with water. In fact, when a mixture of 25 *cc* ACN and 25 *cc* MIBK was added to 50 *cc* of pure water, then, after agitation, the mixture separated immediately into 55 *cc* of a water-rich phase (raffinate) and 45 *cc* of a solvent-rich phase (extract). The compositions of the two phases were measured using an HP gas chromatograph, finding 79% water, 18% ACN, 3% MIBK volume composition for the water-rich phase, and 6% water, 35% ACN and 59% MIBK volume composition for the solvent-rich phase. As shown in Figure 5.1 (see tie line A), these values were within few percent of the equilibrium compositions calculated using the UNIQUAC equation, with parameters given by Sorensen and Arlt (1980).

In addition, when 2 *ppm* dye was added to the system, the dye was found to partition between the two phases, so that at the end of the separation 96% of it was dissolved in the upper, solvent-rich phase, which corresponds to a partition coefficient $p_{sw} = 25$. Comparing this result with that obtained using pure MIBK, we see that acetonitrile is a far better solvent of the dye than MIBK.

Finally, we analyzed the third solvent system, by adding a mixture of 40 *cc* ACN and 10 *cc* MIBK to 50 *cc* of water, finding 25 *cc* of an upper phase with 13% water, 58% ACN and 29% MIBK volume composition, and 75 *cc* of a lower phase with a 64% water, 33% ACN and 3% MIBK volume composition, in agreement, within few percent, with the equilibrium compositions calculated using the UNIQUAC equation (see tie line B in Figure 5.1). In addition, adding the dye, we found that 42% of its original amount was dissolved in the upper phase and 58% in the lower phase, which corresponds to a partition coefficient $p_{sw} = 2.2$.

5.1.3 Comparison between CIPS, LLE and PTE

5.1.3.1 The LLE process

Having saturated the solid particles with crystal violet dye, we performed various extraction experiments, to compare the different processes. First, we performed conventional liquid-liquid extraction (LLE), where the two solvents described in the previous Section were added and stirred isothermally. During this process, at prescribed intervals, the batch was centrifuged, to break the stable emulsion, and the dye concentration in the upper phase was measured. The results are given in Figure 5.2 for pure MIBK (50% MIBK and 50% of our model system), and

in Figure 5.3 for the ACN/MIBK mixture (25 % Acetonitrile, 25% MIBK and 50% of our model system).

Comparing Figures 5.2 and 5.3, we see that at the end of the extraction using the ACN/MIBK mixture, 95% of the dye initially embedded in the particles was dissolved in the upper phase, while with MIBK that amounted to only 45%. This behavior was expected, since acetonitrile is a far better solvent of the dye than MIBK (see previous Section), and is typical of most processes, where water-soluble solvents extract far better than non-water-soluble solvents. What was not expected in these experiments is that the timescale of the extraction using the ACN/MIBK mixture was much shorter than that with pure MIBK, i.e. 10 minutes versus 40 minutes, where by timescale we refer here to the time needed to extract 63% of the dye dissolved in the solvent phase at equilibrium. As discussed in Section 5.1.5, this is due to the higher solubility of the dye in the water-rich phase when we use the ACN/MIBK mixture, so that there is more dye dissolved inside the pores, and the extraction can be completed faster.

5.1.3.2 The CIPS process

First Example. At this point we performed our composition-induced phase separation process, using the same ACN/MIBK solvent mixture that we used for LLE. To do that, our model system (i.e. water, containing 2% of dye-saturated silica gel particles) was first mixed with acetonitrile (25 *cc* ACN to 50 *cc* water), forming a homogeneous mixture that was agitated for ten minutes (see Figure 5.4). Then we added the appropriate amount of MIBK (1 part to 3 parts solution), stirred mildly, and let settle for two minutes, obtaining two phases that separated without the help of a

centrifuge. (Actually, for sake of precision, before analyzing the samples we centrifuged them, to eliminate any residual traces of suspended particles that might disrupt the reading of the spectrophotometer. However, the centrifuge was in no way necessary to separate the two phases.) When the two phases were analyzed, we obtained the results of Figure 5.5 showing that the same equilibrium state as that using LLE was reached, but within a much faster timescale. In fact, as the dye concentration in the water/ACN mixture is about 30 times larger than that in the water phase of the water/MIBK mixture, a reduction of the timescale from 40 minutes to 2 minute was expected.

Table 5.1 summarizes our experimental results, giving the compositions of the phases after separation, the amount of dye in the particles, water-rich and solvent-rich phases, and the equilibrium partition coefficients.

Second example. CIPS can be performed using a wide variety of solvents. In the first example described above we have used as modifier a solvent, i.e. MIBK, which is insoluble with the native solvent, i.e. water, and soluble with the primary solvent, i.e. ACN. However, we could use a modifier which is soluble with water and insoluble with ACN, such as sodium chloride. To show that, we added 50 *cc* of ACN to 50 *cc* of our model system, agitated for 2 minutes, and then we added 5 *g* of sodium chloride. As a result, the system separated immediately into 40 *cc* of an upper phase, with a 33% water, 60% ACN and 0% salt volume composition, and 65 *cc* of a lower phase, with a 58% water, 39% ACN and 3% salt volume composition. In this case we found that the dye would partition between the two phases with a 1:6 ratio, and 85% of the total quantity of dye was dissolved in the upper phase.

5.1.4 CIPS versus TIPS

At this point, a direct comparison between TIPS and CIPS was in order. To this purpose, we performed the TIPS process, adding 50 *cc* of the third solvent system described in Section 5.1.2, to 50 *cc* of our model system, heating the resulting mixture above its 40°C critical temperature, and then cooling it down to ambient, 25°C temperature. We saw that, as expected, two phases formed very rapidly, with 41% of the original amount of dye dissolved in the upper phase and 57% in the lower phase, in agreement with the partition coefficient measurement of Section 5.1.2.

We then performed the same extraction using CIPS, and found the same results, namely we were able to extract 98% of the original amount of dye from the silica gel particles, but only 40% of it was dissolved in the upper phase, due to the relatively low partition coefficient and the fact that the upper phase volume was only 25% of the total volume. As a comparison, in the extraction described in Section 5.1.3.2, we were also able to extract 98% of the original amount of dye from the particles, but, due to the very large partition coefficient, most of it was dissolved in the upper phase. However, this is not a direct comparison between CIPS and TIPS, as we did not optimize the conditions of TIPS. In fact, we could have increased the amount of dye in the upper phase by increasing the quantity of solvents and/or the critical temperature.

Therefore, we may conclude that when we use the same solvent system, CIPS and TIPS have the same extraction efficiency. However, comparing the results described in this Section with those of Section 5.1.3.2, we see that by applying CIPS

we can achieve a higher efficiency than when using TIPS, as we are allowed to use a larger amount of modifier, so that the solvent content in the water-rich phase is reduced. Clearly, we could have achieved the same result by heating the mixture of Section 5.1.3.2 to about 150°C under pressure (to prevent evaporation). However, apart from the obvious cost of heating and cooling the mixture across such a large temperature gap, many organic compounds, such as the products of fermentation broths, cannot be heated to such high temperatures. Therefore, as in single-stage extractions TIPS has no apparent advantages over CIPS, the added expense has no justification.

5.1.5 Theoretical model

The large difference between the extraction efficiencies of LLE and CIPS is due solely to a difference in the transfer rates: eventually, if we wait enough time, the same equilibrium state must be reached. A simple theoretical model can help us understand this phenomenon.

Consider a mass M_p of porous spherical particles of radius immersed in a binary mixture composed of a water-rich phase of mass M_w and a solvent-rich phase of mass M_s. A thin film of the water-rich phase surrounds the particles, so that the system can be schematized as in Figure 5.6 , showing a single capillary pore of length $l \approx a$, in contact at the mouth with a thin film of a well-stirred water-rich phase of thickness d, followed by a well-stirred film of a solvent-rich phase. Initially, a mass m_{tot} of dye is adsorbed on the capillary walls. Then, as time progresses, the water-rich phase removes the dye from the wall, and in turn the solvent-rich phase removes the

dye from the water-rich phase. In general, the concentration profile of the dye will depend on the partition coefficients $p_{pw} = c_p/c_w$, $p_{sw} = c_s/c_w$ and $p_{ps} = c_p/c_s = p_{pw}/p_{sw}$, expressing the ratios between the concentrations of dye at equilibrium in the water-rich phase, c_w, in the solvent phase, c_s and in the particles, c_p. At equilibrium, the fraction of dye extracted, $\epsilon = m_s/ m_{tot}$, where $m_s = c_s M_s$ is the mass of the dye dissolved in the solvent phase, can be easily found to be:

$$\epsilon = \frac{P_{sw}}{1 + P_{sw} + P_{pw}}, \tag{5.1}$$

where the coefficients and are defined as:

$$P_{sw} = \frac{m_s}{m_w} = p_{sw}\frac{M_s}{M_w}; \quad P_{pw} = \frac{m_p}{m_w} = p_{pw}\frac{Mp}{M_w}. \tag{5.2}$$

From this expression one may conclude that the larger is P_{sw} and the better extraction we get. However, this does not take into account the fact that if the characteristic time τ that it takes to reach equilibrium becomes too long, the extraction process becomes inefficient. In fact, this time is inversely proportional to the mean flux in the pores and so to the amount of dye dissolved in the water phase, and therefore is proportional to $(1+ p_{pw})$. In addition, τ is proportional to the amount of dye that leaves the pores, and to the diffusion time $\tau_d = \theta a^2/D$ that takes a solute molecule to exit a pore, where a is the particle radius, D the diffusion coefficient of the solute molecules and θ the tortuosity factor. This analysis can be performed rigorously following Froment and Bischoff (1979), finding that the ratio between the

dye extracted and the total amount of dye as a function of time is equal to $\epsilon[1-exp(-t/\tau)]$, where

$$\tau = \tau_d(1+p_{pw})\left(1-\frac{m_p}{m_w}\right). \tag{5.3}$$

From this equation, after easy manipulations we find:

$$\tau = \frac{\theta a^2}{D}(1+p_{pw})\,\frac{1+P_{sw}}{1+P_{sw}+P_{pw}}. \tag{5.4}$$

This result is valid, provided that the diffusive time τ_d is much smaller than τ, which means assuming that the quasi-steady-state approximation can be applied. In our case, since τ_d is about 30 seconds, this approximation is correct (see Figures 5.2, 5.3 and 5.5). In addition, in Eq. 5.4 we have neglected the desorption time. This approximation, although appropriate in our case, as we saw in Section 5.1.1, might not be valid in some applications. However, we will assume that Eq. 5.4 is correct, since our goal here is not to exactly predict the value of the extraction time, but to understand the role that the different physical parameters play in the diffusion of the dye out of the particle pores.

In Table 5.2 we give the measured values of τ together with their predicted values. Clearly, in predicting the relaxation time, we have assumed a certain value of the diffusive time, $\tau_d \approx 30$ seconds, which is consistent with the particle size $a \approx 100\ \mu m$, a diffusion coefficient $D \approx 10^{-5}\ cm^2/s$ and a tortuosity coefficient $\theta \approx 3$. As we can see, the theoretical predictions, in particular the ratios between the relaxation times obtained using different solvents, are in good agreement with our experimental

results. Note that in the CIPS process the relaxation time was too short to be measured accurately and, in addition, the quasi-steady-state approximation cannot be applied, so that both measurements and predictions should be taken *cum grano salis*.

The most interesting aspect of our results is that in LLE the extraction timescale is several order of magnitude larger than the diffusion timescale, despite the fact that the process is actually diffusion controlled. This analysis can be applied also, for example, to a fermentation broth, even if the transport process in this case is clearly more complex and may involve diffusion across membranes. However, if the desorption process, which in our model has been assumed to be instantaneous (or at least of the same order as τ_d) is slow, with its rate dependent on the solvent used, then our simple model should be modified accordingly. In addition, it should be pointed out that even when the cells are fractured, the fracturing may be incomplete and uneven, and cells can form loose aggregates, unless intense agitation continues during the extraction. Such aggregates will behave like a porous solid, and will hinder extraction, as the solvent cannot wet the particles easily.

Thus our results explain why in some cases the yield for PTE (both CIPS and TIPS) can be much higher than for conventional LLE (see Ullmann *et al.* (1995) and Eliyahu and Ludmer (1995)), especially as the extraction times are normally limited to a few minutes. They also explain the results of Eliyahu and Ludmer, who showed that intense fracturing improves the yield of conventional extraction. CIPS has the additional advantage over TIPS that one can reduce the solvent concentration in the water-rich phase, and thereby increase and improve the yield of a single extraction stage, while PTE would need additional stages to achieve the same result. Our results

also indicate another potential advantage of PTE, especially CIPS, as the ability to choose better, water-soluble solvents for the extraction. Now, in our case, ACN is a much better solvent for the dye than MIBK. We know that this is accidental, as there is no inherent reason why we could not find a better solvent that is not water-soluble. However, although this would improve the yield of the process, it would not affect its long timescale. Now, for natural materials, very often water-soluble solvents are superior to immiscible solvents. In that case, CIPS would have a very large advantage, in addition to the other advantages of a short extraction timescale and the absence of stable emulsions formed. It should be pointed out that CIPS can also be performed using centrifuges, without loosing its advantages of higher yields.

In conclusion, CIPS has clear advantages over both LLE and TIPS, since, unlike LLE, it reaches equilibrium very quickly and, unlike TIPS, it allows us to select solvents that give large extraction yields.

5.3 Phase Separation of Liquid Mixtures in the Presence of Surfactants

In Chapter 3, we have studied the separation process from a macroscopic point of view, discovering that the rate of phase separation in liquid mixtures is very high and does not depend on the presence of emulsifying compounds within the solution. On the other hand, surfactants strongly retard the coalescence rate of two-phase liquid mixtures after isothermal mixing, causing the formation of stable emulsions. This result was somewhat unexpected since deeply quenched, partially

miscible mixtures start to phase separate by forming microscopic droplets, and therefore one would expect that TIPS should be more, not less, influenced by the presence of surfactants. In Chapter 4, we complemented the macroscopic experiments of Chapter 3 with microscopic observations, describing the dynamics of the separation process. In this section, we study the influence of surfactants on the mechanism of drop coalescence, explaining why the phase segregation rate in TIPS appears to be unaffected by the presence of surface-active compounds.

The applications of these results can be found in any liquid-liquid operation involving phase separation, both when emulsions are the final product of the process, and when they are detrimental to it. In the first case, emulsions are actively looked after, such as in cosmetics and food industries, while in the second case, as in most extraction processes, they must be broken using coalescers, centrifuges and skimmers. Separation and extraction via phase transition is an interesting alternative, as it does not introduce unwanted side effects as, for example, in centrifuging, where the products may degrade because of the high shear stress involved. In fact, as shown in the previous section, liquid extraction can be performed in two stages, using our approach. First, the system is brought to the one-phase region of its phase diagram, where ideal mixing is achieved, and the solute can be extracted very efficiently from the native solvent. Then, the system is brought rapidly into its two-phase region, by changing its temperature or its composition. This results into rapid phase separation, with the solute preferentially confined into one of the two phases, even in the presence of impurities or emulsifiers. The fact that coalescence is evidently not slowed down by the presence of emulsion-forming compounds was explained by the

conjecture (Ullmann *et al.*, 1995) that there are no stable or well-defined boundaries between the different phases, to which emulsifier molecules can adhere. In this work, we will provide a more convincing explanation of that phenomenon, based on the fact that phase separation of deeply quenched liquid mixtures is driven by the convective motion induced by capillary forces. In fact, since the process is convection driven, we will show that various compounds can be separated equally fast, independently of their molecular weights, as opposed to the slower separations of heavy molecular weight compounds occurring in the diffusion-driven phenomenon of LLE. Finally, we present a dimensional analysis, and try to explain theoretically the presence, and hence the importance, of attractive and repulsive forces during phase separation in the presence of surfactants.

When surface active compounds are dissolved within a liquid mixture, the phase-separating process becomes, obviously, more complex. The coalescence-retarding mechanism of surfactants, however, has been studied extensively only for systems at local equilibrium, where the composition of the dispersed and continuous phases are constant and equal to their equilibrium values. On the other hand, there is no published data on the influence of surface-active solutes on the coalescence rate of the single-phase domains that form in deeply quenched, phase-separating liquid mixtures.

Stable emulsions in mixtures of mutually immiscible liquids are usually composed of small, 1 μm-size droplets. In this case, as phases are in equilibrium with one another, droplet coalescence is driven only by interfacial tension, i.e. the higher the tension, the more rapid is the coalescence rate. This is why two pure liquids rarely

form a stable emulsion, and a third substance nearly always must be present, to lower the surface tension. These modifiers can be of two types, inducing the formation of either electrical double layers (charge stabilization) or protective layers (steric stabilization) on the droplet surface (Rosen, 1978; Hunter, 1986). Ionic surface-active agents belong to the first type of surfactants, inducing charge stabilization through the adsorption of ions or polyelectrolytes at the surface of the drops. In this case, droplets are stabilized because, on one hand, these electrical double layers tend to prevent the flocculation of equally charged droplets, and, on the other hand, they retard the draining of the liquid film, due to the electroviscous effect (i.e. the electrostatic attraction between droplet interfaces and flowing films) (Rosen, 1978; Hunter, 1986). The second type of surfactants are far less efficient, as they simply form a protective layer at the surface of the drop, thus obstructing mass transport across the interfaces, as it happens with nonionic emulsifiers, polymers or finely divided solids.

5.2.1 The experimental setup

We use the same experimental setup and solvent mixtures as described in section 4.1. Two types of solute were added to the liquid mixture, namely 20 *ppm* of crystal violet and 100 *ppm* of blue dextran. Crystal violet has a 407 molecular weight and dissolves preferentially in the solvent-rich phase, while blue dextran has a 2,000,000 molecular weight and dissolves preferentially in the water-rich phase. Both crystal violet and blue dextran have strong colors, which facilitate the visualization of the phase separation process. In addition, crystal violet is an ionic, surface-active compound, which makes it ideal to study the separation process of liquid mixtures. In

fact, as we have shown in previous works (Ullmann *et al.*, 1995; Gupta *et al.*, 1996), when our solvent mixture is agitated at ambient temperature (i.e. in the two-phase region), the presence of crystal violet dye strongly increases the settling time from 10 *s* (with no dye) to 2 *h* (with 20 *ppm* dye). On the other hand, when the same mixture is heated and cooled across its miscibility curve it separates rapidly, irrespectively of the presence of the dye.

In all our experiments, we started with the mixture in its phase-separated state at a constant temperature of 15°C (see Figure 4.2). Then, the solution was first heated from 15°C to 38°C, mixed thoroughly, and finally it was quenched back to 15°C.

5.2.2 Experimental results

We first visualized the settling process, following the mixing of the critical liquid mixture at constant, 15°C, temperature. Due to the presence of 20 *ppm* crystal violet dye, surface tension was lowered and small drops were stabilized as soon as they formed, thereby causing a stable emulsion to form. Figure 5.7a presents a typical morphology of the emulsion formed in such cases. Microscopically, we saw that the emulsion region was filled with micron-size drops within the continuous phase, which slowly moved upward towards the upper interface, where they coalesced (Figure 5.7b). The lower interface, which macroscopically looked similar to the upper one (see Figure 5.7c), in reality was quite different. In fact, no coalescence occurred there, and the interface was simply the dividing line between the emulsion region, which shrank as drops coalesced at the upper interface, and the lower, water-rich clear phase, which grew as the drops moved up. Therefore, both upper and lower phases

grew as the result of the coalescence of the drops at the upper interface. On the contrary, hardly any coalescence between drops was observed in the middle emulsion region, primarily due to the presence of the coalescence retarding dye on the drop surface.

Completely different morphologies were observed when the critical mixture was quenched from 38°C to 15°C. As it was discussed in Section 4.2.1, and shown in Figures 4.4, 4.5 and 4.7, we see at first the appearance of ~ 10 μm microdomains, which subsequently grow in time. After reaching millimeter size, domains started to experience gravitational effects and the system rapidly separated into two gravity-stabilized regions. The final equilibrium state was reached in no more than 20 s, except for the presence of some small drops that remained in both separated phases. The same behavior was obtained with different surfactant concentrations.

5.2.3 Theoretical Model

5.2.3.1 Capillary forces during phase transition

As discussed in Section 4.3, the body force F_ϕ equals the gradient of the free energy (Hohenberg and Halperin, 1977), and therefore it is driven by the concentration gradients within the mixture (Farrell and Valls, 1989; Jasnow and Vinals, 1996),

$$F_\phi = \frac{\rho}{M_W}\nabla g = \left(\frac{\rho RT}{M_W}\right)\tilde{\mu}\nabla\phi. \qquad (5.5)$$

Physically, F_ϕ tends to minimize the energy stored at the interface, driving, say, A-rich drops towards A-rich region; therefore it is an attractive force, enhancing

the coalescence of droplets. In addition, being proportional to $\tilde{\mu} = \mu_A - \mu_B$, the body force is driven by the surface energy, and therefore can be interpreted as a capillary force, whose magnitude can be easily estimated as,

$$F_\phi \sim \frac{\rho RT\sqrt{\psi - 2}}{aM_W} \sim \frac{\sigma}{a^2(\psi - 2)}. \tag{5.6}$$

5.2.3.2 Colloidal forces in liquids

Colloidal particles, when dispersed within our liquid mixture, experience repulsive forces, either electrostatic or steric. Initially, when there are no sharp interfaces within the system, the surfactants will distribute uniformly, and therefore will not influence the process of phase separation (see Figure 5.8). Later, however, after droplets have formed, surfactants are swept away by the fluid, moving at speeds exceeding 1 *mm/s*, and clustering on the droplet interfaces, where they are at local equilibrium (see Figure 5.8).

Let us compare the magnitude of the capillary force F_ϕ with that of the electrostatic repulsion between two droplets due to the presence of surfactants, assuming that the distance between the droplets is equal to the thickness of their interface, $l = a/\sqrt{\psi - 2}$. Note that, in our case, where $a \sim 0.1\ \mu m$, this distance is of the order of the Debye length, λ_D, for water-based solutions, which is the typical distance among droplets in stable emulsions (Hunter, 1986). As the typical repulsive energy V_R between two droplets in a stable emulsion is of order $10kT$ (Rosen, 1978; Hunter, 1986), where k is the Boltzmann constant, the repulsive force is,

$$f_R \sim \frac{V_{\max}}{\lambda_D} \sim \frac{10kT}{a}\sqrt{\psi - 2} \tag{5.7}$$

The attractive capillary force F_A is equal to the ratio between the body force F_ϕ and the number density n of droplets. Therefore, considering that $n = \phi / \left(\frac{4}{3} \pi r^3 \right)$, where ϕ is the volume fraction of drops, we obtain,

$$F_A \sim 10 r^3 F_\phi \sim \frac{10 r^3 \rho RT \sqrt{\psi - 2}}{a M_W}, \tag{5.8}$$

where we have substituted Eq. 5.6. Finally, defining the ratio ξ between the attractive capillary force (Eq.5.8) and the repulsive electrostatic force (Eq. 5.7) we obtain,

$$\xi = \frac{f_A}{f_R} \sim \frac{\rho N_A r^3}{M_W}, \tag{5.9}$$

where N_A is the Avogadro number. This analysis reveals that, since $\xi >> 1$ for micron-size and larger drops, the attraction forces due to capillary effects are always dominant with respect to the repulsion between drops, caused by the presence of surface-active compounds on their surface.

Obviously when, on the other hand, the mixture is agitated isothermally (i.e. without phase transition), the resulting drops are at equilibrium with the continuous phase, so that $\tilde{\mu} = 0$, and $F_\phi = 0$. Therefore, as there is no attractive force, drops are easily stabilized by any surface active compounds present within the system, resulting into the formation of stable emulsions.

5.3 Solvent extraction of metal ions from contaminated soil

In this section we develop the experimental technique to decontaminate soils, a very serious problem these days, using the CIPS process. As most soils contain

adsorbed water, their wettability by conventional organic solvents is rather poor. In fact, to understand where the advantages of the new remediation process lie, let us list some of the problems encountered by conventional soil extraction by solvents.

- Due to their small solubility in water, most ions move slowly, carried along by the ground water. This is ultimately dangerous, as the ions can eventually reach the water supply.
- Most of the compounds that form stable complexes with metal ions are only weakly soluble in water, and preferentially adsorbed on soil. The low solubility of both ions and complexing agents in water makes water an unsuitable extractant. Now, more powerful solvents can be used instead, that can better dissolve the complexing agents; however, as most of these solvents are insoluble in water, they do not wet the soil particles well, so that their extraction yield is low.
- The solvent that has remained in the soil at the end of the extraction must be removed. Using conventional solvents this removal is expensive in the treatment of excavated soils and sediments, and prohibiting difficult for *in situ* processes. On the other hand, our water-soluble solvents can be easily removed through a water wash.
- Many wet soils, when contacted with solvents, tend to form stable emulsions that settle very slowly. That means that operating a traditional mixer-settler apparatus for the treatment of excavated soils and sediments will present serious difficulties.

All these difficulties can be overcome by using our proposed method, which is briefly summarized in the next Section.

5.3.1 Description of the remediation process

Our remediation process is composed of two stages. First, the contaminants are selectively extracted from the soil by contacting the soil with the carrier solvent in which the appropriate chelating agents have been dissolved. Then, all the effluents are separated by adding a solubility modifier that causes phase separation. This will result in a water-rich stream containing some solvents and traces of contaminants, and a solvent-rich phase, containing the chelating agent together with the contaminants.

The main innovation of the proposed process is the use of environmentally acceptable, water-soluble carrier solvents, such as ethanol, which can be separated from water and soil by adding a solubility modifier. The carrier solvents themselves do not have to be good solvents of the contaminants at all. Their main purpose, in fact, is to carry with them appropriate chelating agents which, being soluble in the solvent mixture, can first penetrate the pores in the soil, and then form complexes with the contaminants which thereby can be washed out of the soil.

First, for sake of simplicity, we shall describe our proposed treatment of excavated soils and sediments (see Figure 5.9 for a schematic description of the process). In this case, the contaminants are first selectively extracted from the excavated crushed soil or sediment, using the carrier solvent in which the selective solvents or chelating agents have been dissolved. Then, in other two mixer-settlers, the soil is contacted first with the carrier solvent, to remove any trace of chelating

agents, and then with water, to remove the carrier solvent. If organic compounds or solvents are present in the soil, the previous treatment will be preceded by a solvent wash, using a mixture of the carrier solvent and water, to remove the organic contaminants. At this point, all the effluents (apart from those used for the removal of the organic pollutants) are combined and separated in a mixer-settler by adding a modifier that causes a phase separation. This will result in a water-rich stream containing some solvents and traces of contaminants, and a solvent-rich phase, containing the chelating agents, the contaminants, the carrier solvent and the modifier. After that, the solvents are separated and the contaminants concentrated by distillation. The contaminants then can be recovered by a number of available methods, while the separated solvent and modifier are sent back to their appropriate places in the process. Concomitantly, in the waste water, the traces of contaminants can be removed by ion exchange and then disposed in concentrated form, together with the solids of the ion exchange.

An equivalent process can be drawn for the *in situ* recovery of metal ions contaminants. Here, we shall use a method very similar that used in enhanced oil recovery, by digging a series of wells (either horizontal or vertical) in the soil. Then, the different stages of the process of Figure 5.9 can be realized by staged pumping, again in analogy with the pumping processes used in enhanced oil recovery. An accurate description of these processes is available (Shumaker, 1980), since a number of demonstration projects have been build, funded by DOE, and these results can be

applied here.[1] In our case, we will first pump pure carrier solvent to displace the organic contaminants, such as chlorinated solvents, which are present, for example, in sites contaminated by uranium. In the next phase, the carrier solvent, mixed with some water and containing the chelating agent, is pumped in the soil to extract the contaminants. Then, the carrier solvent, mixed with some water, is used to remove both the chelating agents and the contaminants from the soil. After that, a water wash will remove the carrier solvent and clean the soil. The treatment of the various effluents is similar to that used in the case of excavated soil and described in Figure 5.9.

The application of our method is not restricted to the decontamination of soil from heavy metals, but can also be extended to the soil remediation of organic hazardous compounds, such as PCB and chlorinated solvents. The fact that our approach can be used *in situ* and in the presence of organic contaminants makes it possible to treat sites which cannot be treated with any of the currently available methods. Finally, it should be stressed that the process described in Figure 5.9 is given here to illustrate the potentials of the proposed technology, but it should not be considered as its only possible application.

5.3.2 Extraction of iron ions from soil

As an example of our extraction process, we used iron ions as a of model of the heavy metals to be extracted, as iron ion concentration can be readily and

[1] The important characteristics of these projects is that they were very successful in oil recovery. Unfortunately, the technology is still too expensive for the current price of crude oil. However, when applied to soil remediation, the economic considerations are of a different nature.

precisely measured spectrometrically. To be sure, the extraction of iron ions from soil is not very important from a practical standpoint; however, learning how to solve the technological problems arising in this case will allow us to determine how to perform successfully much more relevant extractions, such as that of chromium, which is the subject of the next Section. The soil that was used is a volcanic soil typical of the region near Salerno, Italy, with about 15% of organic content, and we will call it Vesuvian soil (mineral analysis in Table C.1, Appendix C).

The iron concentration was measured using a Parker Elmer spectrophotometer, with 8-Hydroxyquinoline (Cheng, Ueno and Imamura, 1982) acting both as an indicator, to measure colorimetrically the iron concentration, and as an extractant. The solvent was a solution of 50% water and 50% acetonitrile, in which we dissolved 1230 *ppm* of 8-Hydroxyquinoline, so that the number of moles of the extractant was, in every test, at least five times larger than that of the iron ions. The calibration curve from the spectrophotometer (i.e. absorbency versus iron ion concentration) was found to be almost linear for concentrations up to 50 *ppm* (Figure C.1, Appendix C).

First, we mixed the Vesuvian soil with a solution of deionized water and $(NH_4)_2Fe(SO_4)_2$, with 0.945 *mg* of iron ions per each gram of soil. At the end, we saw that no detectable quantity of iron ions was dissolved in the water, and therefore, after drying, the soil contained 945 *ppm* of iron ions. As a further check, we performed a blank extraction, by using pure water as solvent, and saw that with 10 *ml* of water added to each gram of contaminated soil, after mixing for 30 minutes, only 1.3% of the iron was extracted.

Next, we performed a series of tests, using our extracting solution, i.e. 50% water and 50% acetonitrile, with 1,230 *ppm* of 8-Hydroxyquinoline. First, we mixed 10 *ml* of solution to each gram of contaminated soil, so that approximately 5 moles of chelants are present per each mole of metal ions. In Figure 5.10 the extraction yield is represented as a function of the mixing time, showing that steady state is reached after less than 10 minutes mixing, with about 75% of the iron ions extracted. It should be stressed that each point of the curve in Figure 5.10 was the result of a separate experiment, in which a different soil sample was used. At this point, we added 5 *ml* MIBK per each gram of soil, seeing that the mixture separates immediately into two phases, with no emulsion formation, and the soil particles confined in the lower, water-rich phase. Measuring the composition of the two phases, we determined that 95% of the initial quantity of iron ions was dissolved in the upper phase and 5% in the lower phase. That means that the partition coefficient of the 8-Hydroxyquinoline/iron ions complexes between the two phases is about 20, as it was confirmed in a separate set of measurements. All these tests were repeated five times, obtaining the same results within a 10% error. Note that at the end of the separation process both solvent and modifier are confined in the upper phase, and therefore can be easily recycled.

Finally, we investigated the influence of the solvents on the extraction yield, using first a 50% water - 50% ethanol, and then a 99% water - 1% ethanol solvent solution (pure water is not a feasible solvent, since it does not dissolve 8-Hydroxyquinoline), with again a 5 to 1 ratio of chelant to metal ions moles. In both cases, we obtained the same results than when using acetonitrile, showing that the

role of the solvent solution is exclusively that of carrying the complexing agent inside the pores of the soil particles. This is an important result, since it shows that a) the amount of solvent required to decontaminate the soil is very limited; b) such solvent does not have to be a good solvent of the metal ions at all, and can therefore be chosen as non-toxic.

5.3.3 Extraction of Chromium (VI) ions from soil

In this Section we present an important application of this approach to decontaminate soils from chromium (VI) ions. It is well known that chromium (VI) compounds are human carcinogens (Brauer and Wetterhahn, 1991), as chromium (VI) ions are readily carried across the human cell membranes, where they are ultimately reduced by intracellular components to chromium (III), which in turn forms stable complexes with DNA (Brauer and Wetterhahn, 1991).

In this set of experiments we used an Appalachian soil (i.e. soil from the Appalachian mountains), with 15% organic content (mineral content is given in Table C.2, Appendix C. The chromium (VI) concentration was measured using spectrophotometer, with Diphenylcarbazide as indicator, using the same procedure as in Cheng, Ueno and Imamura, 1982, page 282. Diphenylcarbazide is a colorless crystalline powder, almost immiscible in water, which produces a highly sensitive color reaction with Cr(VI). As we can see in Figure C.2 (Appendix C), the calibration curve that was obtained at a wavelength of 542 *nm* is fairly linear in the concentration range of interest.

The extracting technique was similar to that used for the extraction of the iron ions. First, the soil was spiked adding 50 *ml* of a water solution containing 20 *ppm* of chromium (VI) ions to each gram of soil and mixing for three hours. At the end, the chromium concentration in water was measured, revealing that 23% of the chromium ions were absorbed (see Table 5.3, step I). This measurement was repeated five times, with identical results.

At this point, we extracted the Cr (VI) ions from the dry Appalachian soil using a solution of 50% water and 50% acetone, containing 500 *ppm* of Diphenylcarbazide. As in the case of iron, the same compound was used for both the photometric determination and the extraction of the chromium ions. In Table 5.3, Case A, we report the results obtained, respectively, after mixing for 2 hours 20 *ml* and 40 *ml* of the extracting solution per each gram of contaminated soil.

The results are expressed in terms of the partition coefficient P, defined as the ratio between the chromium concentration in the extracting solution and that in the soil particles at equilibrium, i.e. $P = Cs / Cp$. Here Cs is the ratio between the mass of the metal ions in the extracting solution and that of the extracting solution, while Cp is the ratio between the mass of the metal ions remained in the soil and that of the soil. Clearly, the partition coefficient appears to be practically constant, equal to about 0.025, independent of the amount of the extracting solution used in the process.

A new set of measurements was performed with wet soil, obtained by soaking each gram of soil with 1.3 *ml* of water for one hour. Surprisingly, we found that the extraction yield improves dramatically, with the partition coefficient increasing from 0.025 to 0.036 (see Table 5.3, Case B).

These measurements were repeated trying to mimic a multiple stage process. To do that, after extracting the soil, we let it dry overnight at ambient conditions, and repeated the extraction process the next day. Not surprising, we found that the partition coefficient was about the same as for the first extraction. In addition, when we performed the process using a 99% water - 1% acetone extracting solution, we found that the yield of the process was unchanged (see Table 5.3), clearly showing that it the extracting agent is the chelant, and not the solvent. In fact, only when we used a 1% water - 99% acetone mixtures the yield of the process was higher, with a partition coefficient of 0.05.

At this point, as the use of acetone has to be ruled out due to environmental considerations, we repeated the experiments replacing acetone with ethanol (Table 5.3). Identical results were obtained, thereby confirming that the extracting agent is the chelant, while the role of the solvent, be it acetone or ethanol, is simply to carry the chelant inside the pores of the soil. In fact, in a separate set of experiments, we saw that whenever the molar ratio between chelants and metal ions become less than 2, the yield of the process becomes much smaller.

Finally, we studied the kinetics of the extraction process by measuring the percent of chromium extracted as a function of time, using both dry and wet soil samples. The extracting solution was a solution composed of 1% water and 99% ethanol, with a 5/1 molar ratio of Diphenylcarbazide to chromium ions. The results are plotted in Figure 5.11, showing that, while for dry soils the equilibrium concentration was reached after 60 minutes, for wet soils the extraction process was much faster and took only about 10 minutes. As for the case of iron, each point of the

curves in Figure 5.11 was the result of a separate experiment, in which a different soil sample was used, thereby validating the analytical method used to determine the ion concentrations. Again, each test was repeated five times, finding identical results within a 10% error.

5.3.4 Extraction of cadmium ions from soil

The extraction of cadmium ions was performed using an identical procedure as with the chromium ions, using 1,5-diphenylthiocarbazone as chelating agent (Cheng, Ueno and Imamura, 1982). First, samples of Vesuvian soil were spiked by adding 1 g of soil to 50 *ml* of a 2 *ppm* solution of cadmium oxide. After 3 hours stirring, we saw that about 25% of the cadmium ions were absorbed by the soil (see Table 5.4). The extracting solution consisted of a mixture of 99% distilled water and 1% ethanol, containing 2 *ppm* of 1,5-diphenylthiocarbazone. The results of the first and second extractions, reported in Table 5.4, show that the extraction yield was very similar to that of chromium, with approximately 50% of the cadmium present in the sample removed in each extraction, and a partition coefficient of about 0.045.

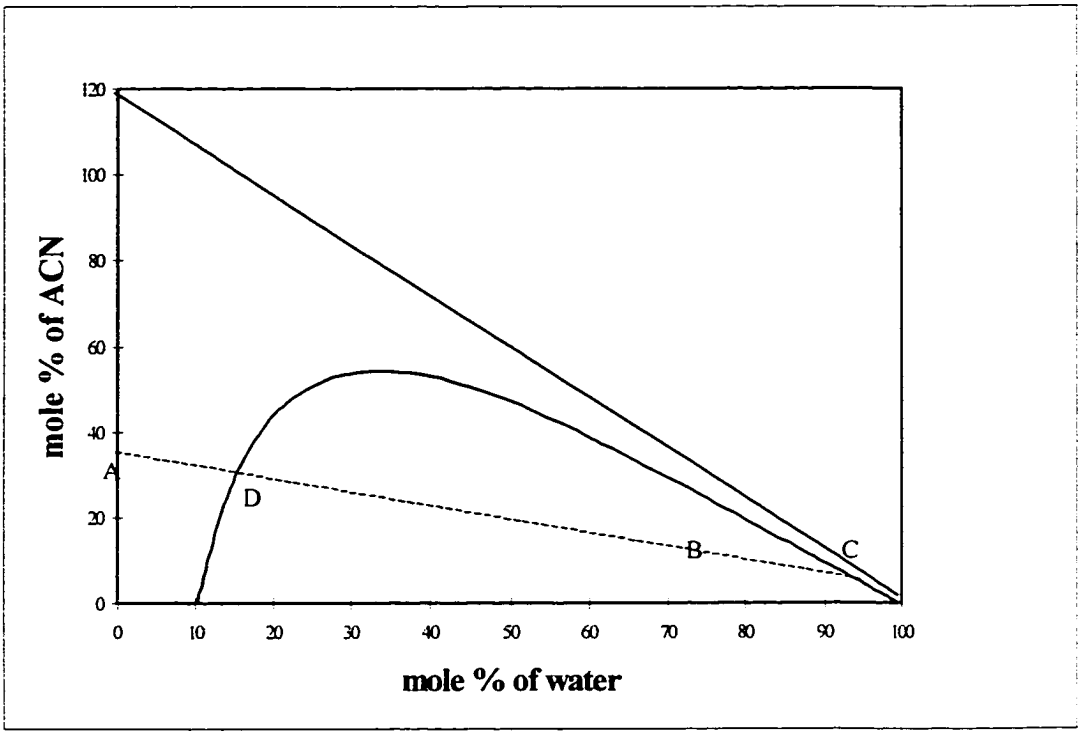

Figure 5.1: Phase Diagram for ACN-water-MIBK.

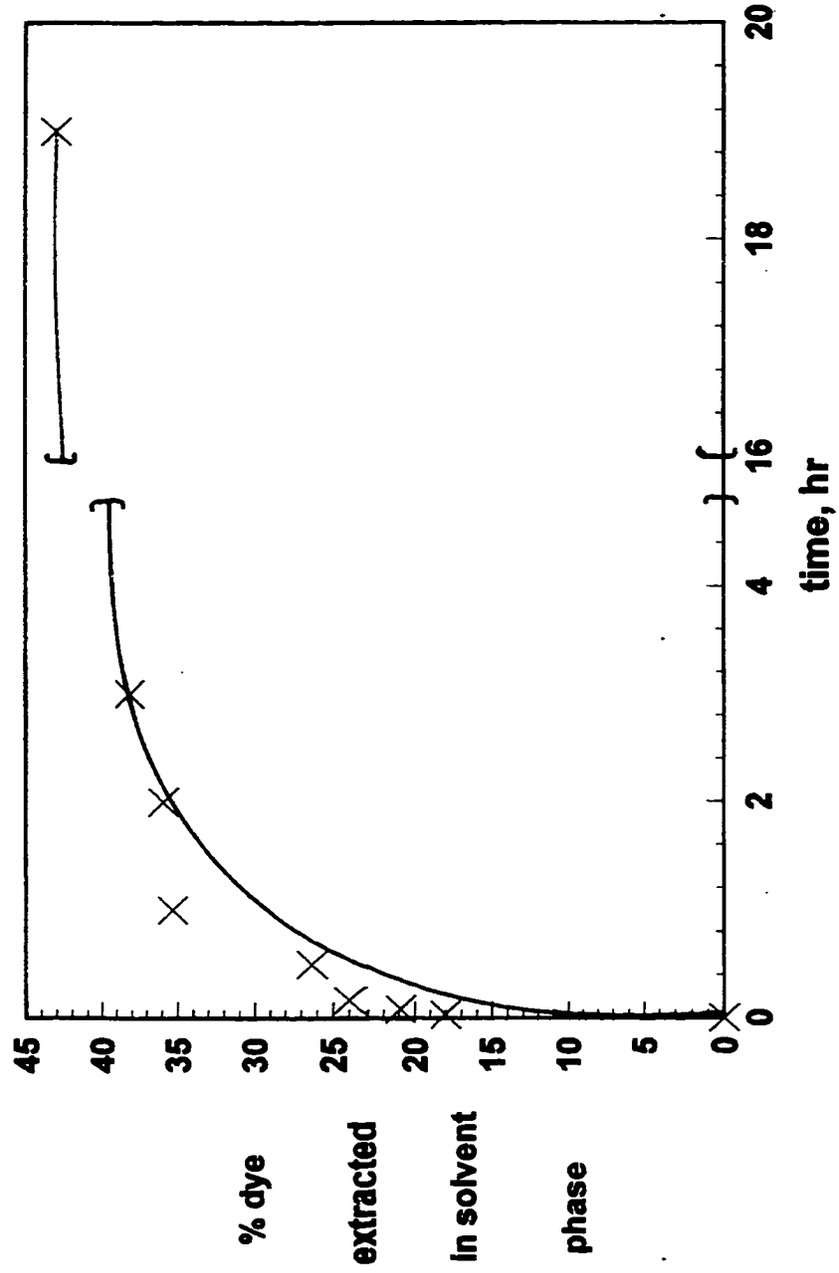

Figure 5.2: LLE: Water, MIBK, 2ppm dye, 2% particles.

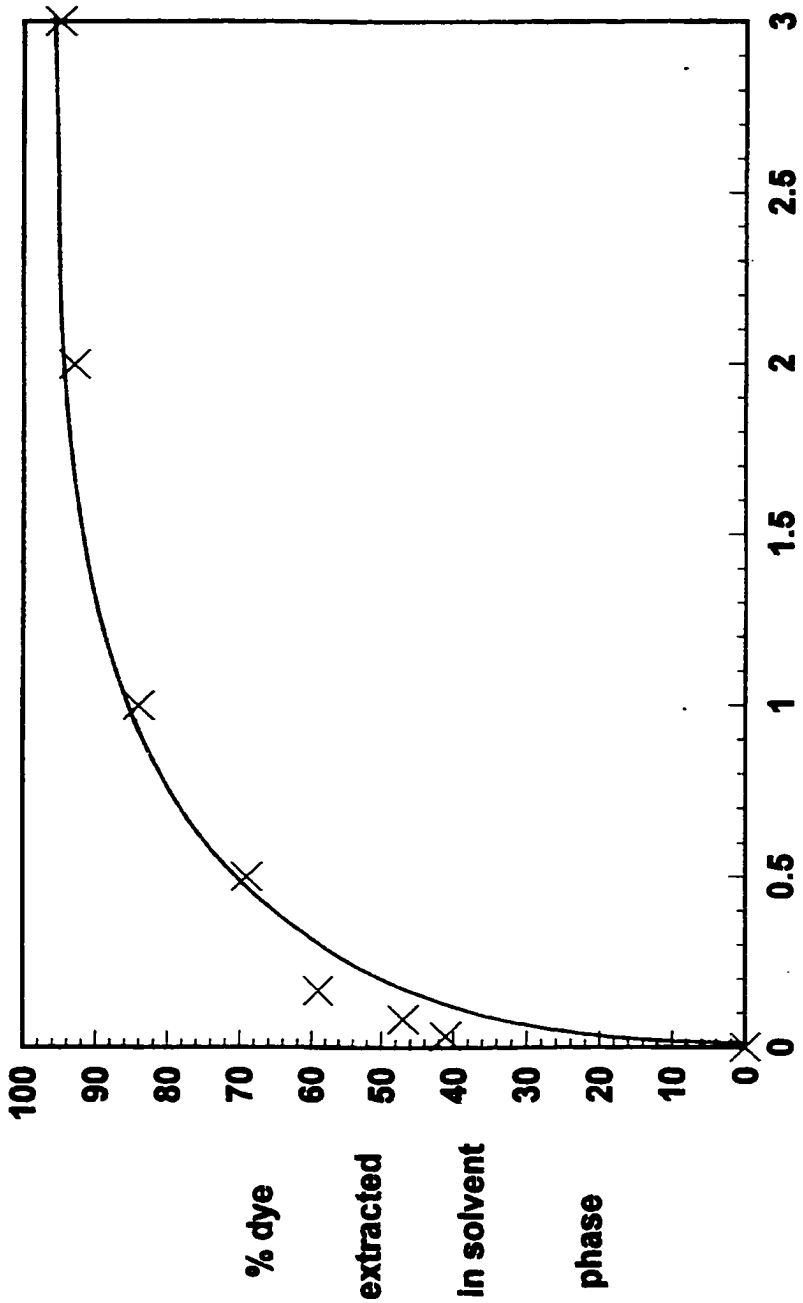

Figure 5.3: LLE: ACN, Water, MIBK, 2ppm dye, 2% particles.

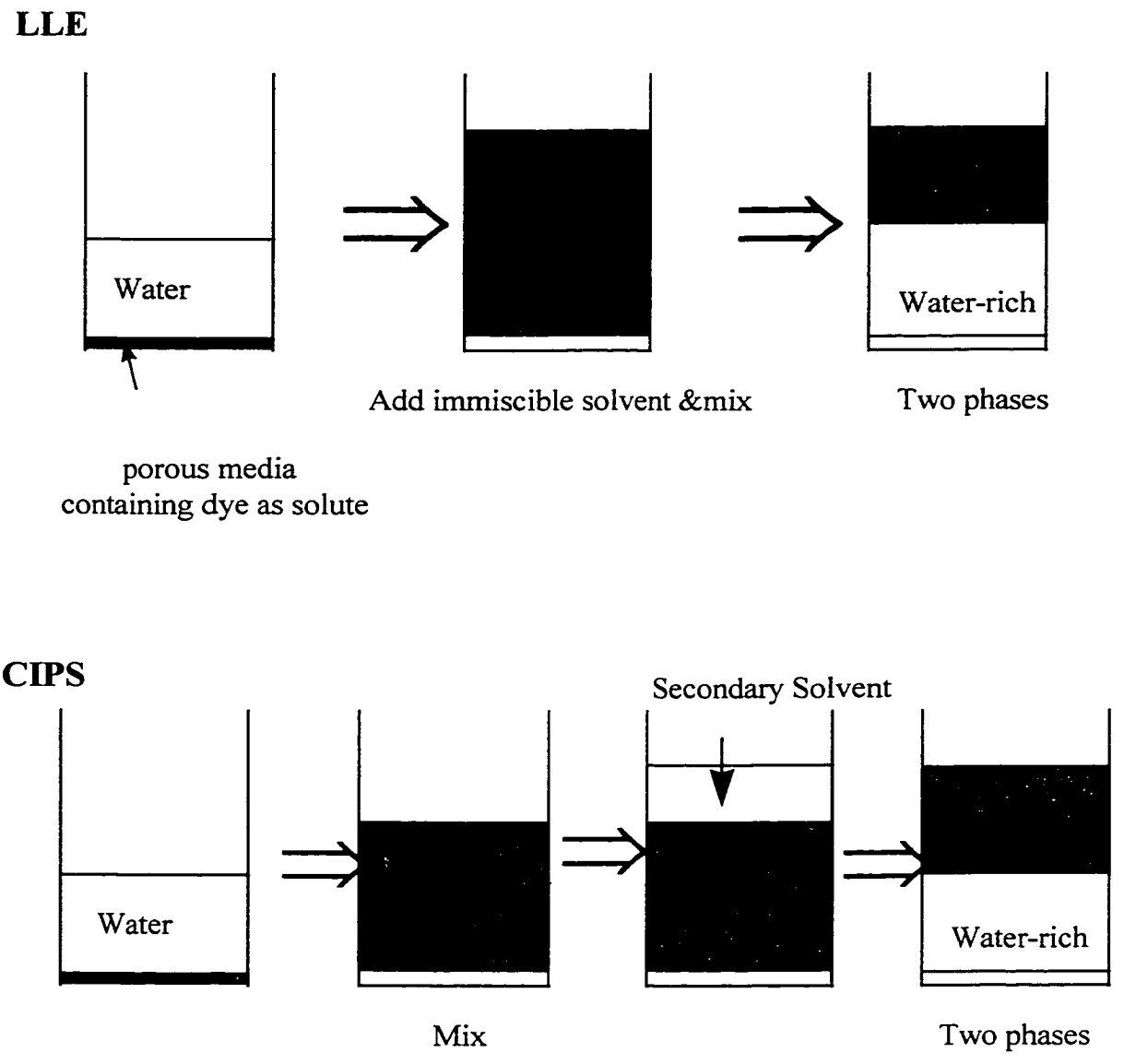

Figure 5.4: Extraction from porous media using LLE and CIPS process.

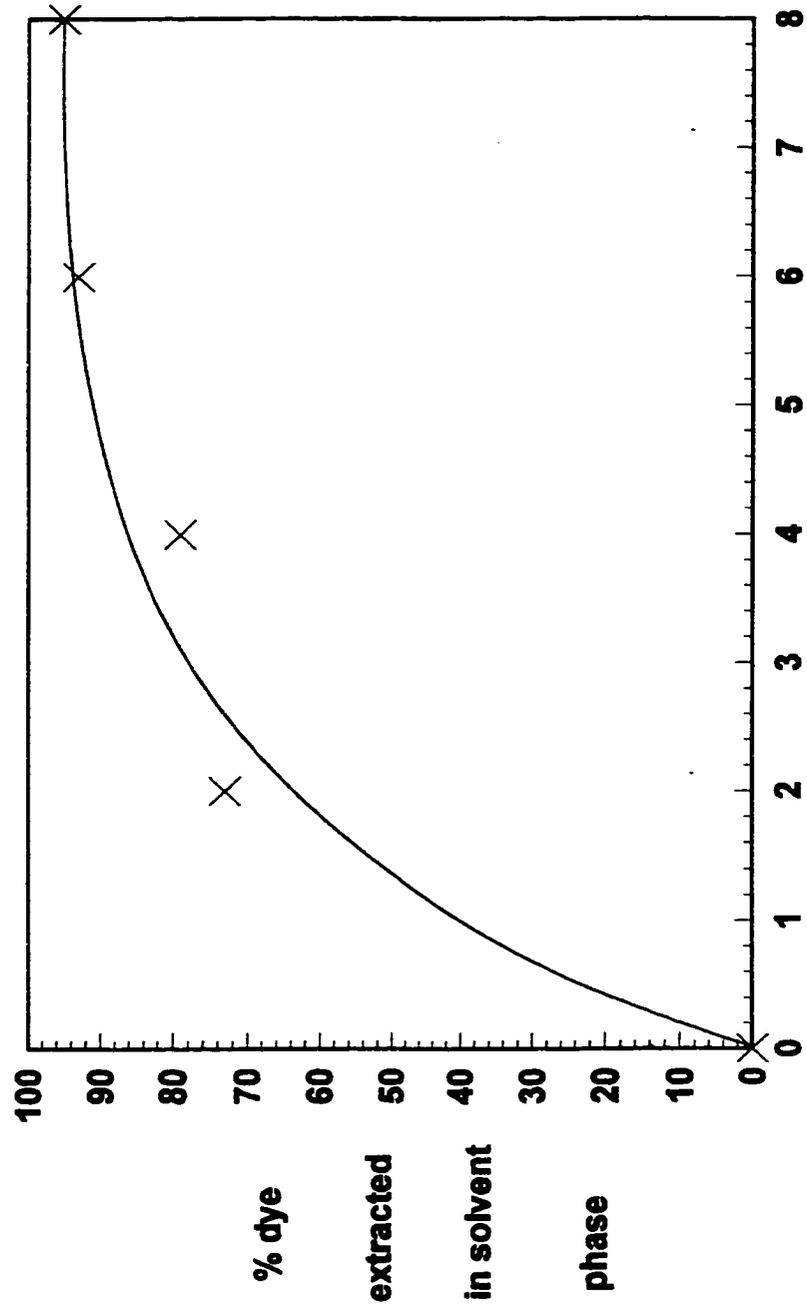

Figure 5.5: CIPS: ACN, Water, MIBK, 2ppm dye, 2% particles.

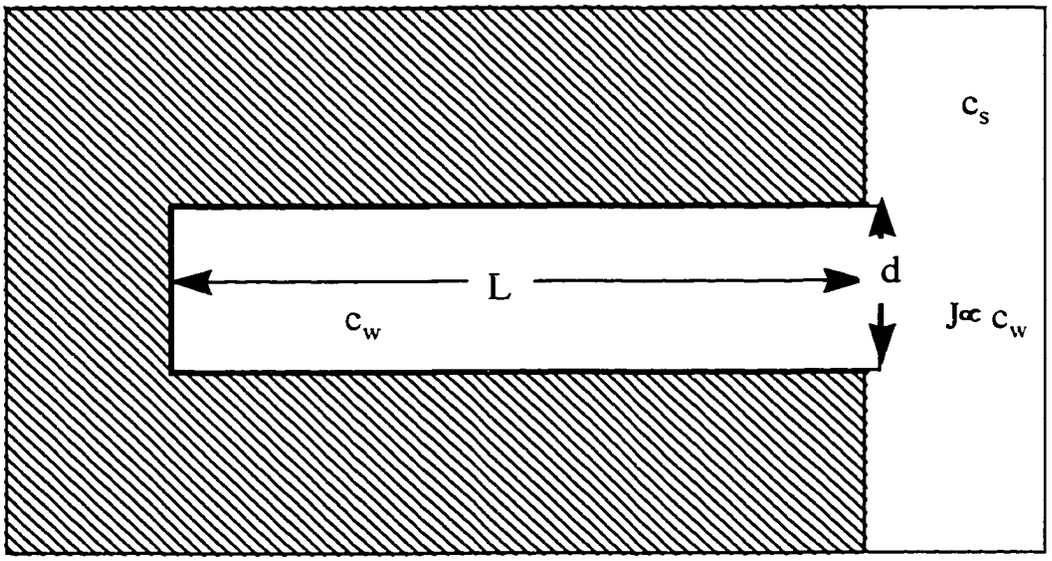

Figure 5.6: Schematics of the pore geometry.

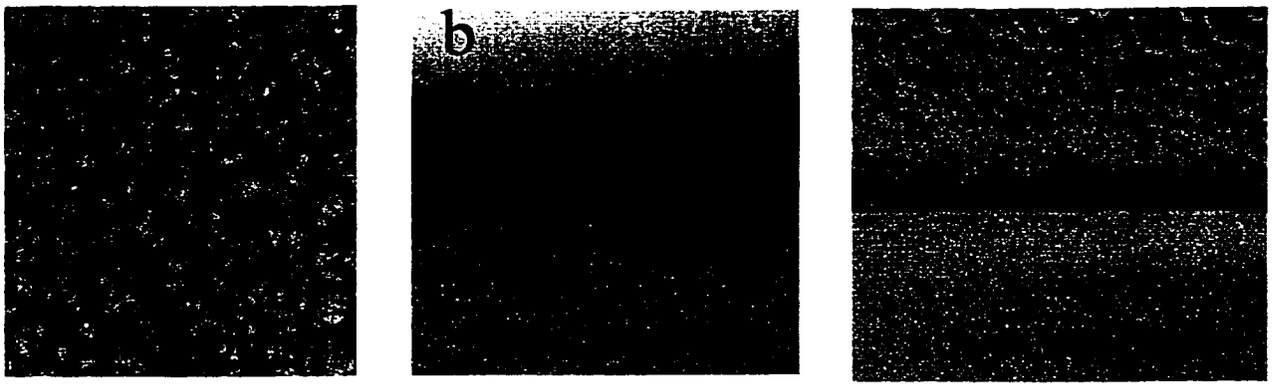

Figure 5.7 : Morphology of the liquid mixture in its two-phase state after it has been mixed isothermally.

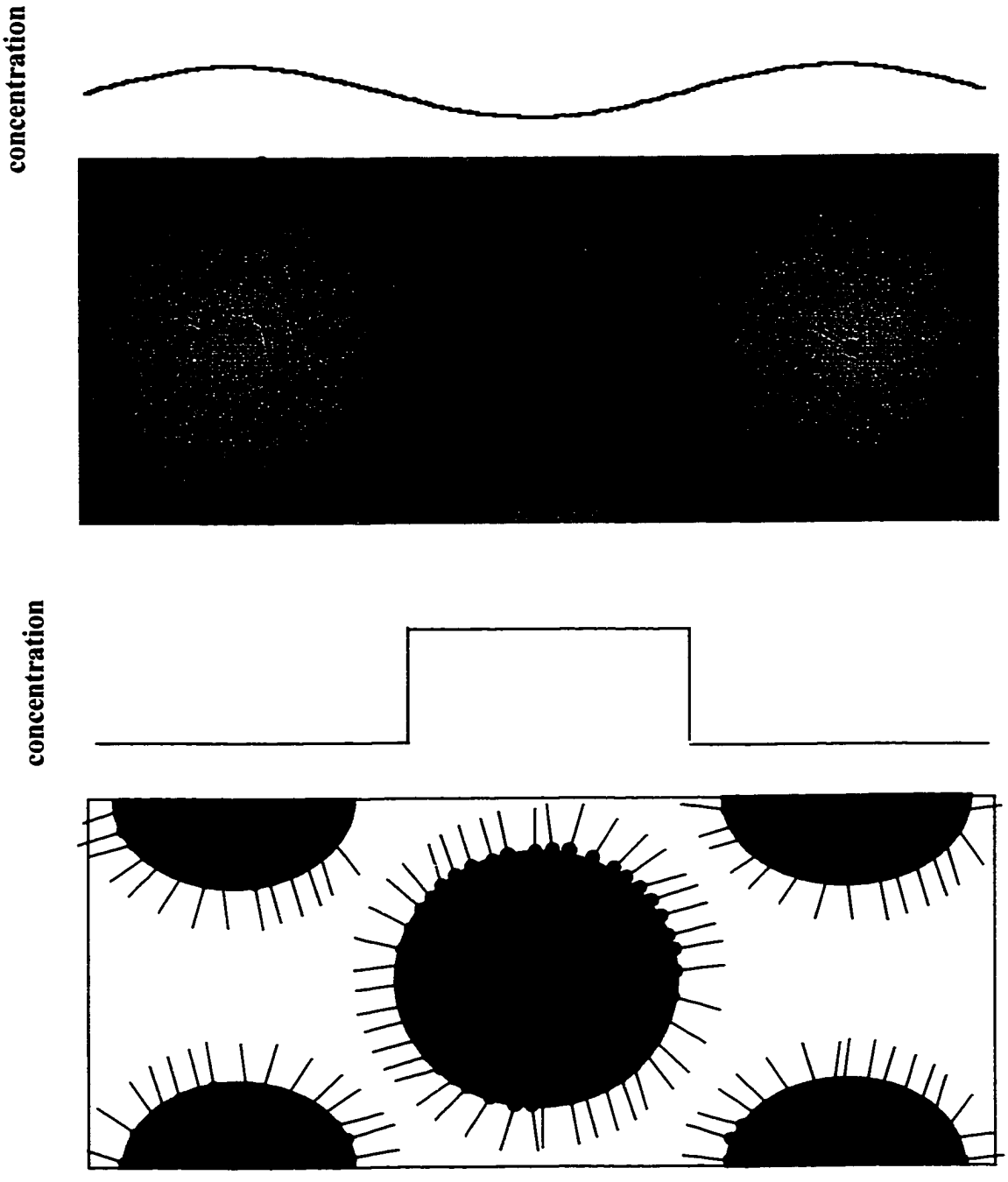

Figure 5.8: Distribution of surfactant molecules at the early stage of phase separation (above), and after the formation of single-phase domains (droplets), separated by sharp interfaces (below).

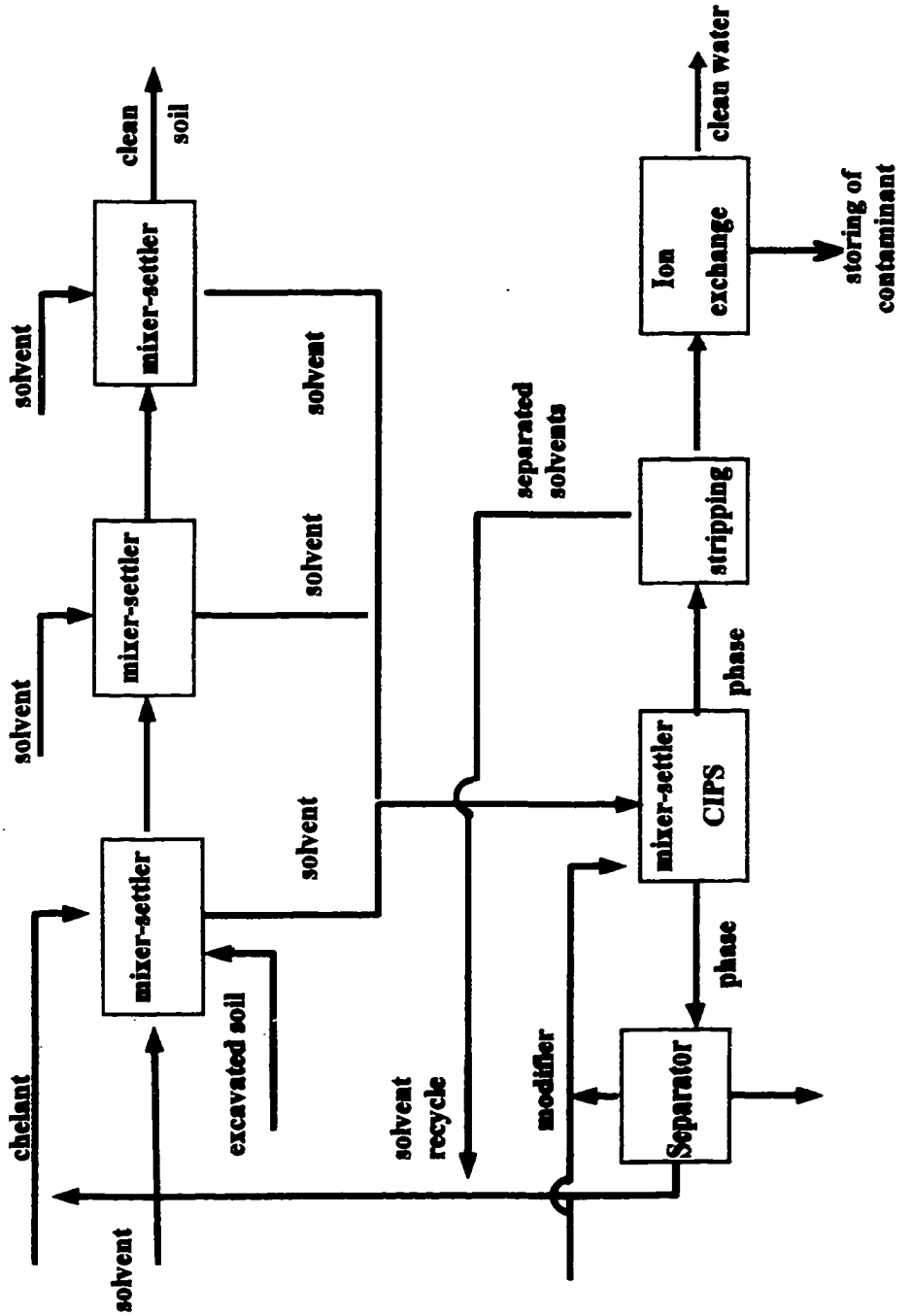

Figure 5.9: Schematics of the new soil remediation process.

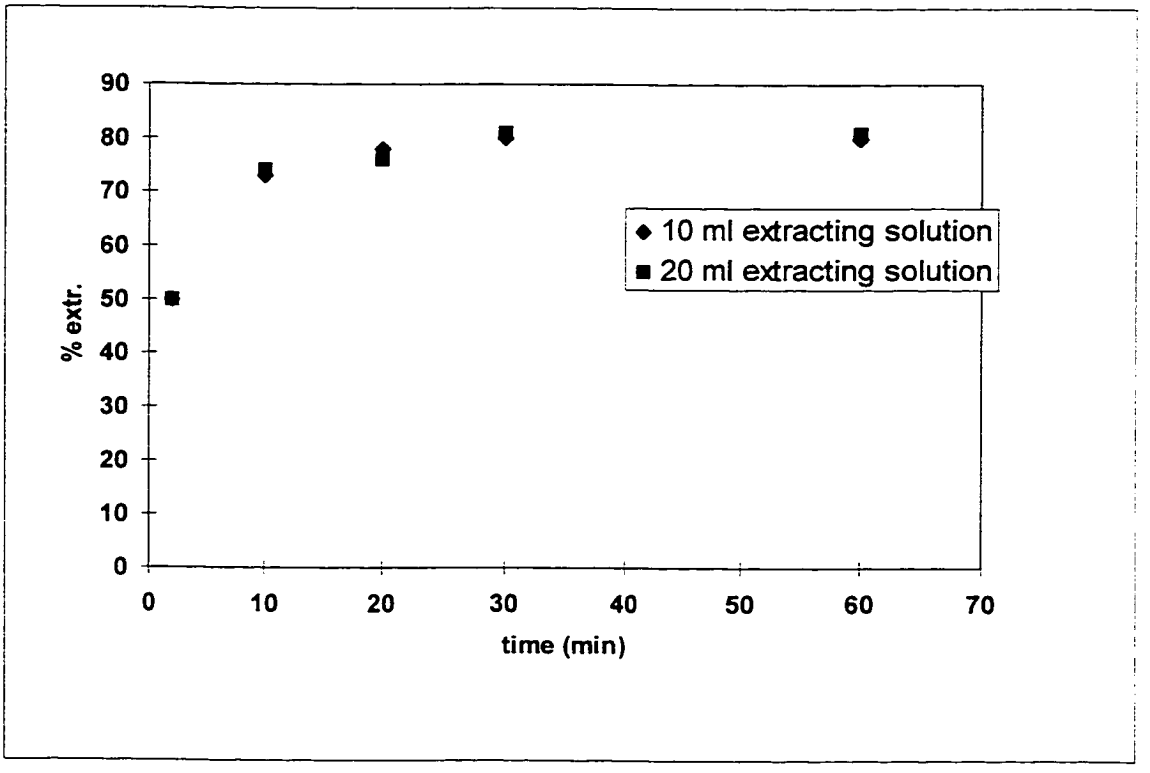

Figure 5.10: Recovery of the iron ions as a function of time.
Per each gram of soil, we have used 10 ml and 20 ml of a extracting solution.

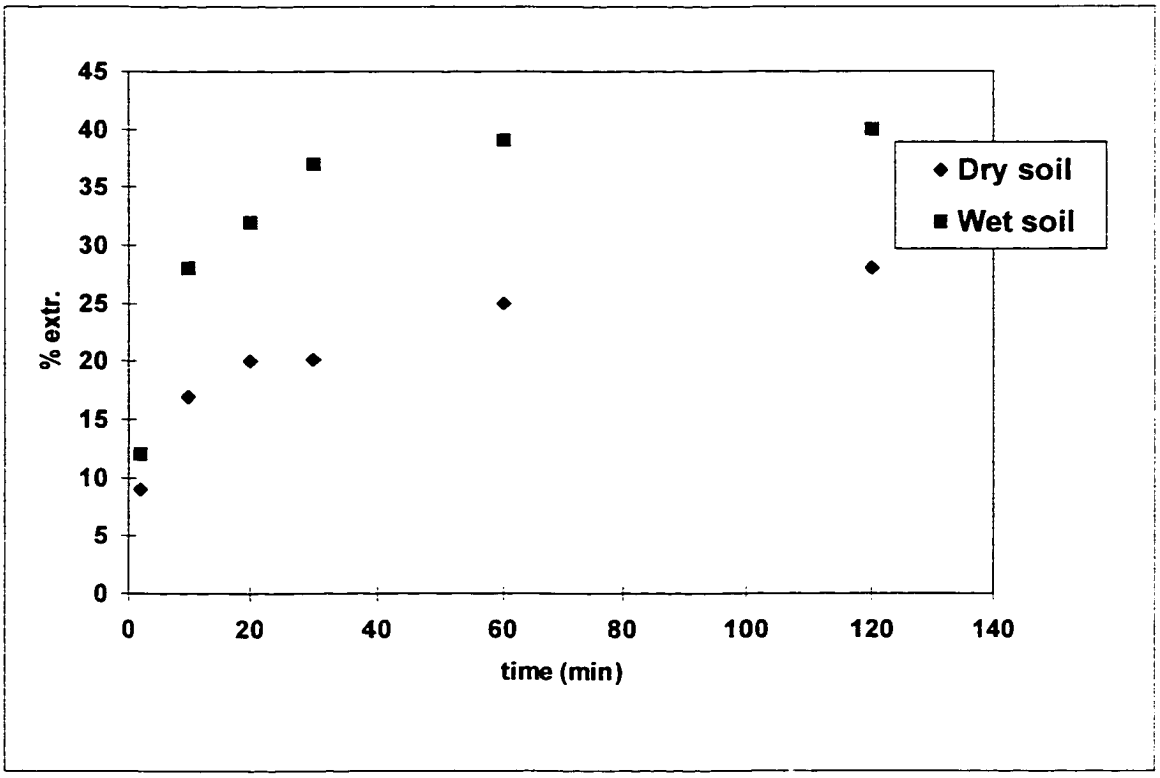

Figure 5.11: Recovery of the chromium ions as a function of time.
Per each gram of soil, we have used 20 ml of a
99% water - 1% ethanol solution,
with a 5:1 Diphenylcarbazide to chromium ions molar ratio.

Table 5.1: Equilibrium Data of LLE and CIPS Extraction Processes

	Global Composition	Solvent Phase Composition	Water Phase Composition	Ratio, solvent phase to water phase	% dye solvent phase	% dye water phase	% dye solid phase	p_{pw}	p_{sw}
LLE	50% MIBK, 50% Water, Total 200cc	98% MIBK, 2% Water, Total 100cc	3% MIBK, 97% Water, Total 100cc	1	44	9	47	263	5
LLE/ CIPS	25% MIBK, 25% ACN, 50% Water	59% MIBK, 35% ACN, 6% Water	3% MIBK, 18% ACN, 79% Water	0.82	95	4	1	22	25
CIPS*	33.3 % ACN 66.6% Water				99		1	0.75	

* before modifier addition to homogeneous phase; solvent phase = water phase

p_{pw} = conc. of dye in particle phase/ conc. of dye in water rich phase
p_{sw} = conc. of dye in solvent rich phase/ conc. of dye in water rich phase

All concentrations are based on unit weight.
All partition coefficients were measured separately.

Table 5.2: Experimental (τ) and predicted (τ`) values of the extraction relaxation time.

	Global Composition	τ	$p_{pw}(1- m_p/m_{total})$	τ`
LLE	50% MIBK, 50% Water, Total 200cc	40 min.	140	70 min.
LLE	25% MIBK, 25% ACN, 50% Water	10 min	22	11 min.
CIPS*	25% MIBK 25% ACN, 50% Water	< 2 min.	0.75	45 sec.

* *Before modifier addition to homogeneous phase; solvent phase = water phase*

Table 5.3: Extraction of Chromium (VI) ions from soil.

Step I: Amount of Cr(VI) ions adsorbed by the soil			**Cr(VI) in water before mixing**	**Cr(VI) in water after mixing**	**Cr (VI) adsorbed by soil**	**Percent of Cr(VI) adsorbed by soil**	
			0.2 mg	0.154 mg	0.046 mg	23%	
Step II: Cr(VI) extraction from soil[1]			**Cr(VI) in soil initially**	**Cr(VI) in soil after process**	**Cr(VI) extracted**	**Percent of Cr(VI) extracted**	**Partition coefficient**
Case A	Cr(VI) extracted from 1 g of dry soil using an extracting solution (vol. V) composed of 50% water and 50% acetone.	V = 20 ml	0.046 mg	0.0308 mg	0.0152 mg	33%	0.025
		V = 40 ml	0.046 mg	0.0234 mg	0.0226 mg	49%	0.024
Case B	Cr(VI) extracted from 1 g of wet soil using 20 ml of the following extracting solutions:	50% water and 50% acetone.	0.046 mg	0.0266 mg	0.0194 mg	42%	0.036
		99% water and 1% acetone.	0.046 mg	0.0264 mg	0.0196 mg	42%	0.036
		99% water and 1% ethanol.	0.046 mg	0.026 mg	0.0200 mg	43%	0.038

[1] All cases use a 5/1 molar ratio of Diphenylcarbazide to chromium ions.

Table 5.4: Extraction of Cadmium ions from soil.

Step I: Amount of Cd ions adsorbed by the soil	**Cd in water before mixing**	**Cd in water after mixing**	**Cr (VI) adsorbed by soil**	**Percent of Cd adsorbed by soil**
	0.6 mg	0.422 mg	0.178 mg	29%

Step II: Cd extraction from soil	**Cd in soil initially**	**Cd in soil after process**	**Cd extracted**	**Percent of Cd extracted**	**Partition coefficient**
Cd extracted from 1 g of wet soil in two successive extractions using 20 ml of a 99% water and 1% ethanol.	0.046 mg	0.0308 mg	0.0152 mg	33%	0.025
	0.046 mg	0.0234 mg	0.0226 mg	49%	0.024

Chapter 6

Conclusions

6.1 Dynamics of the phase separation in liquid mixtures

In this work, phase separation of fluid mixtures is studied experimentally by direct visualization in the range 10-400 μm. The system is quenched to a reduced temperature $|T - T_c|/T_c \sim 0.1$, with quenching rate $dT/dt \sim 3°C/s$. Two experimental procedures are considered. In the first, so-called "homogeneous" case, the solution is first heated to a temperature above the coexistence curve, then mixed thoroughly, and finally it is quenched back to the initial temperature, below the coexistence curve. In the second, so-called "gradient" case, after being heated, the solution is kept at the high temperature for two hours without mixing, and only then it is quenched. In the gradient case we see that before the quench the mixture is still mostly demixed, with the exception of a thin, few millimeters thick layer around the phase interface, where a concentration gradient is present.

In the homogeneous case we find that, as in the case of shallow quenches, interconnected domains and well-separated droplets are formed, depending on whether the system undergoes critical or off-critical quenches, respectively. As expected, we find that the typical size of single-phase domains grew linearly in time, with a growth rate $dR/dt \sim 100\ \mu m/s$, which is a few order of magnitude larger than that measured for shallow quenches. The growth rate that we obtain is about three times larger for interconnected domains than for droplets. This last result is new. In addition, since the equilibrium composition of the system keeps changing as the temperature of the mixture decreases, "double phase separation" is observed, thus confirming Tanaka's observations (Tanaka, 1995). The typical velocity of single-phase domains is also measured, obtaining a value, $\sim 100\ \mu m/s$, which is of the same magnitude as the growth rate.

In the gradient case, focusing the experimental apparatus on the region presenting a sharp initial composition gradient, we see that, after the quench, the system remains unchanged for about 3 seconds, until suddenly a sharp interface appears. Only then, we see drops appearing and moving towards the interface, where they coalesce. At later times, analyzing the few scattered drops that are suspended within the mixture, forming what in the engineering literature is called secondary emulsion, we find that their mean radius R grow in time as t^{γ}, where the exponent $\gamma = 0.30 \pm 0.04$ is in agreement with the theory of Lifshitz and Slyozov (Lifshitz and Slyozov, 1961).

The behavior of a phase-separating mixture is well described by the model H (Hohenberg and Halperin, 1977), which predicts that after an initial diffusion-driven stage leads to a non-uniform concentration field, a concentration-gradient-induced material flux

is generated, which is orders of magnitude larger than its diffusive counterpart, and drives the successive process of phase segregation. Based on this model, we derive an expression estimating the growth rate of single-phase domains [cf. Eqs. 4.14 and 4.15], which is in excellent agreement with our experimental results. In addition, the presence of this concentration-gradient-induced driving force explains why in the gradient case we do not observe any drop large enough to be observed using our experimental apparatus.

6.2 Phase separation of liquid mixtures in the presence of surfactants

Here, we compare two different processes involving mixtures of two partially miscible liquids, initially in their two-phase state: in the former, the mixture is agitated isothermally, while in the latter it is heated and cooled across its miscibility curve, inducing phase transition. The most important result of this study is that while, as expected, coalescence rate and settling time in the first case are strongly influenced by the presence of emulsifiers within the mixture, this is not so when the mixture undergoes phase transition. In fact, we found that in this case phase separation was rapid, irrespective of whether surface-active compounds were added.

In this work, we offer a clear explanation of this phenomenon. First, we show by microscopic visualization that the morphology of a liquid mixture in the presence of surfactants after isothermal mixing and that during phase separation are radically different from each other. The emulsions that form after isothermal mixing are composed of a tightly packed suspension of micron-size drops, which hardly move, and coalesce only at

the edge of the emulsion region. This accounts for the slow settling time observed macroscopically, and the fact that the presence of surface-active compounds does stabilize the emulsion. On the other hand, when the mixture is brought across its miscibility curve, it is composed of drops moving rapidly and coalescing, revealing that the process is driven by convection and not by diffusion. This conclusion is confirmed by the fact that at the end of phase separation, the partition coefficient of a solute (i.e. the ratio between its concentration within the two phases) equals its equilibrium value, irrespective of the molecular weight of the solute. In fact, we saw that the extraction times of crystal violet and blue dextran were the same, although these compounds have 407 and 2,000,000 molecular weights, respectively.

These experimental results are explained, at least qualitatively, using the model *H*, where fluid convection is driven by a body force F_ϕ, which is proportional to the gradients in the system composition. The model *H* predicts that after an initial stage, characterized by long range concentration fluctuations, the system separates into single phase domains, with sharp interfaces. The body force can be identified with the traditional capillary interaction, which drives the motion of the single phase domains and acts as an attractive interparticle force. As surfactant molecules are convected by the fluid motion, they rapidly cluster on the droplet interfaces, inducing electrostatic repulsion. A simple dimensional analysis shows that the coalescence-enhancing attractive capillary force F_ϕ is much larger than the repulsive force among drops, which is due to the presence of surfactants, thereby showing why indeed surface active compounds do not appear to influence the settling time of phase separating liquid mixtures.

6.3 Concentration-Induced Phase Separation Process

In this work we also present a novel separation method named Concentration Induced Phase Separation or CIPS. The CIPS process is composed of two mixing stages: first, the system to be extracted is mixed with a primary solvent, which is soluble with the native solvent; then, a modifier is added, which is insoluble with either the native or the primary solvent. Immediately after the addition of the modifier, the system separates rapidly into two coexisting phases, even in the presence of emulsion-forming impurities.

CIPS is conceptually similar to the Temperature-Induced Phase Separation, or TIPS, described in Ullmann *et al.* (1995), where a mixture of native and primary solvents is heated and cooled across its coexistence curve. In fact, when the same solvent system is used, CIPS gives the same results as TIPS, provided that the temperature differential of TIPS is workable. The similarity of the two methods was demonstrated experimentally.

The advantages of CIPS over the conventional Liquid-Liquid Extraction, or LLE, process can be summarized as follows.

- **Improved extraction yield.** When the solute is adsorbed on solid particles, CIPS has a clear advantage over LLE, since, by using primary solvents that are miscible with the native solvent, it does not have the wetting problems that are encountered in LLE, where insoluble or partially miscible solvents are used. This is particularly important in the extraction of natural products and fermentation broths.

- **Ability to handle emulsion-forming systems.** Unlike LLE, CIPS is almost unaffected by the presence of surface-active agents, and no stable emulsions are formed.
- **Equipment savings.** Since we do not need to use centrifuges to break stable emulsions, as we do when using the traditional LLE process, the equipment required to perform CIPS is only a tank. Even when a distillation equipment is required to separate the primary solvents from the modifier, CIPS is still significantly cheaper to perform than LLE.
- **Lower product degradation.** Any possible shear stress damage to large solute molecules is prevented in the CIPS process, where only a mild mixing is required, as opposed to the high centrifugation of traditional LLE. In addition, the fact that in the CIPS process a small amount of the native solvent is contained in the extract will help preventing the unfolding of large solute molecules, such as proteins.
- **Use of water-soluble solvents.** The CIPS process allows the use of water-soluble solvents, which, despite being in general good solvents of biological materials, cannot be used in conventional extraction processes.

Now, most of these advantages over traditional LLE are also shared by TIPS. Like the CIPS process, TIPS takes place rapidly, and is not much affected by the presence of surface active agents in the native system. In addition, since during the heating stage the native and primary solvents are miscible, the resistance to extraction of the solute through the cell interfaces is greatly reduced; in fact, we found that when we used the same

solvents the extraction efficiency of the CIPS and TIPS processes was the same, and consistently larger than that of traditional LLE. Therefore it appears that TIPS, like the CIPS process, has many significant advantages over the traditional LLE process, at least for cases in which either stable emulsions are formed or the solute is sensitive to shear. Yet, comparing CIPS with TIPS, we may conclude that CIPS has the following advantages:

- **Improved extraction yield.** Since there is no concern that high temperatures may be required to reach the single-phase region, the final compositions of the water-rich and solvent-rich phases can be adjusted over a wider range. Consequently, the partition coefficient of the solute to be extracted between the two phases can be higher, to achieve the desired separation.
- **No need for separate heat transfer equipment.** The extraction can be carried out in a single vessel, e.g., a fermentation vessel. Alternatively, low cost settlers may be used for large volume production. In addition, the difficulty of rapidly cooling large amounts of liquid is eliminated. In fact, since mixing is always much faster than cooling, the reemulsification that takes place during slow cooling cannot occur here.
- **Larger flexibility in the choice of solvents.** The range of primary and secondary solvents that can be used is much greater due to the elimination of the temperature constraint.

Conversely, TIPS has the following advantage over CIPS:

- **Possibility of multistage processes.** Since the same system of solvents is alternately heated and cooled, it is simpler to have multistage extractions.

However, this advantage must be weighted against the much higher single-stage efficiency of CIPS.

To conclude, we list the areas of applications where the PTE process may bring significant advantages. They include:

- **The extraction of a fermentation broth both in batch and continuous processes.** This avoids the need to centrifuge and gives better yields due to better contact during the mixing stage.
- **The extraction of different compounds from natural plants or animal materials.** Due to the presence of a single water-rich phase, improved contacting between the solvent and the material to be extracted is achieved. Here there is no water-solvent interface and no wetting problems, and the solvent can easily penetrate the cell walls, thereby increasing the yield of the process.
- **Replacement of solvents which are environmentally objectionable,** e.g. in extraction processes using chlorinated solvents. The CIPS process is not only more powerful and versatile, but also permits the use of solvents which are environmentally friendly.

Appendix A

Measurement of the Diffusion Coefficient

An experimental study was performed to find the diffusion coefficient of our solvent mixture. Two cases were considered, a) solvent diffusing into another solvent, and b) dye diffusion into the solvent. Using these diffusion coefficient values we get an estimate of the concentration fields of solvent and dye inside the cell in the Gradient Case.

1) Solvent Diffusivity: Here, we measure the diffusivity of water in acetonitrile. We start with an initial condition, where the lower 1 *cm* part of a vial is filled with pure water, and the upper 1 *cm* of vial contains acetonitrile. Since the two liquids are miscible at room temperature, they start diffusing into each other. Using a syringe, we take the samples out at the known time and position, and analyze it using GC. The analysis of the phase composition was conducted using an HP 5890 Gas Chromatograph. The GC conditions are given in Table C.3 (Appendix C).

To find the equilibrium concentration, we first mix the solution, and then analyze it. It should be mentioned here that to find concentration at different times, different vials were taken for each data point. Each data point on the figure is an average of the three data points. Also, in the vial we add teflon beads to, a) avoid any disturbance in the solution while taking the solvent out, and b) to break convection currents that may develop in absence of beads. Now we plot these data points and fit for unknown value of diffusion coefficient D using the following equation:

$$\frac{C(z,t)}{C_\infty} = 1 + \frac{4}{\pi}\sum_{n=1}^{\infty}\frac{(-1)^n}{(2n-1)}\cos\left(\frac{(2n-1)}{2}\frac{\pi z}{L}\right)\exp^{-\alpha_n^2 Dt}; \alpha_n = \left(\frac{2n-1}{2L}z\right) \quad ...(1)$$

On fitting data points as in Figure A.1 using the above equation, we find $D_{acetonitrile\text{-}water} \approx 8 \times 10^{-5}\ cm^2/s^1$. This value can now be used to get the concentration field of solvent inside the solution for various times.

Figure A.1: Water diffusion in ACN.

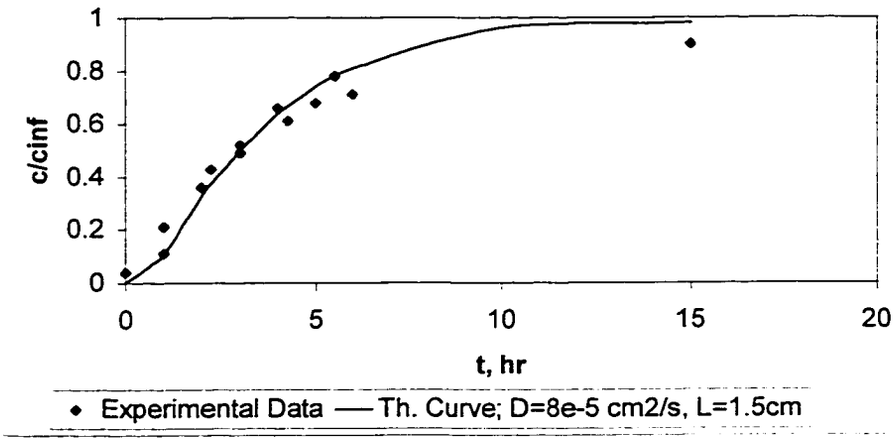

2) Dye Diffusivity: We take the same vial set up, as described earlier, but here, we do the measurements using He-Ne Laser. Since our crystal violet dye or Oil Red O dye have a different peak absorbance wavelength (590 and 514 *nm* respectively) than the laser (633 *nm*) used, we choose Blue Nile dye to match the laser wavelength. This dye has also same order of molecular weight as like other mentioned dyes. Dye color stability with time was checked, and it was found that Blue Nile does not lose its absorbance

[1] Wilke-Chang equation for dilute solution estimates $D_{water\text{-}acetonitrile} \approx 4\times10^{-5}$ cm^2/s.

capacity in our experimental time frame. It was also confirmed that it does not get absorb or react with the teflon beads. We start with an initial condition, where the lower 1 *cm* part of a vial is filled with water + dye, and on top of it we have 1 *cm* water layer with no dye. The dye concentration is then measured in terms of voltage using our experimental set up (Figure A.2), and calculated using a pre-determined calibration curve (Figure A.3). The data points (Figure A.4) are fitted for the diffusion coefficient, D, as before. This gives $D_{water\text{-}dye} \approx 3 \times 10^{-5}\ cm^2/s$, confirming that the dye used diffuses slower than the solvent.

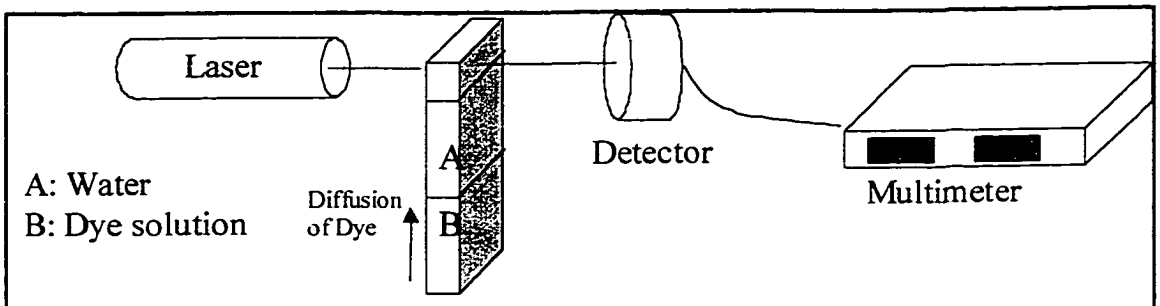

Figure A.2: Dye diffusion coefficient measurement using He-Ne Laser.

Figure A.3: Calibration curve of Blue Nile dye

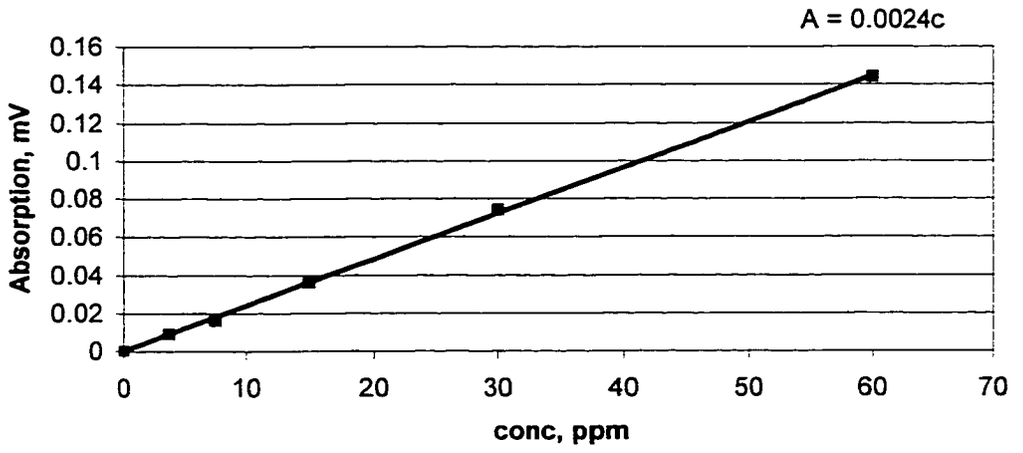

Figure A.4: Blue Nile diffusion in Water

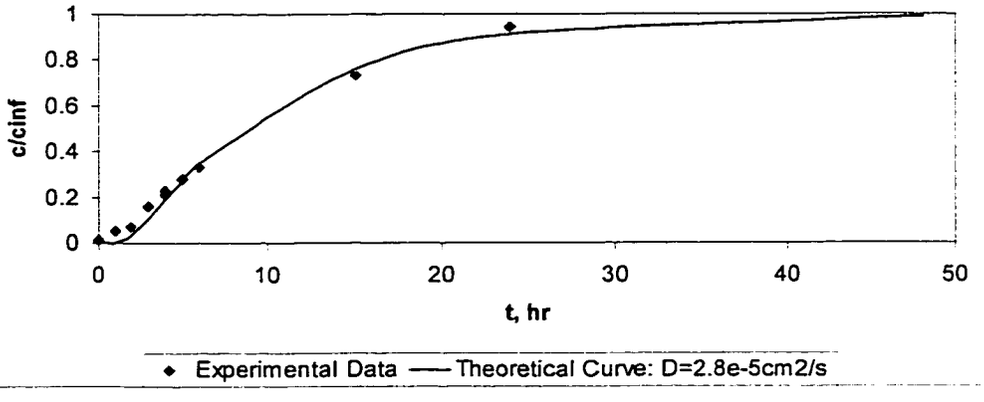

Appendix B

Phase Dynamics Modeling

Here we intend to extend and generalize the model developed previously (Mauri *et al.* (1996)). The base of this theoretical approach is thermodynamic theory proposed by Cahn and Hilliard (1958, 1959). We study the initial stages of separation, neglecting the non-linear terms. This approximation is satisfactory for very short times. Unlike previous treatments, we here consider that for deep quenches the Margules coefficient Ψ changes with time and position.

Linear stability analysis for deep quenches

We consider the homogeneous mixture of two species A and B with mole fraction $\phi_A = \phi$ and $\phi_B = 1-\phi$, respectively, contained in a closed vessel at pressure P, and initially at temperature T_0. Assuming that convection is negligible (i.e., the viscosity of the system is very large), the generalized chemical potential $\tilde{\mu}$ can be expressed as (Mauri *et al.*):

$$\tilde{\mu} = \mu_0 + \ln\frac{\phi}{1-\phi} + \underline{\psi}(1-2\phi) - a^2\nabla^2\phi \qquad \text{(B.1)}$$

where μ_0 is a constant.

Defining, $u = \frac{\phi - \phi_0}{\phi_0}$, and rewriting equation B.1 for $\phi_0 = 1/2$, we obtain:

$$\tilde{\mu} = \mu_0 + \ln\frac{1+u}{1-u} - u\underline{\psi} - \frac{1}{2}a^2\nabla^2 u \qquad \text{(B.2)}$$

which, for small u, reduces to

$$\tilde{\mu} = \mu_0 + 2u + \frac{2}{3}u^3 - u\underline{\psi} - \frac{1}{2}a^2\nabla^2 u \qquad \text{(B.3)}$$

Now, the continuity and constitutive equations are given by

$$\frac{\partial \phi}{\partial t} + \nabla . J = 0, \text{ where } \quad \boldsymbol{J} = - D \nabla \tilde{\mu} . \tag{B.4}$$

that is:

$$\frac{\partial u}{\partial t} = D\left(-2\psi \nabla^2 u - 4\nabla u \nabla \psi - 2u\nabla^2 \psi - a^2 \nabla^4 u\right) \tag{B.5}$$

with $\psi = \underline{\psi} - 2$

Nondimensionlizing in terms of the macroscopic half thickness, L, of cell, we obtain:

$$\frac{\partial u}{\partial t} = \frac{D}{L^2}\left(-2\psi \overline{\nabla}^2 u - 4\overline{\nabla} u \overline{\nabla} \psi - 2u\overline{\nabla}^2 \psi - \frac{a^2}{L^2}\overline{\nabla}^4 u\right) \tag{B.6}$$

Here, since a is very small in comparison to the macroscopic dimension considered, we neglect the last term. Rewriting this equation in 1-D and defining $\tau_D = L^2/D$ we have,

$$\frac{\partial u}{\partial t} = = \frac{1}{\tau_D}\left(-2\psi \; u_{\bar{z}\bar{z}} - 4u_{\bar{z}}\psi_{\bar{z}} - 2u\psi_{\bar{z}\bar{z}}\right) \tag{B.7}$$

subjected to

B.C's $\qquad \frac{\partial}{\partial \bar{z}}\left[(u\psi\right]\|_{\bar{z}=\pm 1} = 0$

I.C. $\qquad u = u_0 = 0 \qquad$ *at t=0.*

Margules Coefficient in terms of time and space

Since at time $t = 0$ the cell is put in contact with a heat bath at temperature T_∞ the temperature inside the cell is given by,

$$\frac{\partial T}{\partial t} = \alpha \frac{\partial^2 T}{\partial^2 z} \tag{B.8}$$

subjected to the following conditions,

B.C's $$\frac{\partial T}{\partial z}\Big|_{\bar{z}=\pm 1} = \mp \frac{h}{k}(T - T_\infty)$$

I.C. $$T = T_0$$

where, T_0 is initial temperature of the mixture.

The solution of the above equation for large Biot number is given by,

$$\frac{T - T_\infty}{T_0 - T_\infty} = \frac{4}{\pi} \sum_{n=1}^{\infty} e^{-n^2 \frac{\pi \alpha t}{4L^2}} \cos\left[(2n+1)\bar{z}\right] \tag{B.9}$$

where $\alpha = k/\rho c_p$.

Assuming that the coexistence curve can be approximated as a parabola,

$$\frac{T_c - T}{T_c} = 4\left(\phi_e - \frac{1}{2}\right)^2 \tag{B.10}$$

Near the critical point we find (Mauri *et al.* (1996)),

$$\left|\phi_e - \frac{1}{2}\right| = \frac{\sqrt{3}}{2}\left(\frac{\psi - 2}{2}\right)^{1/2} \tag{B.11}$$

After easy manipulation of above two equations, we see that,

$$T = T_c - \frac{3T_c}{\psi_c}(\psi - \psi_c) \tag{B.12}$$

which on substituting in eq. B.9 gives

$$\frac{\psi - \psi_\infty}{\psi_0 - \psi_\infty} = \frac{4}{\pi} \sum_{n=1}^{\infty} e^{-n^2 \frac{t}{\tau_T}} \cos\left[(2n+1)\bar{z}\right] \tag{B.13}$$

where, $\psi_0 = \psi(T_0)$ and $\psi_\infty = \psi(T_\infty)$, while $\tau_T = 4L^2/\pi\alpha$.

One of the interesting feature in expressing the above equations in terms of τ_D and τ_T is that, since the model depends on mixture properties only, it can predict the behavior of any liquid mixture. t is left in dimensional form to see the "real" time behavior.

Model predictions

Equation B.7 coupled with equation B.13 was analytically solved using the Implicit Crank-Nicolson method. In Figure B.1 the composition of the mixture is plotted as a function of space for short times ("real" time, $t << \tau_D, \tau_T$). It is observed that following a temperature quench a symmetric solution is obtained, as expected, with the mixture separating into two phases near the walls. The concentrations of two phases were found to grow exponentially with time, and this explains, to an extent, the fast phase separation process observed experimentally. The phase separation is observed to be fastest near to the wall. The region close to the center-line undergoes a much slower temperature change; which could explain the "secondary nucleation" observed in the late stages. This solution, however, does not give the steady state solution. This is because after some time non-linear terms become dominant and they can not be further neglected in the present linear analysis.

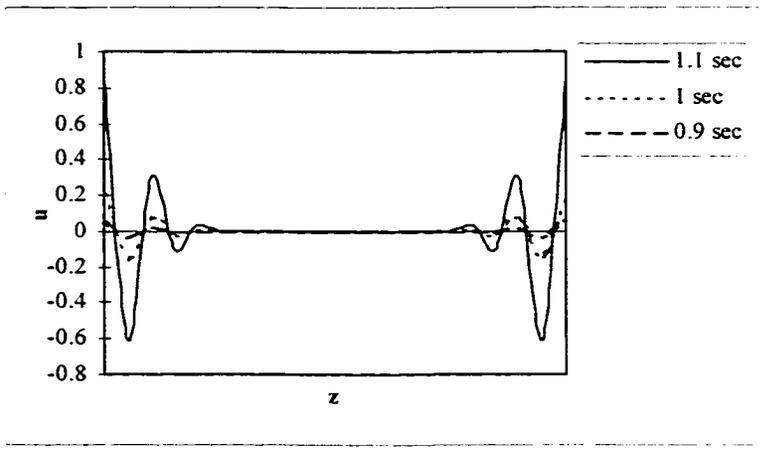

Figure B.1: Composition as a function of time and space.

Appendix C

Table C.1 - Characteristics of the Vesuvian soil.

pH (1/2.5 soil/water):	7.8
Composition	(% by weight)
Organic carbon	15.6
Silicon	20
Aluminum	10
Iron	7
Size Distribution	(% by weight):
Coarse (0.2-2 mm)	51.9
Fine (0.002-0.2 mm)	28.6
Silt (0.0002-0.002 mm	9.7
Clay (< 0.0002 mm)	9.8

Table C.2 - Characteristics of the Appalachian soil.

pH (1/2.5 soil/water):	7.8
Composition	(% by weight)
Organic carbon	18.6
Silicon	14.5
Aluminum	13
Iron	9
Size Distribution	(% by weight):
Coarse (0.5 – 0.2 mm)	24.4
Fine (0.2-0.02 mm)	39.6
Silt (0.02-0.002 mm)	18.8
Clay (< 0.0002 mm)	17.2

Table C.3: GC conditions for water-ACN-toluene analysis.

Oven temperature	110°C
Detector temperature	160°C
Inlet temperature	160°C
Column flow	5 cc/min
Column + auxiliary flow	35 cc/min
Column + auxiliary flow + reference flow	80 cc/min
capillary column	0.53 μm
sample size	0.1 μl

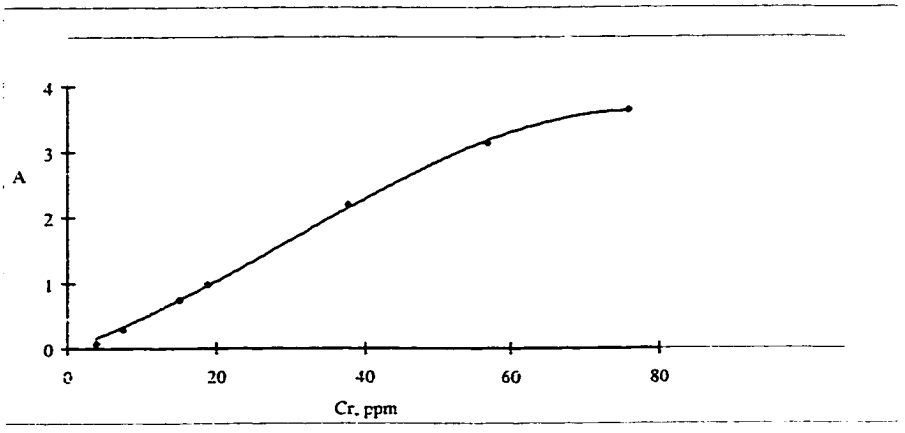

Figure C.1: Calibration curve of iron ion complex in 50% water and 50% acetonitrile solution, in which 1,230 ppm of 8-Hydroxyquinoline are dissolved.

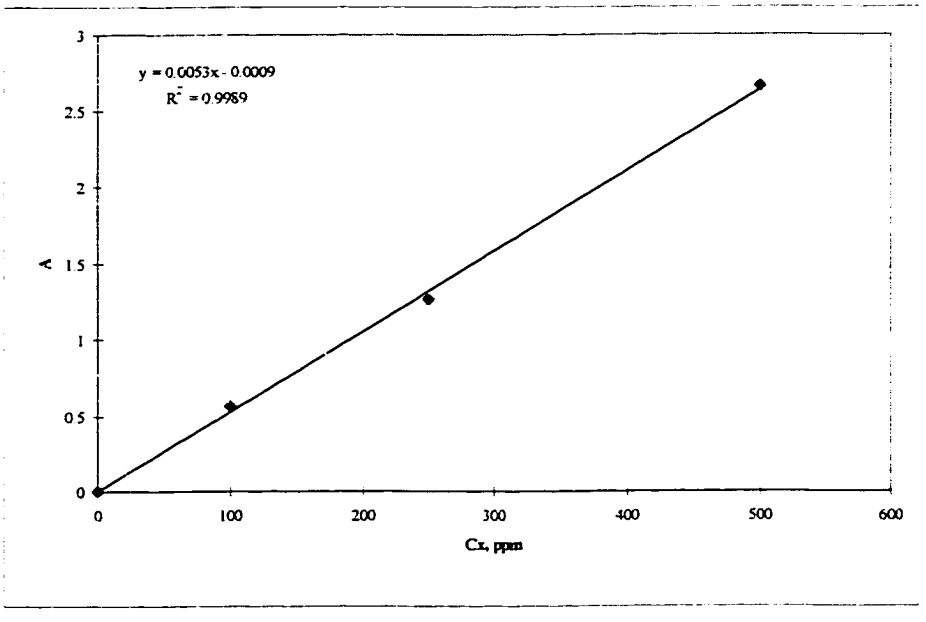

Figure C.2: Calibration curve of chromium ion complex in 50% water and 50% acetone solution, in which 500 ppm of Diphenylcarbazide are dissolved.

References

1. Adamson, A.W., *Physical Chemistry of Surfaces*; John Wiley and Sons, New York, 1967.
2. Bates, F.S., and Wiltzius, P., *J. Chem. Phys.* **91**, 3258, 1989.
3. Beysens, D., Guenoun, P., Sibille, P. and Kumar, A., *Phys. Rev. E* **50**, 1299, 1994.
4. Binder, K., Nucleation Barriers, Spinodals, and the Ginzburg Criterion, *Phys. Rev. A* **29**, 341, 1984.
5. Brauer, S.L. and Wetterhahn, K., *J. Am. Chem. Soc.* **113**, 3001-3007, 1991.
6. Cahn, J.W., Hilliard, L.E., *J. Chem. Phys.* **28**, 258, 1958; **31**, 688, 1959.
7. Cavanaugh, T.J., Russo, A.P. and Nauman, E.B; Designing Polymer Blends, *CHEMTECH* 32-37, 1996.
8. Cheng, K.L., Ueno, K., Imamura T., *Handbook of Organic Analytical Reagents*; CRC Press: New York, 253-267 and 277-283, 1982.
9. Chou, Y.C. and Goldburg, W.I., *Phys. Rev. A* **20**, 2105, 1979; **23**, 858, 1981.
10. Church, J.M. and Shinnar, R., Stabilizing Liquid-Liquid Dispersions by Agitation, *Ind. Eng. Chem.* **53**, 479-484, 1961.
11. Cohn, R.H., and Jacob, D.T., Acetone Impurity Effects on Binary Fluid Mixture Methanol-Cyclohexane, *J. Chem. Phys.* **80**(2), 856, 1984.
12. Cummins, H.Z. and Levanyuk, A.P., *Light Scattering Near Phase Transitions*, North-Holland Publishing Company, 1983.
13. Cumming, A., Wiltzius, P., Bates, F.S. and Rosedale, J.H., *Phys. Rev. A* **45**, 885, 1992.
14. Cussler, E.L., *Diffusion: Mass transfer in fluid systems;* Cambridge University Press, Cambridge, 1991.
15. de Gennes, P.G., Dynamics of Fluctuations and Spinodal Decomposition in Polymer Blends, *J. Chem. Phys.* **72**(9), 4756, 1980.
16. Debenetti, P.G., *Metastable Liquid Concepts and Principles*; Princeton University Press, Princeton, NJ, 1996.
17. Domb, C. and Green, M.S., *Phase Transition and Critical Phenomena*; Academic Press, NY, 1972.
18. Domb, C. and Lebowitz, J.L., eds., Academic Press, London, 1983.

19. Edler, P.M., *Porous Media: Geometry and Transports*; Butterworth Heinemann, 1992.

20. Eliyahu, N. and Ludmer, Z., Mass Transfer across Microorganism Cell Walls and Phase Separation during Batch Extraction with Organic Solvent Mixtures, *Abstracts of Papers*, 1995, AIChE Annual Meeting, Miami, FL; American Institute of Chemical Engineers: New York, 1995.

21. Farrell, J.E. and Valls, O.T., Spinodal Decomposition in a Two-Dimensional Fluid Model, *Physical Review B* **40**, 7027, 1989; **43**, 630, 1991.

22. Francis, A.W., *Critical Solution Temperatures*, Advances in Chemistry, Series 31, American Chemical Society, 1961.

23. Froment, G.F. and Bischoff, K.B., *Chemical Reactor Analysis and Design*; Wiley, New York, 267, 1979.

24. Gordon, P.; *Principles of Phase Diagrams in Material Systems*; McGraw-Hill Book Company, 1968.

25. Gu, T., Gu, Y., Zheng, Y., Wiehl, P.E., Kopchick, J.J., Phase Separation of Acetonitrile-Water Mixture in Protein Purification, *Separation Technology* **4**, 258-60, 1994.

26. Guenoun, P., Gastaud, R., Perrot, F., and Beysens, D., Spinodal Decomposition Patterns in an Isodensity Critical Binary Fluid: Direct-Visualization and Light-Scattering Analyses, *Physical Review A* **36**, 4876, 1987.

27. Guillaume, Y.C. and Guinchard, C.; ACN Clusters in Water/ACN Mixture, with Implications for the RPLC Weak Polar Solute Retention, *Analytical Chemistry* **69**, 183-9, 1997.

28. Gunton, J.D., Miguel, M.S., Sahni. P.S., *Phase Transition and Critical Phenomena*, Vol. 8; Academic Press, London, 267-421, 1983.

29. Gupta, R., Mauri, R., Shinnar, R., Liquid-Liquid Extraction using the Composition-Induced Phase Separation Process, *Ind. Eng. Chem. Res.* **35**, 2360-2368, 1996.

30. Hales, B.J., Bertrand, G.L., and Hepler, L.G., *J. Phys. Chem.* **70**, 3970, 1966.

31. Hashimoto, T., Nishimura, K., Takeuchi, Y., *Phys. Lett.* **65A**, 250, 1978

32. Hennion, M., Ronzaud, D., and Guyot, P., *Acta Metallica* **30**, 599, 1982.

33. Hono, K. and Hirano K.I., *Phase Transitions* **10**, 223, 1987.

34. Hunter, R.J., *Foundations of Colloid Science*, Vol. I, Ch. 7; Claredon Press, Oxford, 1986.

35. Katz, J.L. and Wiederisch, H. *J. Collid. Interf. Sci.*, **61**, 351, 1977.

36. King, M.E., Patha, R.W., Sontum, S.F., A Laser Refraction Method for Measuring Liquid Diffusion Coefficient, *Journal of Chemical Education*, **Sept. 1989**, *v.66*, p. 787-90.

37. Laddha, G.S. and Degaleesan, T.E., *Transport Phenomena in Liquid Extraction*, Tata McGraw-Hill, New Delhi, 1978.

38. Landdolt-Bornstein, *Numerical Data and Functional Relationships in Science and Technology*, II/2c: Solution Equilibria, 1964, Springer Verlag, 1950ff.

39. Langer, J.S., *Systems Far from Equilibrium*; edited by Garrido, Springer, Berlin, 1980.

40. Lifshitz, E.M. and Slyozov, V.V. *J. Phys. Chem. Solids* **19**, 35, 1961.

41. Littlewood, A.B., *Gas Chromatography: Principles, Techniques and Applications*, Academic press, 1970.

42. Ludmer, Z. and Shinnar, R., Solubility in Binary Mixtures at the Immiscibility Critical Point, *AIChE J.* **33**, 1776, 1987.

43. Ludmer, Z., Shinnar, R., Yakhot, V., Countercurrent Separation Process and Apparatus, *U.S. Patent*, No. 4,954,260, 1990.

44. Lupis, C.H.P, *Chemical Thermodynamics of Materials*, Elsevier, NY, 1983.

45. Mauri, R., Shinnar, R., Triantafyllou, G., Spinodal Decomposition in Binary Mixtures, *Phys. Rev. E.* **53**, 2613-2623, 1996.

46. McNair, H.M. and Bonelli, E.J.; *Basic Gas Chromatography*; Varien, 1968.

47. Nowakowski, B. and Ruckenstein, E., *J. Chem. Phys.* **94**, 1991, and references therein.

48. Rowlinson, J.S., *Liquid-Liquid Mixtures*; 2nd Edition, Plenum, NY, 1969.

49. Shinnar, R. and Mauri, R., Concentration Induced Phase Separation (CIPS) process, *U.S. Patent*, No. 8,274,546, 1995.

50. Shinnar, R., On the Behavior of Liquid Dispersions in Mixed Vessels, *Journal of Fluid Mechanics* **10**, 259-75, 1961.

51. Shumaker, M.M., *Enhanced Recovery of Residual and Heavy Oils*; Noyyes Data Co.: Park Ridge, NJ, 1980.

52. Siggia, E.D., *Physical Review A.* **20**, 595, 1979.

53. Snyder, R.B., and Eckert, C.A., *J. Chem. Engg. Data* **18**, 282, 1973.

54. Sorensen, J.M. and Arlt, W.; *Liquid-Liquid Equilibrium Data Collection*, Chemistry Data Series, Vol I-III, DECHEMA, Frankfurt, 1980.

55. Stephen, H., Stephen, T., and Silcock, H., *Solubilities of Inorganic and Organic Compounds*; 7 parts, Pergamon, 1979.

56. Stenland, C. and Pettitt, M., Binary-Solution Critical Opalescence, *Journal of Chemical Education* **72**, 560-4, 1995.

57. Stround, S.W. and Ransley, H.M.P., *British Patent*, 760, 351, (October 10, 1956).

58. Tanaka, H., *J. Chem. Phys.* **107**, 3734, 1997, and references therein.

59. Tanaka, H., Araki, T., Spontaneous Double Phase Separation Induced by Rapid Hydrodynamic Coarsening in Two-Dimensional Fluid Mixtures, *Phys. Rev. Lett.* **81**, 389, 1998.

60. Treybal, R.E., *Liquid Extraction*; McGraw Hill, New York, 1963.

61. Treybal, R.E., *Mass-Transfer Operations*; 3rd Edition, McGraw Hill, New York, 1981.

62. Tveekrem, J.L., and Jacob, D.T., Impurity Effects in Near-critical Binary-Fluid Mixture *Phys. Rev.*, **27(5)**, 2773, 1983.

63. Ullmann, A., *Liquid-Liquid Extraction Using Solvent Mixtures with Critical Points of Miscibility*; PhD Thesis, City University of New York, New York, 1993.

64. Ullmann, A., Ludmer, Z. and Shinnar, R., Novel Continuous Multistage Extraction Column Based on Phase Transition of Critical-Solution Mixtures, *Chemical Engineering Science*, **52**, 567-81, 1997.

65. Ullmann, A., Ludmer, Z. and Shinnar, R., Phase Transition Extraction Using Solvent Mixtures with a Critical Point of Miscibility *AIChE J.*, **41**, 488, 1995.

66. Van der Waals, J.D., Z. Phys. Chem. **13**, 657, 1894, reprinted in J. Stat. Phys. **20**, 200, 1976.

67. Vladimirova, N., Malagoli, A., Mauri, R., Two-dimensional Model of Phase Segregation in Liquid Binary Mixtures *Phys. Rev. E.*, submitted.

68. Walas, S.M., *Phase Equilibria in Chemical Engineering*; Butterworth Publishers, 1985.

69. Whitaker, S. and Pigford, R.L.; Thermal Diffusion in Liquids: Measurement and a Molecular Model *Ind. Eng. Chem.*, **50**, 1062-32, 1958.

70. White, W.; *Close-Up Photography*; Kodak Workshop Series, 1984.

71. White, W.R. and Wiltzius, P. *Phys. Rev. Lett.* **75**, 3012, 1995.

72. Wong, N.C. and Knobler, C.M., Light Scattering of Phase Separation in Isobutyric + Water-Mixtures *J. Chem. Phys.*, **69**, 725, 1978.

73. Zettlemoyer, A.C. *Nucleation*, Marcel Dekker, 1969.